A new liquid scintillation counting technique to resolve mixtures of two pure beta-emitting radionuclides

Winifred Margaret van Wyngaardt (née Morris)

Thesis presented for the degree of
Doctor of Philosophy
in the department of Chemistry
University of Cape Town

November 2007

Supervisor: Dr. B.R.S. Simpson
Co-Supervisor: Prof. G.E. Jackson

I, the undersigned, hereby declare that the work contained in this thesis is my own original work, and that it has been conducted under the supervision of Dr. B.R.S. Simpson (Radioactivity Standards Laboratory, National Metrology Institute of South Africa) and Prof. G.E. Jackson (Department of Chemistry, University of Cape Town). The computer programs used in this study were those in general use in the laboratory and were developed and modified by colleagues in the field.

With the exception of duly acknowledged extracts, no part of this research contains previously published material of others. No part of this work has been submitted in the past for a degree, nor is it being submitted for another degree at this or another university.

Signature: ……. Date: …….

ABSTRACT

A new liquid scintillation counting technique to resolve mixtures of two pure beta-emitting radionuclides

Winifred Margaret van Wyngaardt
Submitted November 2007

Methods currently available for the accurate activity resolution of dual-label solutions of pure β-emitting radionuclides are mostly time consuming and involve much effort. The goal of this thesis was therefore to devise a simpler method to achieve the same objective. The technique developed is based on elements of two liquid scintillation counting techniques that are widely used to measure single-radionuclide solutions, namely the triple-to-double coincidence ratio (TDCR) efficiency calculation technique and the CIEMAT/NIST efficiency tracing method. Double- and triple-coincidence count rates, together with the figure-of-merit P determined from an external tracer, provide sufficient information to extract the component activities of a source in a simple manner.

The mathematical basis for the method is demonstrated and equations are derived to estimate statistical uncertainties, taking correlation effects into account. A simulation based on counting statistics was performed to assess the practicality of the method under normal counting conditions and to validate the derived uncertainty formulae. A critical overview of the underlying photon statistics of liquid scintillation counting is also given, together with clarification of various descriptions published in the literature.

Further insight into the applicability of the new method was achieved by measuring a range of activity compositions of various radionuclide pairs, in particular ^{14}C-^{63}Ni, ^{33}P-^{35}S, ^{32}P-^{33}P and ^{32}P-^{35}S. In all of these experiments, the best results were obtained when the tracer standard used was the same as the low energy component of the mixture. The accuracy of the results for the mixtures of low-energy radionuclides, ^{14}C-^{63}Ni and ^{33}P-^{35}S, was excellent and mostly matched the best achievable by existing methods. The results obtained for the ^{32}P-containing mixtures (with large energy differences) were not as good, showing deviations from the gravimetrically prepared activities that were larger than the estimated uncertainties.

The successful demonstration of this new technique provides a useful extension to the application of the TDCR detector. In addition, owing to the method being particularly sensitive to incorrectly determined efficiencies, it shows potential as a tool to gauge the accuracy of various aspects relating to the efficiency model used.

PUBLICATIONS AND PRESENTATIONS FROM THIS THESIS

W.M. Van Wyngaardt, B.R.S. Simpson, A simple counting technique for measuring mixtures of two pure β-emitting radionuclides. Nucl. Instr. and Meth. A 564 (2006) 339.

W.M. van Wyngaardt, B.R.S. Simpson, G.E. Jackson, Further investigations of a simple counting technique for measuring mixtures of two pure β-emitting radionuclides. Appl. Radiat. Isot. 66 (2008) 1012. Presented orally by W.M. van Wyngaardt at the International Conference on Radionuclide Metrology and its Applications (ICRM 2007), Cape Town, South Africa in September 2007.

W.M. van Wyngaardt, B.R.S. Simpson, Standardization of S-35 by the TDCR efficiency calculation technique. Accepted for poster presentation at the Liquid Scintillation Conference (LSC 2008), Davos, Switzerland in May 2008. To be published in the conference proceedings in a special edition of the journal Radiocarbon.

FULL PUBLICATION RECORD

W.M. Morris, B.R.S. Simpson, Preparation of solid water-equivalent radioactive standards. Appl. Radiat. Isot. 60 (2004) 557.

B.R.S. Simpson, W.M. Morris, The standardization of ^{33}P by the TDCR efficiency calculation technique, Appl. Radiat. Isot. 60 (2004) 465.

B.R.S. Simpson, W.M. Morris, Direct activity determination of ^{54}Mn and ^{65}Zn by a non-extrapolation liquid scintillation method. Appl. Radiat. Isot. 60 (2004) 475.

L. Mo, B. Avci, D. James, B. Simpson, W.M. van Wyngaardt, J.T. Cessna, C. Baldock, Development of activity standard for ^{90}Y microspheres. Appl. Radiat. Isot. 63 (2005) 193.

Winifred M. van Wyngaardt, Bruce R.S. Simpson, Preparation and use of standards for a comparison exercise among users of ^{131}I capsules in South Africa. Physica Medica XXI (2005) 101.

W.M. Van Wyngaardt, B.R.S. Simpson, A simple counting technique for measuring mixtures of two pure β-emitting radionuclides. Nucl. Instr. and Meth. A 564 (2006) 339.

W.M. Van Wyngaardt, B.R.S. Simpson, Absolute activity measurement of the electron-capture-based radionuclides ^{139}Ce, ^{125}I, ^{192}Ir and ^{65}Zn by liquid scintillation coincidence counting. Appl. Radiat. Isot. 64 (2006) 1454.

B.R.S. Simpson, W.M. Van Wyngaardt, Activity measurements of the high-energy pure β-emitters ^{89}Sr and ^{90}Y by the TDCR efficiency calculation technique. Appl. Radiat. Isot. 64 (2006) 1481.

P. Cassette, G.H. Ahn, T. Alzitzoglou, I. Aubineau-Lanièce, F. Bochud, E. Garcia Torano, A. Grau Carles, A. Grau Malonda, K. Kossert, K.B. Lee, J.P. Laedermann, B.R.S. Simpson, W.M. van Wyngaardt, B.E. Zimmerman, Comparison of calculated spectra for the interaction of photons in a liquid scintillator. Example of ^{54}Mn 835 keV emission. Appl. Radiat. Isot. 64 (2006) 1471.

A.C. Razdolescu, R. Broda, P. Cassette, B.R.S. Simpson, W.M. Van Wyngaardt, The IFIN-HH triple coincidence liquid scintillation counter. Appl. Radiat. Isot. 64 (2006) 1510.

B.R.S. Simpson, W.M. Van Wyngaardt, Activity measurement of phosphorus-32 in the presence of pure beta-emitting impurities. S. Afr. J. Sci. 102 (2006) 361.

W.M. van Wyngaardt, B.R.S. Simpson, G.E. Jackson, Further investigations of a simple counting technique for measuring mixtures of two pure β-emitting radionuclides. Appl. Radiat. Isot. 66 (2008) 1012.

B.R.S. Simpson, W.M. van Wyngaardt, Absolute activity of ^{133}Ba by liquid scintillation coincidence counting using the 4π(e,X)-γ extrapolation technique. Appl. Radiat. Isot. 66 (2008) 929.

To Gerhard

ACKNOWLEDGEMENTS

I would like to thank the following people, who made the completion of this thesis possible:

- My friend, colleague and supervisor in this study, Bruce Simpson, for his expert guidance, for his meticulous and timely review of this thesis and for his remarkable patience.
- My co-supervisor, Graham Jackson, for his continued interest and encouragement in this work.
- My colleagues in Radionuclide Metrology, for sharing their knowledge and experience with me.
- The Management of the National Metrology Institute of South Africa, formerly the National Metrology Laboratory of the CSIR, for providing me with the opportunity to study towards a PhD, and for financial support, time and encouragement.
- The Department of Science and Technology for the award of the Women Scientist Fellowship.
- My friend Ester, for sharing her exceptional wisdom with me and for helping me to see light when the task at hand seemed to be overwhelming.
- My family, for their unwavering support and encouragement. Thank you Ma, Daddy, Elsa, Hannelie, Wim, Francia, Dalene, Irene, Adele and Cebella – for providing an incentive for me to hurry up.
- My husband Gerhard, for running our home single-handedly for a very long time, for encouragement, for never-ending patience and for never giving up on me.

CONTENTS

CHAPTER 5 Experimental – measuring mixtures of ^{32}P, ^{33}P and ^{35}S

CHAPTER 6 Conclusions

APPENDIX A Probability distributions

APPENDIX B The figure-of-merit *P* (and *M*) for one-, two- and three-phototube detectors

APPENDIX C Measurement of correction factors

APPENDIX D The statistical uncertainty in N_t / N_d

LIST OF FIGURES

LIST OF TABLES

CHAPTER 1 Introduction

1.1 Beta decay

The radionuclides studied in this thesis were all pure beta minus (β^-) emitters. Beta minus decay occurs in unstable nuclei containing a proton/neutron imbalance with an excess of neutrons. During such a β transition a neutron (n) is converted to a proton (p^+), and a beta particle (β^-) and antineutrino ($\bar{\nu}$) are formed to conserve charge and mass/energy [1]

$$n \rightarrow p^+ + \beta^- + \bar{\nu}. \qquad (1.1)$$

The beta particle is ejected from the nucleus as an electron together with the antineutrino, which is an uncharged particle with a tiny rest mass. Beta decay can be described in more detail by the Standard model [2] whereby the so-called weak interaction allows a *down* quark from the neutron (consisting of two *down* quarks and one *up* quark) to change to an *up* quark, thereby forming a proton (consisting of one *down* quark and two *up* quarks). The process is mediated by the exchange of a virtual W^- boson, which decays to an electron and an electron anti-neutrino.

When a radionuclide decays purely by β emission and the β decay occurs directly to the ground state of the daughter, the radionuclide is known as a pure β-emitter. There are not many such radionuclides. In a booklet [3] summarising the nuclear decay data of the 249 radionuclides most often used or encountered in medicine and industry, only eleven pure β-emitters (^{3}H, ^{14}C, ^{32}P, ^{33}P, ^{35}S, ^{63}Ni, ^{79}Se, ^{90}Sr, ^{106}Ru, ^{135}Cs and ^{209}Pb) and another twelve that are essentially pure β-emitters (^{36}Cl, ^{45}Ca, ^{85}Kr, ^{89}Sr, ^{90}Y, ^{91}Y, ^{99}Tc, ^{143}Pr, ^{147}Pm, ^{151}Sm, ^{185}W and ^{206}Tl) are listed. The decay scheme of ^{14}C is given in Fig. 1.1.

Beta decay is characterised by the total energy released during the β transition, E_{max}. For pure β-emitters E_{max} equals the difference between the atomic masses of the ground states of the parent and daughter nuclides, expressed in units of energy [5]. This decay energy is shared between the electron and antineutrino in a statistical manner so that, for a large number of transitions, the electron energies will range from zero to E_{max} and *vice versa* for the energies of the antineutrino. A continuous β energy spectrum is obtained which will overlap, at least

in the low energy region, with that of any other β-emitter. The β spectrum of ^{14}C is given in Fig. 1.2 as a typical example.

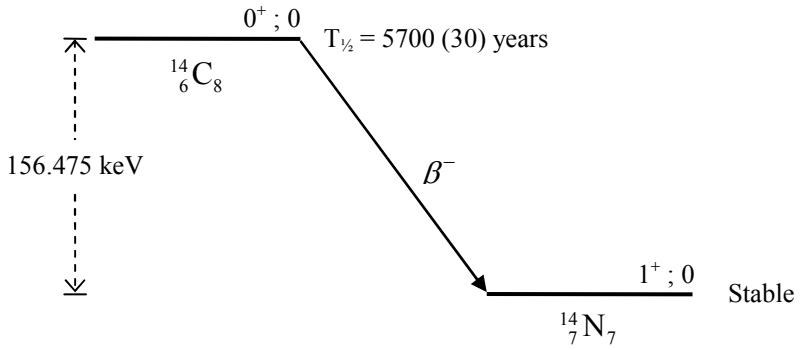

Fig. 1.1 Decay scheme of ^{14}C [4]. The decay schemes of other pure β-emitters will be similar.

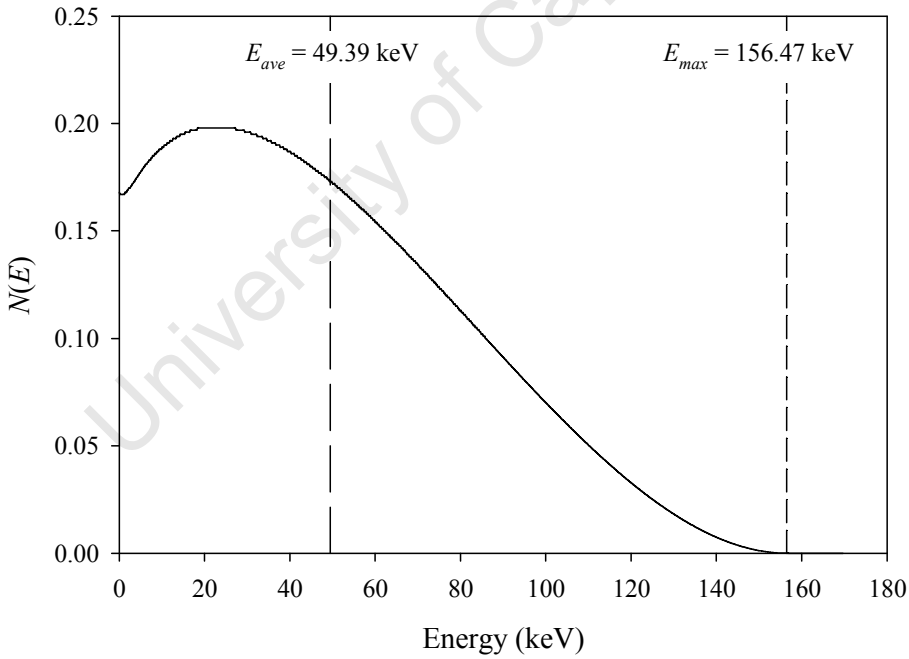

Fig. 1.2 The theoretical β spectrum of ^{14}C was generated from the Fermi theory of β decay using routines from the program EFFY 2 [6]. $N(E)$ gives the number of β particles with energy between E and $E+dE$. The average energy is given by [5]

$$E_{ave} = \int_0^{E_{max}} E\,N(E)dE \Big/ \int_0^{E_{max}} N(E)dE\,. \qquad (1.2)$$

The spectra of other β-emitters will be similar with energies ranging from zero to the specific maximum energy of the particular radionuclide.

1.2 The measurement of pure β-emitting radionuclides

For the direct or absolute standardisation of radionuclides the detection efficiency must be established without reference to a tracer standard [7]. To achieve this accurately for pure β-emitting radionuclides is particularly difficult. Some of the more widely-used methods [8] are summarised below.

1.2.1 Proportional counting

Since the 1960s proportional counting in 4π geometry has been widely used for the standardisation of radionuclides, including pure β-emitters [9]. In this type of detector, the original ion pair formed by the interaction of a decay particle with the detector gas is multiplied linearly by subsequent electron collisions with the gas under the influence of an applied electric field [10]. The counting gas, which may be pressurised to increase the interaction probability, is often methane or a 90:10 mixture of argon:methane [8]. Self-absorption within the solid sources used prevents some of the original ion pairs from reaching the detector, thereby reducing the detection efficiency in a manner that is difficult to quantify. This is of particular significance for radionuclides with low-energy emissions such as ^{204}Tl [11], a pure β-emitter with a 3 % electron-capture branch [4]. Self-absorption can be estimated by linear extrapolation to zero source mass [11, 12, 13] or by $4\pi\beta$-γ efficiency tracing using a β-γ emitter of similar β energy to the radionuclide of interest [14]. As examples of its ongoing importance, proportional counting was recently used for standardisations of ^{89}Sr [13, 14] and ^{32}P [12] as part of international intercomparisons.

1.2.2 Internal gas proportional counting

A method that relies on similar detection principles for the measurement of gaseous samples such as $^{3}H_2$, $^{14}CO_2$ and ^{85}Kr is internal gas proportional counting [15]. The radionuclide sample is mixed directly with a suitable counting gas so that self-absorption effects are eliminated. Corrections are, however, required for end effects, the wall effect and the loss of very low energy β particles [16]. The results of an international intercomparison of the measurement of ^{85}Kr gas and of $^{3}H_2$ gas mixed with N_2 showed agreement to within the specified uncertainties [17]. Internal gas proportional counting can also be used for the

measurement of tritiated water after quantitative reduction to $^{3}H_2$ gas [18, 19]. For tritium measurement, this method usually sets the standard against which results obtained by other methods, for example liquid scintillation counting, are compared [20, 21], although the uncertainties obtainable with the different methods are comparable.

1.2.3 Liquid scintillation counting

Liquid scintillation counting has been widely used for the measurement of radionuclides since the early 1950s [22]. For this mode of detection a radionuclide sample in solution is mixed with a liquid scintillation cocktail. The decay energy is transferred, via the solvent, to the scintillator molecules of the cocktail, which emit photons of light upon de-excitation. The photons are detected by one or more photomultiplier tubes (more correctly called electron-multiplier phototubes). The light output is related to the decay energy although the intensity is non-linearly reduced by quenching effects [23]. The process of liquid scintillation counting is described in more detail in Section 2.2 of this thesis.

Today liquid scintillation counting is used by most national radionuclide metrology laboratories for the accurate measurement of pure β-emitting radionuclides [23]. It is also the preferred method adopted at the National Metrology Laboratory of South Africa (NMISA) Radioactivity Standards laboratory. Two sophisticated methods based on efficiency calculation are usually applied for this purpose. The direct triple-to-double coincidence ratio (TDCR) efficiency calculation technique [24, 25, 26, 27, 28] makes use of the ratio of the measured triple- and double-coincidence count rates to calculate the detection efficiency of the radionuclide of interest, while the CIEMAT/NIST efficiency tracing method [29, 30, 31] relies on an external ^{3}H tracer standard to do this. Both methods are described in detail in Chapter 2.

Some examples where the TDCR method has been used for absolute activity measurement are ^{3}H [32], ^{14}C [32], ^{33}P [33], ^{63}Ni [28, 32, 34], ^{89}Sr [35], ^{90}Y [35] and ^{99}Tc [32]. The CIEMAT/NIST method has been used for the measurement of ^{14}C [29, 31], ^{32}P [29], ^{36}Cl [29], ^{45}Ca [36], ^{63}Ni [34], ^{79}Se [37], ^{89}Sr [13, 29], ^{90}Y [38], ^{99}Tc [29] and ^{185}W [29], among others. The TDCR method was successfully applied in an international intercomparison of ^{3}H [20] and both methods achieved good results in international intercomparisons of ^{63}Ni [39] and ^{90}Y

[40].

Of the methods discussed in this section, only liquid scintillation counting is widely used for the routine measurement of radionuclides in, for example, environmental and bioscience applications. This is aided by the availability of automatic liquid scintillation analysers which are able to count large numbers of samples without much user interaction, easy sample preparation and the ability to measure coloured, chemically quenched or relatively large volume samples.

1.2.4 Other methods

Other methods that are less widely used for the measurement of pure β-emitting radionuclides include measurement with a windowless 4π-CsI(Tl) sandwich spectrometer [13, 41], calorimetry [42, 43], cryogenic microcalorimetry [44, 45, 46] and Cherenkov counting [47, 48].

1.3 The need to measure mixtures of pure β-emitting radionuclides

It is often necessary or useful to measure mixtures of pure β-emitting radionuclides in the same sample, although the continuous nature and overlap between spectra of different β-emitters makes this challenging. A few typical examples are given below, with mention of the methods generally used for measurements. The measurement methods are discussed in more detail in Section 1.4.

1.3.1 The determination of impurities in radionuclide metrology

For the direct application of the methods described in the previous section, the sources being measured must be radioactively pure. During the production of certain radionuclides, for example ^{32}P, impurities are formed which are difficult to separate out chemically and which do not decay away quickly compared to the half-life of the radionuclide under consideration. For absolute activity measurements, the impurity content must then be determined and corrected for. When the impurity is also a pure β-emitter, it is in effect necessary to measure

a mixture of two or more pure β-emitting radionuclides. In recent international intercomparisons of ^{32}P with possible impurities of ^{33}P and ^{35}S, most participants resolved the mixtures by measuring the solution repeatedly over an extended time period to follow the decay of the individual components [12, 49 – 52]. The method is accurate but time consuming.

1.3.2 Environmental monitoring for nuclear contamination

Beta-emitters such as ^{3}H, ^{14}C, ^{36}Cl, ^{89}Sr, ^{90}Sr, ^{90}Y and ^{99}Tc are products of the nuclear fuel cycle and the environment surrounding nuclear facilities is routinely monitored for possible contamination [53]. Mixtures of different elements are chemically separated before measurement when possible. Alternatively mixtures must be resolved by suitable measurement techniques.

Of the radionuclides mentioned above, ^{89}Sr, ^{90}Sr and ^{90}Y are of particular importance. Immediately after a nuclear accident the short-lived ^{89}Sr ($T_{½}$ = 50.57 days [4]) is formed in significant excess compared to ^{90}Sr [54]. However, the long-lived ^{90}Sr ($T_{½}$ = 28.79 years [4]) has a long biological half-life of about 10 years so that it poses a serious health risk together with its radioactive daughter ^{90}Y ($T_{½}$ = 2.6708 days [4]) [55]. Some methods have been developed to rapidly measure these radioisotopes to assess the radiation hazard due to a nuclear incident. For example, the spectrum unfolding method was used to measure ^{89}Sr and ^{90}Sr after chemical separation of ^{90}Y [56] and spectral deconvolution was used to measure mixtures of ^{90}Y, ^{90}Sr and ^{89}Sr [57]. Both methods gave good results, also for low-level samples.

There is also a need to determine ^{14}C in the presence of ^{3}H. As an example, the ^{14}C levels in samples of milk and agricultural produce from various sites in the USA were monitored for contamination. The sample material was combusted, and the resultant carbon dioxide converted to benzene for measurement by liquid scintillation counting [58]. Counting windows were set to eliminate any ^{3}H. No significantly elevated results were obtained in the vicinity of nuclear facilities or as a result of fallout from the Chernobyl accident [59, 60].

1.3.3 Biological science

Double-label experiments have been widely used as a tool to study the biochemical reaction mechanisms and pathways whereby natural molecules are synthesised by living organisms. ^{14}C is often incorporated into the carbon backbone of the precursor molecule as a reference against which the retention, dilution or loss of the other label (e.g. ^{3}H or ^{32}P) can be measured to provide information regarding the specific reaction taking place [61]. For example, determining the mechanism for a cyclization reaction [62]; determining the specific hydrogen atoms removed during an oxidation reaction [63]; and demonstrating that a specific one of two enantiomers (non-superimposable mirror images) is used exclusively in a biosynthesis reaction [64]. In these applications automatic liquid scintillation analysers are usually used to resolve mixtures.

1.3.4 The study of nutrient uptake in plants

Nitrogen, calcium, phosphorus, sulphur and potassium are important nutrients for plants. The stable isotope ^{15}N and radionuclides ^{45}Ca, ^{32}P, ^{33}P, ^{35}S and ^{86}Rb (as a chemical equivalent of K) are useful tracers for studies of nutrient uptake. A mixture resolution method for use in fertiliser studies was developed whereby ^{86}Rb is measured by Cherenkov counting and the activities of ^{33}P and ^{35}S determined by repeated liquid scintillation counting over a lengthy decay time [65].

In an actual field experiment the nutrient uptake from the forest floor and the lower part of the rooting zone was compared between Norway spruce (conifer) and broad-leaved birch trees in mixed stands on different soils [66]. In one part of this study a solution of ^{45}Ca and ^{32}P was applied at two depths around various trees and the uptake of the radio tracers estimated from the leaves. ^{32}P was measured by Cherenkov counting and ^{45}Ca determined by liquid scintillation counting. In another part of the study ^{32}P and ^{33}P were applied at different depths together with ^{86}Rb. The intention was to measure ^{86}Rb with a NaI γ-detector, ^{32}P by Cerenkov counting and ^{33}P by liquid scintillation counting, but variable quenching due to Fe^{3+} prevented the separation of the two phosphorous isotopes.

1.4 Methods currently available to measure mixtures of pure β-emitting radionuclides

Of the detection methods mentioned in Section 1.2 for the measurement of pure β-emitters, only liquid scintillation counting has widespread use for the measurement of solutions containing two or more pure β-emitting radionuclides in the same sample. This is not easy to achieve. Some of the more widely used and/or accurate methods are described below.

1.4.1 Methods programmed into automatic liquid scintillation analysers

The methods described below are often programmed into commercial automatic liquid scintillation analysers and are well-suited for routine use.

1.4.1 (a) Conventional Dual Label-DPM methods

The conventional Dual Label-DPM methods rely on the setting of two adjoining counting windows to resolve mixtures of two pure β-emitting radionuclides [67]. Quench correction curves of detection efficiency vs. a quench indicating parameter are collected for both pure components in each counting region. Measuring the quench indicating parameter of a mixed radionuclide source and collecting counts from both windows allow the determination of the component count rates and activities.

The Exclusion method is one of the original Dual Label-DPM methods. The counting windows are set so that the lower window contains counts from both components and the upper window excludes all counts of the lower energy radionuclide [67, 68]. For this method the maximum β-energies of the components must differ by at least a factor of 3 or 4. The method is not commonly used today due to the development of techniques that give better detection efficiencies.

For the Inclusion method, two windows are set such that significant overlap of counts occurs from both radionuclides in each counting region, i.e., there is spilldown of the high energy component into the low energy region and spillup of events from the low energy component to the high energy region [67]. However, quenching changes the positions of the spectra. To maintain optimal counting conditions an automated window tracking method is applied that

adjusts the windows so that the spilldown and spillup remain constant with increased quench. Window settings for certain radionuclide pairs are often built in by the manufacturer of the liquid scintillation analyser, alternatively, optimal window settings must be determined experimentally [67, 69]. The method can be extended to resolve three radionuclides by setting three counting windows and collecting three quench correction curves.

Application of the Dual Label-DPM method to mixtures of ^{3}H (E_{max} = 18.6 keV) and ^{14}C (E_{max} = 156.5 keV) for ^{14}C/^{3}H count rate ratios of between 3 and 48 gave relative discrepancies from the experimentally prepared activities that were mostly < 2 % for ^{14}C and mostly < 15 % for ^{3}H, depending on the ratios [68]. In another experiment mixtures of ^{14}C and ^{3}H with activity ratios between 40.1/1 and 1/10 gave relative discrepancies of < 10 % for ^{14}C and mostly < 20 % for ^{3}H when ^{14}C/^{3}H equalled 2/1 or less [70]. In this study unreliable results were obtained for ^{3}H when ^{14}C/^{3}H ≥ 10/1.

1.4.1 (b) The Full Spectrum-DPM method

The Spectrum "unfolding" or Full Spectrum-DPM method relies on the Spectral Index of the Sample (SIS) to resolve mixtures of two radionuclides [55, 56, 67]. Counting is performed over the full energy spectrum without the setting of counting windows. The SIS reflects the pulse height-energy distribution of a spectrum and is unique for each radionuclide for a specific quench state [67]. The SIS value is directly related to the weighted mean pulse height of the spectrum, calculated from the channel numbers and counts per channel [71]. The relationship between the SIS values of individual pure β-emitters and that of a mixed radionuclide source, SIS_T, is given by [56]

$$SIS_T = \frac{SIS_L \cdot N_L + SIS_H \cdot N_H}{N_T}. \qquad (1.3)$$

SIS_L and SIS_H are the SIS indices of the lower and higher energy components of the pure spectra at the same quench state as the mixture source and N_L and N_H are the counts collected from each component, with $N_T = N_L + N_H$. If the quench state of a mixed radionuclide source is known, SIS_T can therefore be used to unfold the energy spectrum into its component spectra. To apply the method, quench correction curves of detection efficiency vs. a quench indicating parameter (e.g. tSIE) and SIS vs. tSIE are collected for the two pure components. It follows from Eq. (1.3) that the count rates of the two components, CPM_L and CPM_H, are

given by [56, 67]

$$CPM_L = \frac{SIS_H - SIS_T}{SIS_H - SIS_L} \cdot CPM_T \text{ and } CPM_H = \frac{SIS_T - SIS_L}{SIS_H - SIS_L} \cdot CPM_T, \quad (1.4)$$

where CPM_T is the count rate of the mixture source and SIS_H and SIS_L were determined from the SIS vs. tSIE quench correction curves. The count rates are converted to activities by comparison with the efficiency vs. tSIE calibration curve. For this method, it is recommended that the maximum β energies of the radionuclides must differ by a factor of 3 or more and the activity ratios must be between 1:25 and 25:1.

Application of the Full Spectrum-DPM method to mixtures of ^{90}Y (E_{max} = 2280.1 keV) and ^{90}Sr (E_{max} = 546.0 keV) for activity ratios of ^{90}Y/^{90}Sr between 0 and 1 gave relative discrepancies from the expected activities of < 2 % for ^{90}Sr and < 30 % for ^{90}Y, depending on the activity ratio [69].

1.4.1 (c) General comments

These methods available with automatic liquid scintillation analysers are relatively easy to use, although determination of counting windows for the DL-DPM method requires some competence from the analyst. For good results it is important that the standards for the determination of quench correction curves exactly match the mixture source in terms of the liquid scintillator cocktail used, the type and size of the counting vial and the total source volume [67].

These methods are only applicable to radionuclide pairs with energies that differ significantly and require single-radionuclide solutions of the components for the collection of quench correction curves. Instead of using pure standards for the determination of quench curves, these methods can be used together with the CIEMAT/NIST efficiency tracing method. The required detection efficiencies are then calculated and non-standardised sources can be used to determine the quench correction curves from the single-radionuclide solutions [55].

1.4.2 Spectral deconvolution

Spectral deconvolution [68, 70, 72] is a powerful method for the standardisation of mixed radionuclide sources. The method makes use of pulse height spectra of the pure components that correspond to the same quench state as the mixed radionuclide source to unfold the composite spectrum. However, spectra of the pure components can be collected only at a limited number of quench states. The technique described below provides a method whereby the required spectra are obtained mathematically from the limited set.

Spectra are collected for each of the pure components in different quench states and for the mixture solution, using a liquid scintillation spectrometer. The spectra are fitted by Fourier spectral functions (for logarithmic pulse-height spectra) or by Chebyshev spectral functions (for linear pulse-height spectra) [70]. This enables the transformation of the fitted spectra (of the pure components) by channel rearrangement and in addition aids in smoothing out statistical fluctuations. The transformed spectra are interpolated to calculate the pure spectra at the required quench states [70]. If X and Y are the radionuclides in the mixture, the fitted mixture spectrum, $y(X+Y)$, is unfolded by obtaining the coefficients, a and b, for which the difference between $y(X+Y)$ and the interpolated pure spectra, $y(X)$ and $y(Y)$, are minimised for all i channels. This is expressed mathematically by [70, 72]

$$\min\left\{\sum\left[y_i(X+Y)-ay_i(X)-by_i(Y)\right]^2\right\}. \tag{1.5}$$

The unfolding is further optimized by iterative shifting of the pure spectra up and/or down the channel axis to account for gain change, or by iterative adjustment of the quench state used for the calculation of the pure spectra [70, 72]. The coefficients give the component count rates, which are converted to activities using the CIEMAT/NIST method [29].

The spectral deconvolution method has been successfully applied to mixtures of increasing difficulty, namely ^{3}H (E_{max} = 18.6 keV) and ^{14}C (E_{max} = 156.5 keV) [68, 70]; ^{90}Y (E_{max} = 2280.1 e/keV) and ^{90}Sr (E_{max} = 546.0 keV) [57, 4]; ^{45}Ca (E_{max} = 256.4 keV) and ^{35}S (E_{max} = 167.1 keV) [70, 4]; and mixtures that were previously thought to be inseparable, ^{14}C and ^{35}S [72]. An indication of the accuracy attainable is briefly summarised. For ^{14}C/^{3}H count rate ratios of between 1.8 and 103 the relative discrepancies from the experimentally prepared activities were < 1 % for ^{14}C and mostly < 3 % for ^{3}H, depending on the ratios [68]. Mixtures of ^{14}C and ^{3}H with activity ratios between 40.1/1 and 1/10 gave larger relative discrepancies

of < 3 % for ^{14}C and < 6 % for ^{3}H, and more so for the two extreme mixtures [70]. Various mixture ratios of ^{90}Y/^{90}Sr gave relative discrepancies which were mostly < 2 % [57]. Similarly, various mixture ratios of ^{45}Ca and ^{35}S gave relative discrepancies of < 1.6 % for ^{45}Ca and < 4 % for ^{35}S [70]. Mixtures of ^{14}C and ^{35}S with activity ratios between 10.5/1 and 1/11.8 gave relative discrepancies of mostly < 5 % for the component with the higher activity and mostly < 30 % for the smaller component, for samples with low quenching [72].

Comparison of the results given above with those in Section 1.4.1 show that spectral deconvolution is currently the most powerful technique for resolving two-component mixtures by spectroscopy. However, the method requires single-radionuclide solutions of each component to be available so that spectra can be collected at different quench states and the complex programs developed for the fitting, transforming, interpolation and unfolding of spectra may limit usage by the general user.

1.4.3 Following the decay over time

Mixtures of radionuclides can be resolved by measuring the solution repeatedly over a time that is long compared to the half-life of the short-lived components [49]. For a three-component mixture the count rate at a time *t* after the reference date, $N(t)$, equals the sum of the individual decay corrected count rates such that [49, 50, 52]

$$N(t) = N_1 \exp(-\lambda_1 t) + N_2 \exp(-\lambda_2 t) + N_3 \exp(-\lambda_3 t), \tag{1.6}$$

where N_1, N_2 and N_3 are the count rates as specified on the reference date and λ_i are the respective decay constants. In addition,

$$N_i = A_i \varepsilon_i, \text{ for } i = 1 \text{ to } 3, \tag{1.7}$$

where A_i are the individual radionuclide activities on the reference date and ε_i the detection efficiencies, which must remain constant for the duration of the experiment. By fitting the set of count rates collected over time to Eq. (1.6) by a weighted least squares fitting procedure, the individual reference count rates can be obtained. The count rates can be converted to activities by the CIEMAT/NIST efficiency tracing method [49, 51, 52] or by the TDCR method [50, 52]. The method of following the decay over time was successfully applied to the measurement of ^{32}P, containing impurities of ^{33}P and ^{35}S, in two international intercomparisons [12, 49 – 52]. The solutions were measured repeatedly for periods of one to four months, with the extracted ^{32}P activity concentrations being reported with uncertainties at

about the 0.5 % level (1σ). The activity concentrations of the impurities were specified with uncertainties of about 5 % relative to the activity of the major radionuclide [49, 50].

This method is only applicable to radionuclides with suitably short half-lives. Generally, the accuracy obtainable is dependent on the activity ratios and differences in the half-lives of the components, with mixtures of radionuclides with similar half-lives and small component ratios being more difficult to resolve [49]. The long period of time required is a distinct disadvantage of the method. The stringent requirement of unaltering source efficiency during this period also poses difficulties.

1.4.4 Sequential Cherenkov and liquid scintillation counting

Cherenkov radiation refers to the photons produced when a charged particle travels through a transparent medium at a speed greater than the speed of light in the medium [73]. This effect can be used for the detection of β particles with energies > 263 keV, using an ordinary liquid scintillation analyser with water-based sources instead of a liquid scintillation cocktail [47].

This form of radiation has been used advantageously to measure mixtures of two radionuclides when the decay energy of one component is high enough to be measured by Cherenkov counting but not the other [74]. The aqueous sample is first measured by Cherenkov counting, taking into account colour quenching effects, to determine the activity of the high energy component. A suitable liquid scintillation cocktail is then added to the source, and the total activity determined by the ^{14}C efficiency tracing method [75]. The activity of the low energy component is determined by subtraction. This procedure has been successfully applied to mixtures of ^{32}P-^{14}C, ^{32}P-^{35}S, ^{32}P-^{45}Ca, ^{36}Cl-^{35}S and ^{36}Cl-^{45}Ca among others, and gave results that agreed with the prepared values to within 5 % [74]. This method is easy to apply in a routine laboratory but the detection efficiencies must be determined carefully to achieve reliable results.

1.5 Thesis motivation

The methods currently available for the simultaneous measurement of two pure β-emitting radionuclides in the same sample appear to either be “black boxes” for routine work, or, if

better accuracy is required, to be time consuming and involving a lot of effort. The methods rely on one or more of the following: complex setting of counting windows and tracking of the windows to account for quenching, distinct differences in the β energies, the collection of quench correction curves for the pure components, spectral unfolding, spectral deconvolution and/or lengthy counting times.

The aim of this thesis was to develop a simple *counting* technique capable of resolving the activities of mixtures of two pure β-emitting radionuclides. The new method should be easy to execute experimentally and give accurate results for a wide range of radionuclide pairs. The intention was to achieve the activity resolution without any of the inconveniences, conditions and/or complexities associated with currently available methods. The development of a technique based on liquid scintillation counting seemed most likely to be able to satisfy these objectives. At the same time the availability of a triple phototube detection system provided the possibility of broadening its scope beyond just activity standardisation. The basic idea followed was therefore to utilise aspects of the TDCR technique, together with the CIEMAT/NIST approach for establishing detection efficiencies. This concept, in principle, fulfilled the criteria outlined above and was subsequently investigated in detail. The following intermediate objectives were identified:

- To gain a thorough understanding of the calculation of liquid scintillation counting detection efficiencies by reviewing models based on photon statistics. To clarify different approaches and resulting formulae into a comprehensible summary.
- To determine a mathematical basis for the new method.
- To undertake a simulation to gauge whether the method would be feasible under normal counting conditions, taking into consideration the effect of counting statistics. Also to gain insight into uncertainties due to counting statistics and the expected correlation effects.
- Once satisfied that the new method showed promise, to undertake experimental work on a variety of mixture pairs to verify that the method is indeed viable in practice. Also to assess the accuracy of the new method and to gain insight into various factors that might affect the general applicability of the method.

1.6 References

[1] M.F. L'Annunziata, Nuclear radiation, its interaction with matter and radioisotope decay, in: M.F. L'Annunziata (Ed.), Handbook of radioactivity analysis, second ed., Academic Press, New York, 2003, pp. 14 – 20.

[2] http://www2.slac.stanford.edu/vvc/theory/weakinteract.html

[3] M.-M. Bé, C. Dulieu, V. Christé, Mini table de radionucléides 2007, Laboratoire National Henri Becquerel, EDP Sciences, France, 2007, pp. 8 – 131.

[4] M.-M. Bé, B. Duchemin, C. Morillon, E. Browne, V. Chechev, A. Egorov, R. Helmer, E. Schönfeld, Nucleide 2000. Nuclear and atomic decay data, Version 2-2004. BNM-CEA/DTA/LPRI, Saclay, France, 2004.

[5] NCRP Report No. 58, A handbook of radioactivity measurements procedures, second ed., National Council on Radiation Protection and Measurements, Bethesda, 1985, pp. 350 – 352.

[6] E. Garcia-Toraño, A. Grau Malonda, EFFY, a new program to compute the counting efficiency of beta particles in liquid scintillators, Comp. Phys. Commun. 36 (1985) 307.

[7] NCRP Report No. 58, A handbook of radioactivity measurements procedures, second ed., National Council on Radiation Protection and Measurements, Bethesda, 1985, pp. 16 – 18.

[8] S. Pommé, Methods for primary standardization of activity, Metrologia 44 (2007) S17.

[9] NCRP Report No. 58, A handbook of radioactivity measurements procedures, second ed., National Council on Radiation Protection and Measurements, Bethesda, 1985, pp. 100 – 109.

[10] G.F. Knoll, Radiation detection and measurement, third ed., John Wiley & Sons, Inc., New York, 2000, pp. 159 – 188.

[11] L. Johansson, G. Sibbens, T. Altzitzoglou, B. Denecke, Self-absorption correction in standardisation of ^{204}Tl, Appl. Radiat. Isot. 56 (2002) 199.

[12] P.A.L. da Cruz, A. Iwahara, E.M.O. Bernardes, C.J. da Silva, The absolute standardization of ^{32}P and ^{204}Tl at LNMRI, Appl. Radiat. Isot. 60 (2004) 415.

[13] T. Altzitzoglou, B. Denecke, L. Johansson, G. Sibbens, Standardisation of ^{89}Sr using three different methods, Appl. Radiat. Isot. 56 (2002) 447.

[14] I. Csete, L. Szücs, A. Zsinka, Standardization of ^{89}Sr at the National Office of Measures, Appl. Radiat. Isot. 56 (2002) 467.

[15] NCRP Report No. 58, A handbook of radioactivity measurements procedures, second ed., National Council on Radiation Protection and Measurements, Bethesda, 1985, pp. 109 – 113.

[16] M.P. Unterweger, Primary radioactive gas standards (excluding radon), Metrologia 44 (2007) S79.

[17] J.L. Makepeace, F.E. Clark, J.L. Picolo, N. Coursol, E. Günther, M.P. Unterweger, Intercomparison of internal proportional gas counting of ^{85}Kr and ^{3}H, Nucl. Instr. and Meth. A 339 (1994) 343.

[18] J.L. Makepeace, F.E. Day, E. Günther, M.A. Unterweger, Intercomparison of measurement of tritiated water by internal proportional gas counting, Nucl. Instr. and Meth. A 369 (1996) 458.

[19] D. Stanga, P. Cassette, Improved method of measurement for tritiated water standardization by internal gas proportional counting, Appl. Radiat. Isot. 64 (2006) 160.

[20] J. Makepeace, T. Altzitzoglou, P. Cassette, P. Dryák, E. Günther, F. Verrezen, R. Broda, B. Simpson, M. Unterweger, International comparison of measurements of the specific activity of tritiated water, Appl. Radiat. Isot. 49 (1998) 1411.

[21] D. Stanga, I. Moreau, P. Cassette, Standardization of tritiated water by two improved methods, Appl. Radiat. Isot. 64 (2006) 1203.

[22] M.F. L'Annunziata, M.J. Kessler, Liquid scintillation analysis: principles and practice, in: M.F. L'Annunziata (Ed.), Handbook of radioactivity analysis, second ed., Academic Press, New York, 2003, pp. 347 – 364.

[23] R. Broda, P. Cassette, K. Kossert, Radionuclide metrology using liquid scintillation counting, Metrologia 44 (2007) S36.

[24] B.R.S. Simpson, B.R. Meyer, Direct determination of the activity of non-gamma-emitting radionuclides by the TDCR efficiency calculation technique: a review of the present status, NAC Report NAC/92-02 (1992).

[25] B.R.S. Simpson, B.R. Meyer, Further investigations of the TDCR efficiency calculation technique for the direct determination of activity, Nucl. Instr. and Meth. A 312 (1992) 90.

[26] P. Cassette, R. Vatin, Experimental evaluation of TDCR models for the 3 PM liquid scintillation counter, Nucl. Instr. and Meth. A 312 (1992) 95.

[27] R. Broda, A review of the triple-to-double coincidence ratio (TDCR) method for standardizing radionuclides, Appl. Radiat. Isot. 58 (2003) 585.

[28] A.C. Razdolescu, R. Broda, P. Cassette, B.R.S. Simpson, W.M. van Wyngaardt, The IFIN-HH triple coincidence liquid scintillation counter, Appl. Radiat. Isot. 64 (2006) 1510.

[29] A. Grau Malonda, E. Garcia-Toraño, Evaluation of counting efficiency in liquid scintillation counting by pure β-ray emitters, Int. J. Appl. Radiat. Isot. 33 (1982) 249.

[30] B.M. Coursey, A. Grau Malonda, E. Garcia-Toraño, J.M. Los Arcos, The standardization of pure-beta-particle-emitting radionuclides, Trans. Amer. Nucl. Soc. 50 (1985) 13.

[31] B.M. Coursey, W.B. Mann, A. Grau Malonda, E. Garcia-Toraño, J.M. Los Arcos, J.A.B. Gibson and D. Reher, Standardization of carbon-14 by $4\pi\beta$ liquid scintillation efficiency tracing with hydrogen-3, Appl. Radiat. Isot. 37 (1986) 403.

[32] B.R.S. Simpson, B.R. Meyer, Direct activity measurement of pure beta-emitting radionuclides by the TDCR efficiency calculation technique, Nucl. Instr. and Meth. A 339 (1994) 14.

[33] B.R.S. Simpson, W.M. Morris, The standardization of ^{33}P by the TDCR efficiency calculation technique, Appl. Radiat. Isot. 60 (2004) 465.

[34] R. Collé, B.E. Zimmerman, P. Cassette, L. Laureano-Perez, ^{63}Ni, its half-life and standardization: Revisited, Appl. Radiat. Isot. 66 (2008) 60.

[35] B.R.S. Simpson, W.M. van Wyngaardt, Activity measurements of the high-energy pure β-emitters ^{89}Sr and ^{90}Y by the TDCR efficiency calculation technique, Appl. Radiat. Isot. 64 (2006) 1481.

[36] L. Rodriguez Barquero, J.M. Los Arcos, A. Grau Malonda, E. Garcia-Toraño, LSC standardization of ^{45}Ca by the CIEMAT/NIST efficiency tracing method, Nucl. Instr. and Meth. A 339 (1994) 6.

[37] P. Bienvenu, P. Cassette, G. Andreoletti, M.-M. Bé, J. Comte, M.-C. Lépy, A new determination of ^{79}Se half-life, Appl. Radiat. Isot. 65 (2007) 355.

[38] K. Kossert, H. Schrader, Activity standardization by liquid scintillation counting and half-life measurements of ^{90}Y, Appl. Radiat. Isot. 60 (2004) 741.

[39] P. Cassette, T. Altzitzoglou, R. Broda, R. Collé, P. Dryak, P. De Felice, E. Gunther, J.M. Los Arcos, G. Ratel, B. Simpson, F. Verrezen, Comparison of activity concentration measurement of ^{63}Ni and ^{55}Fe in the framework of the Euromet 297 project, Appl. Radiat. Isot. 49 (1998) 1403.

[40] B.E. Zimmerman, G. Ratel, Report of the CIPM Key Comparison CCRI(II)-K2.Y-90, Metrologia, 42 (2005) 06001.

[41] B. Denecke, Absolute activity measurements with the windowless 4π-CsI(Tl)-sandwich spectrometer, Nucl. Instr. and Meth. A 339 (1994) 92.

[42] R. Collé, Classical radionuclide calorimetry, Metrologia 44 (2007) S118.

[43] W.B. Mann, M.P. Unterweger, The NBS/NIST Peltier-effect microcalorimeter: a four-decade review, Appl. Radiat. Isot. 46 (1995) 185.

[44] R. Collé, B.E. Zimmerman, A dual-compensated cryogenic microcalorimeter for radioactivity standardizations, Appl. Radiat. Isot. 56 (2001) 223.

[45] E. Leblanc, P. de Marcillac, N. Coron, J. Leblanc, M. Loidl, J.F. Metge, J. Bouchard, A new absolute method for the standardization of radionuclides emitting low-energy radiation, Appl. Radiat. Isot. 56 (2002) 245.

[46] M. Loidl, E. Leblanc, J. Bouchard, T. Branger, N. Coron, J. Leblanc, P. de Marcillac, H. Rotzinger, T. Daniyarov, M. Linck, A. Fleischmann, C. Enss, High-energy resolution X-ray, gamma and electron spectroscopy with cryogenic detectors, Appl. Radiat. Isot. 60 (2004) 363.

[47] A. Grau Carles, A. Grau Malonda, Radionuclide standardization by Cherenkov counting, Appl. Radiat. Isot. 46 (1995) 799.

[48] A. Grau Malonda, A. Grau Carles, The anisotropy coefficient in Cherenkov counting, Appl. Radiat. Isot. 49 (1998) 1049.

[49] T. Altzitzoglou, Analysis of triple-label samples by liquid scintillation spectrometry, Appl. Radiat. Isot. 60 (2004) 487.

[50] F. Jaubert, P. Cassette, Standardization of a ^{32}P solution containing pure-beta impurities using the TDCR method in liquid scintillation counting, Appl. Radiat. Isot. 60 (2004) 601.

[51] L. Rodríguez Barquero, E. García-Toraño, J.M. Los Arcos, Standardization of ^{32}P/^{33}P and ^{204}Tl by liquid scintillation counting, Appl. Radiat. Isot. 60 (2004) 615.

[52] B.R.S. Simpson, W.M. van Wyngaardt, Activity measurement of phosphorus-32 in the presence of pure beta-emitting impurities. S. Afr. J. Sci. 102 (2006) 361.

[53] G.T. Cook, C.J. Passo, Jr., B. Carter, Environmental liquid scintillation analysis, in: M.F. L'Annunziata (Ed.), Handbook of radioactivity analysis, second ed., Academic Press, New York, 2003, pp. 537 – 607.

[54] E.I. Vapirev, P.A. Grozev, L.I. Botsova, A.V. Hristova, Beta-spectroscopic separation of ^{90}Sr, ^{90}Y and ^{89}Sr with a scintillation detector, J. Radioanal. Nucl. Chem. Art. 173 (1993) 293.

[55] T. Altzitzoglou, J.J. Larosa, C. Nicholl, Measurement of ^{90}Sr in bone ash, Appl. Radiat. Isot. 49 (1998) 1313.

[56] K.H. Hong, Y.H. Cho, M.H. Lee, G.S. Choi, C.W. Lee, Simultaneous measurement of ^{89}Sr and ^{90}Sr in aqueous samples by liquid scintillation counting using the spectrum unfolding method, Appl. Radiat. Isot. 54 (2001) 299.

[57] A. Grau Malonda, L. Rodriguez Barquero, A. Grau Carles, Radioactivity determination of ^{90}Y, ^{90}Sr and ^{89}Sr mixtures by spectral deconvolution, Nucl. Instr. and Meth. A 339 (1994) 31.

[58] J.B. Moore, J.E. Noakes, J.D. Spaulding, Environmental monitoring of ^{14}C in milk and agricultural samples, in: J.E. Noakes, F. Schönhofer, H.A. Polach (Eds.), Liquid scintillation spectrometry 1992, Radiocarbon, Tucson, Arizona, 1993, pp. 447 – 453.

[59] John Greenwald, Deadly meltdown, Time, May 12 (1986) 11.

[60] The Chernobyl Forum: 2003–2005, Chernobyl's legacy: health, environmental and socio-economic impacts and recommendations to the governments of Belarus, the Russian Federation and Ukraine, D. Kinley III (Ed.), IAEA Division of Public Information, IAEA, Vienna, 2006, pp. 10 – 11.

[61] M.F. L'Annunziata, Agricultural biochemistry: reaction mechanisms and pathways in biosynthes, in: M.F. L'Annunziata, J.O. Legg (Eds.), Isotopes and radiation in agricultural sciences, Vol. 2 (animals, plants, food and the environment), Academic Press Inc., Orlando, Florida, 1984, pp. 151 – 162.

[62] R.J.H. Williams, G. Britton, T.W. Goodwin, The biosynthesis of cyclic carotenes, Biochem. J. 105 (1967) 99.

[63] E. Leete, D.H. Lucast, Loss of tritium during the biosynthesis of meteloidine and scopolamine from [N-methyl-^{14}C, 6β, 7β-$^{3}H_2$]tropine, Tetrahedron Lett. 38 (1976) 3401.

[64] E. Leistner, R.N. Gupta, I.D. Spenser, A general method for the determination of precursor configuration in biosynthetic precursor-product relationships. Derivation of pipecolic acid from D-lysine, and of piperidine alkaloids from L-lysine, J. Am. Chem. Soc. 95 (1973) 4040.

[65] A. Noor, M. Zakir, B. Rasyid, Maming, M.F. L'Annunziata, Cerenkov and liquid scintillation analysis of the triple label ^{86}Rb-^{35}S-^{33}P, Appl. Radiat. lsot. 47 (1996) 659.

[66] P.-O. Brandtberg, J. Bengtsson, H. Lundkvist, Distributions of the capacity to take up nutrients by *Betula* spp. and *Picea abies* in mixed stands, For. Ecol. Manage. 198 (2004) 193.

[67] M.F. L'Annunziata, M.J. Kessler, Liquid scintillation analysis: principles and practice, in: M.F. L'Annunziata (Ed.), Handbook of radioactivity analysis, second ed., Academic Press, New York, 2003, pp. 418 – 429.

[68] A. Grau Carles, M.T. Martin-Casallo, A. Grau Malonda, Spectrum unfolding and double window methods applied to standardization of ^{14}C and ^{3}H mixtures, Nucl. Instr. and Meth. A 307 (1991) 487.

[69] M.H. Lee, K.H. Chung, G.K. Choi, C.W. Lee, Measurement of ^{90}Sr in aqueous samples using liquid scintillation counting with full spectrum DPM method, Appl. Radiat. Isot. 57 (2002) 257.

[70] A. Grau Carles, A new linear spectrum unfolding method applied to radionuclide mixtures in liquid scintillation counting, Appl. Radiat. Isot. 45 (1994) 83.

[71] M.F. L'Annunziata, M.J. Kessler, Liquid scintillation analysis: principles and practice, in: M.F. L'Annunziata (Ed.), Handbook of radioactivity analysis, second ed., Academic Press, New York, 2003, pp. 370 – 372.

[72] A. Grau Carles, L. Rodriguez Barquero, A. Grau Malonda, Standardization of ^{14}C and ^{35}S mixtures, Nucl. Instr. and Meth. A 235 (1993) 234.

[73] M.F. L'Annunziata, Cherenkov counting, in: M.F. L'Annunziata (Ed.), Handbook of radioactivity analysis, second ed., Academic Press, New York, 2003, pp. 719 – 797.

[74] H. Fujii, M. Takiue, Radioassay of dual-labeled samples by sequential Cherenkov counting and liquid scintillation efficiency tracing technique, Nucl. Instr. and Meth. A 273 (1988) 377.

[75] M.F. L'Annunziata, M.J. Kessler, Liquid scintillation analysis: principles and practice, in: M.F. L'Annunziata (Ed.), Handbook of radioactivity analysis, second ed., Academic Press, New York, 2003, pp. 400 – 403.

CHAPTER 2 The TDCR and CIEMAT/NIST methods

2.1 Introduction

Pure β-emitting radionuclides are generally measured using liquid scintillation counting. Measurement of such radionuclides on uncalibrated counting systems became possible with the development of theory [1] to calculate the detection efficiency of a source in terms of a single floating parameter, the figure-of-merit, that characterises the liquid scintillation detection system. This chapter describes the underlying principles of two developments based on this theory, namely, the absolute triple-to-double coincidence ratio (TDCR) efficiency calculation technique [2,3] and the CIEMAT/NIST efficiency tracing method [4,5].

2.2 Liquid scintillation counting

For liquid scintillation counting, a source is usually prepared by mixing a radionuclide solution homogeneously with a liquid scintillation cocktail. The basic liquid scintillation process can be explained by means of Fig. 2.1 for a general cocktail consisting of a fluorescent aromatic scintillator dissolved in an aromatic solvent. With the decay of a pure β-emitter, the unstable nuclide de-excites by expelling an energetic electron from the nucleus. Most of this energy is absorbed by the abundant solvent molecules [6,7], which in turn transfer the energy to the scintillator molecules in an energy-favourable process. The excited scintillator molecules so formed rapidly de-excite through the process of fluorescence, emitting photons of light, some of which will be detected by a photomultiplier tube. The intensity of the light produced is a function of the energy and type of radioactive decay. The presence of other compounds in the source affects the amount of light available for detection at different steps of the scintillation process. Chemical quenchers interfere with the solvent-scintillator energy transfer, while coloured compounds may absorb some of the emitted light, thus reducing the amount of light reaching the phototube.

Fig. 2.2 gives a schematic diagram of the detection of a liquid scintillation source by a photomultiplier tube. Some of the photons formed in the scintillator interact with the

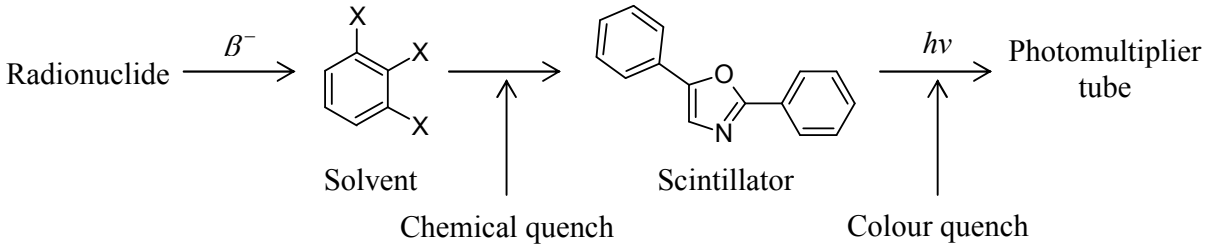

Fig. 2.1 The basic liquid scintillation process [6].

photocathode and cause the emission of photoelectrons. These electrons are accelerated by the potential applied between the electrodes of the phototube and multiplied linearly through interaction with a series of dynodes. The electrical pulses from the anode of the photomultiplier are amplified and processed by electronic circuits. The whole detection and amplification process is such that the output pulse is proportional to the original number of photons [9,10].

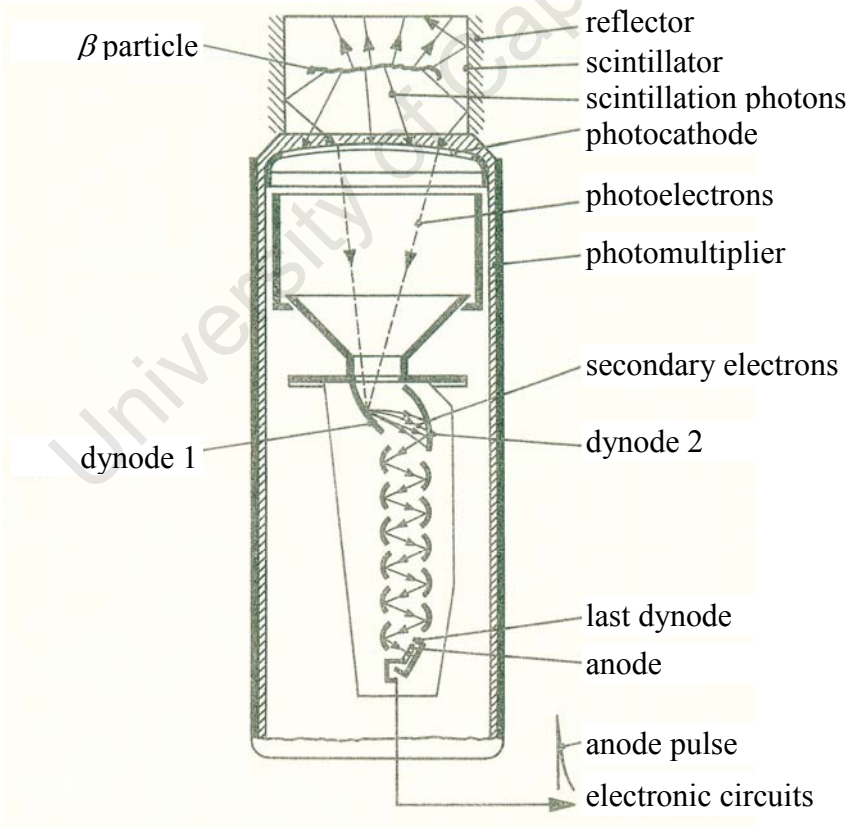

Fig. 2.2 The detection of particles emitted within a liquid scintillation source by a photomultiplier tube [8].

2.3 The calculation of detection efficiency

2.3.1 Single phototube detection efficiency of a mono-energetic electron

To calculate the efficiency of a phototube, the detection of the interaction of an electron with a liquid scintillator is viewed as a combination of random processes, detailed later. The resulting photon statistics can be described [11,12] by means of the binomial distribution and, under certain conditions, by the Poisson distribution, both of which are reviewed in Appendix A. The random process under study is viewed as a number of repeated, independent Bernoulli (or binary) trials. This implies that each trial has only two possible outcomes, generally referred to as success and failure [13]. In addition, the probability of success for each trial is the same and the outcome of one trial is not affected by the outcomes of previous trials.

The notation used to derive an expression for the detection efficiency is shown schematically in Fig. 2.3. In Stage 1, the interaction of a mono-energetic electron of energy E with a liquid scintillation source gives rise to the formation of, on average, N primary photons [11]. If the source is viewed by a single phototube, m of the N photons will reach the phototube and interact with the photocathode. The distribution of m is determined by the light collection efficiency of the scintillator, ξ. In Stage 2 of the detection, the interaction of m photons gives rise to the formation of l photoelectrons that impinge on the first dynode of the phototube and are detected. The overall efficiency of the phototube, ε_p, describes the probability of formation and detection of photoelectrons.

Starting with Stage 2, the probability that the interaction of m photons causes the emission and detection of l photoelectrons in a phototube with overall efficiency ε_p can be described by the binomial distribution [11] *

$$b\left(l,m,\varepsilon_p\right)=\frac{m!}{l!\left(m-l\right)!}\varepsilon_p^{l}\left(1-\varepsilon_p\right)^{m-l},\ l=0,1,2,\ldots m. \tag{2.1}$$

* The binomial distribution [14]

$$b\left(x,n,p\right)=\frac{n!}{x!\left(n-x\right)!}p^{x}\left(1-p\right)^{n-x},\ x=0,1,2,\ldots n$$

is widely applicable to all processes with a constant success probability. It computes the probability $b\left(x,n,p\right)$ of getting exactly x successes in n independent Bernoulli trials, where each trial has an individual success probability of p. The mean of the distribution $\bar{x}=np$ and the variance $\sigma^2=np\left(1-p\right)$.

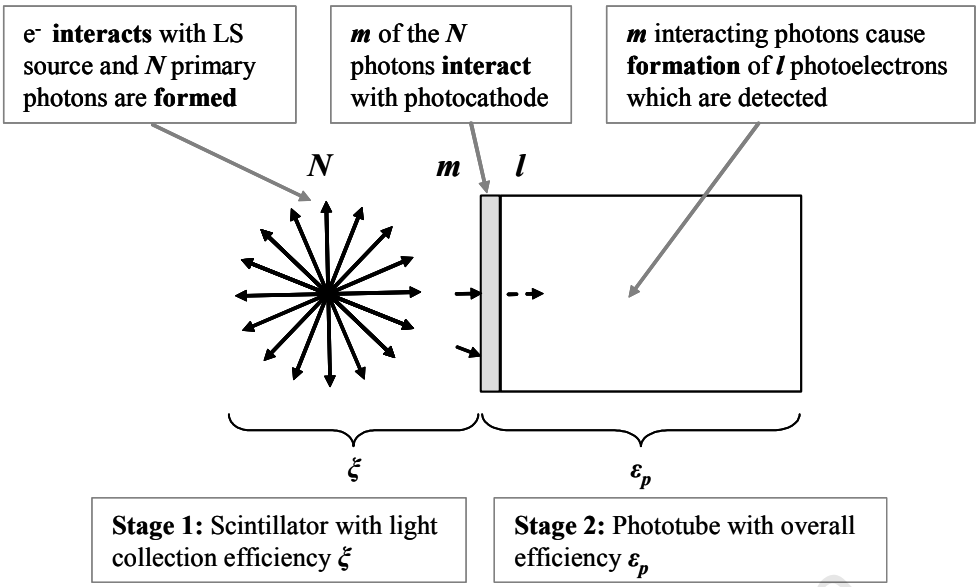

Fig. 2.3 Schematic diagram showing the photons formed by the interaction of a mono-energetic electron with a liquid scintillator (LS) and detection by a single phototube.

In terms of the formal definition of the binomial law [14], l is the number of successes in m repeated, independent trials, ε_p is the success probability for the process, and the probability of counting exactly l successes is given by the distribution $b(l,m,\varepsilon_p)$. The phototube efficiency is made up of a number of components such that $\varepsilon_p = \mu\varepsilon_q\delta$, with μ the spectral matching factor of the emission spectrum of the scintillator and the absorption spectrum of the photocathode, ε_q the quantum efficiency of the photocathode and δ the photoelectron collection efficiency at the first dynode.

Using Eq. (2.1), the probability to detect no photoelectron when m photons interact with the photocathode (zero detection probability) is

$$b(0,m,\varepsilon_p) = (1-\varepsilon_p)^m \tag{2.2}$$

and the complement of the zero detection probability

$$\varepsilon_s(m) = 1 - b(0,m,\varepsilon_p) = 1-(1-\varepsilon_p)^m \tag{2.3}$$

gives the probability to detect at least one photoelectron.

Returning to Stage 1 of the process, the number of photons m reaching the photocathode out of N primary photons formed can similarly be described by the binomial distribution

$$b(m,N,\xi)=\frac{N!}{m!(N-m)!}\xi^{m}(1-\xi)^{N-m},\ m=0,1,2,\ldots N, \tag{2.4}$$

where ξ is the light collection efficiency of the scintillator and ξN gives the expected number of photons reaching the photocathode. As is described in Appendix A.2, the binomial distribution given in (2.4) can be approximated by a Poissonian one [11] *

$$P(m,\xi N)=\frac{(\xi N)^{m}\exp(-\xi N)}{m!},\ m=0,1,2,\ldots N \tag{2.5}$$

if the individual success probability ξ is low and the number of trials N high enough so that the mean number of successes ξN is large and constant. These conditions are usually satisfied in the measurement of radioactivity. For short-lived radionuclides the counting time must be short compared to the half-life to ensure that N remains constant during the experiment [12]. In the above approximation, the mathematics is simplified because the distribution is a function of ξN and not of ξ and N individually.

Under conditions where the Poisson approximation is valid, the distributions given by Eqs. (2.3) and (2.5) can be combined and simplified with the aid of power series [11] so that the single phototube detection probability (efficiency) is given by the Poisson probability to detect at least one photoelectron for N primary photons formed:

$$\varepsilon_s = 1-P(0,\varepsilon_0 N)=1-\exp(-\varepsilon_0 N). \tag{2.6}$$

Here $\varepsilon_0=\xi\varepsilon_p=\xi\mu\varepsilon_q\delta$ is the overall optical efficiency of the scintillator/phototube system and $\varepsilon_0 N$ gives the total number of photoelectrons expected to arrive at the first dynode of the phototube.

* The binomial distribution becomes computationally cumbersome when the number of trials is very large. If, in addition to n being very large, p is close to zero so that np is finite and constant [12,15], the Poisson distribution [14]

$$P(x,np)=\frac{(np)^{x}\exp(-np)}{x!},\ x=0,1,2,\ldots n$$

is a convenient but accurate approximation of the binomial distribution. It computes the probability $P(x,np)$ of getting exactly x successes when the average number of successes is np. The mean of the distribution $\bar{x}$ equals the variance, i.e., $\bar{x}=\sigma^2=np$.

2.3.2 Single phototube detection efficiency for a β-emitting radionuclide

The number of primary photons formed in response to the interaction of an electron with a liquid scintillator varies non-linearly according to the electron energy and can be described by [11]

$$N = \frac{LF(E)E}{h\nu} = \frac{LQ(E)W(E)E}{h\nu}. \tag{2.7}$$

$LF(E)$ gives the scintillation yield, i.e., the fraction of the electron energy which is transformed to light energy, with $h\nu$ the average energy of the emitted photons. L is the energy conversion factor and $F(E)$ the relative scintillation efficiency. The latter is the product of the ionisation quenching function $Q(E)$ and the function $W(E)$ that accounts for the wall effect.

Ionisation quenching plays a significant role at low energies. Because a low energy electron will transfer its energy to the scintillation cocktail over a short distance (dE/dx large), the excited solvent molecules are in close proximity to each other. This increases the probability of interaction between the excited molecules and less energy is transferred to the fluorescent scintillator molecules [16]. This reduction in energy can be calculated by numerical integration of the semi-empirical Birks formula [1,17]

$$Q(E) = \frac{1}{E}\int_0^E \frac{dE}{1 + kB(dE/dx)}, \tag{2.8}$$

where k is the rate constant for ionisation quenching and $B(dE/dx)$ is the specific ionisation density. The two constants are combined to form the kB-value, which is determined for the specific scintillator. In practice, once the computation of $Q(E)$ is complete, the values are fitted with a rational function and this function is substituted for $Q(E)$ in further calculations.

The wall-effect, which describes the escape of high energy electrons from the scintillator before the full energy transfer has occurred, can be ignored for the calculation of the detection efficiency, provided that quenching is not severe for higher energies [18]. Eq. (2.7) can then be replaced by

$$N = \frac{LQ(E)E}{h\nu}. \tag{2.9}$$

The detection efficiency for a pure β-emitter with continuous energy spectrum from 0 to a maximum of E_m is obtained by substituting Eq. (2.9) into (2.6) and integrating this function weighted by the normalised β spectrum, $S(E)$, over the β energy range [4,19]

$$\varepsilon_s = \int_0^{E_m} S(E)\left[1-\exp\left\{\frac{-\varepsilon_0 LQ(E)E}{h\nu}\right\}\right]dE\,. \tag{2.10}$$

$S(E)$ is calculated from the Fermi theory of β decay. The energy independent components can be combined into a single parameter P such that

$$\varepsilon_s = \int_0^{E_m} S(E)\left[1-\exp\{-PQ(E)E\}\right]dE\,, \tag{2.11}$$

where $P=\varepsilon_0 L/h\nu$ is the figure-of-merit of the system. This is consistent with the formulation of Gibson [1], who defined P as the number of electrons at the first dynode of the phototube per keV deposited in the liquid scintillator. Quenching attenuates the energy transfer process such that $P=gP_0$ where P_0 is the figure-of-merit for the unquenched system and g is the energy-independent relative quenching factor [1]. It is important to note that to calculate the detection efficiency for a given quench state, it is not necessary to explicitly know ξ, ε_p, μ, ε_q, δ, ε_0, $h\nu$, P_0 nor g. Simply determining the free parameter P, a combination of these unknown quantities, is sufficient.

2.3.3 Double- and triple-phototube detection efficiency for a β-emitting radionuclide

Liquid scintillation detectors are generally designed to make use of two or three phototubes in coincidence to reduce the effect of thermionic noise and afterpulsing. For a system in which the phototubes are efficiency-matched, the detection efficiency formulae are [3]

$$\varepsilon_d = \int_0^{E_m} S(E)\left[1-\exp\{-PQ(E)E\}\right]^2 dE \tag{2.12}$$

for two phototubes in coincidence,

$$\varepsilon_t = \int_0^{E_m} S(E)\left[1-\exp\{-PQ(E)E\}\right]^3 dE \tag{2.13}$$

for three phototubes in coincidence, and [20]

$$\varepsilon_D = \int_0^{E_m} S(E)\left(3\left[1-\exp\{-PQ(E)E\}\right]^2 - 2\left[1-\exp\{-PQ(E)E\}\right]^3\right)dE \tag{2.14}$$

for the logical sum of the double coincidences. P denotes the figure-of-merit of a single phototube such that $P=\varepsilon_0 L/2h\nu$ for each phototube in a matched two-phototube detection

system and similarly $P = \varepsilon_0 L/3hv$ for a three-phototube system. Here ε_0, the overall optical efficiency of the complete detection system, is given by the sum of each phototube's optical efficiency, with each tube viewing a fraction of the *N* primary photons formed. At a first glance it appears as if *P* is different for one-, two- and three-phototube systems. If, for a matched system, it is assumed that an equal number of photons are incident on each photocathode (ξ the same for each phototube) and the photoelectric efficiency (ε_p) of each phototube is the same, then $\varepsilon_0 = 2\xi\varepsilon_p$ for a two-phototube system and $\varepsilon_0 = 3\xi\varepsilon_p$ for a three-phototube detector and thus the value of *P* is the same for each phototube of a two- or three-phototube system. This is explained in more detail in Appendix B.

It is important to note that in Refs. [4] and [19], the figure-of-merit *M* is defined as the ratio of the energy deposited in the liquid scintillator and the average number of photoelectrons emitted by all photocathodes in the system. Thus, $M = hv/\varepsilon_0 L$, and this formula is applicable to one-, two- or three-phototube detection systems. *M* is the inverse of *P* and, because it considers the whole detection system rather than a single phototube,

$$M = hv/\varepsilon_0 L = hv/2\xi\varepsilon_p L = 1/2P \tag{2.15}$$

for a matched two-phototube system and

$$M = hv/\varepsilon_0 L = hv/3\xi\varepsilon_p L = 1/3P \tag{2.16}$$

for a matched three-phototube system.

2.4 The TDCR technique

In the triple-to-double coincidence ratio (TDCR) efficiency calculation technique, the ratio between the triple- and double-coincidence count rates is used to fix the figure-of-merit, from which the detection efficiencies and ultimately the activity of a source can be calculated. A matched three-phototube detection system is generally required. The photoelectric efficiencies ε_{pi} of the phototubes are likely to be different and matching is achieved by moving the source relative to the phototubes to alter the light collection efficiencies ξ_i so that the products $\xi_i\varepsilon_{pi}$ are equal.

The double- and triple-coincidence count rates N_d and N_t of a source consisting of a pure β-emitting radionuclide dissolved in liquid scintillator are recorded simultaneously. For the

given quench state [3]

$$N_d = N_0 \varepsilon_d \text{ and } N_t = N_0 \varepsilon_t , \tag{2.17}$$

where N_0 is the disintegration rate of the source and ε_d and ε_t are the actual double- and triple-coincidence detection efficiencies. An accurate determination of the efficiency values is obtained by combining the experimental measurement with theory in the following manner. The ratio of the two efficiencies equals the ratio R of the measured count rates,

$$\frac{\varepsilon_t}{\varepsilon_d} = \frac{N_t}{N_d} = R , \tag{2.18}$$

and the efficiencies can be expressed theoretically as functions of a single floating parameter, the figure-of-merit P, as shown in Eqs. (2.12) and (2.13). Eq. (2.18) can thus be re-written as

$$\frac{\varepsilon_t(P)}{\varepsilon_d(P)} = R \tag{2.19}$$

and the unique value of P that solves the equation determined iteratively. Once P is known for the specific value of R measured, the efficiency estimates follow directly and the measured source activity is given by

$$N_0 = \frac{N_d}{\varepsilon_d(P)} = \frac{N_t}{\varepsilon_t(P)} . \tag{2.20}$$

An example is shown in Fig. 2.4, where the theoretically calculated ε_d, ε_t and TDCR values are given as functions of P for ^{63}Ni, demonstrating the monotonic relationship that makes the technique feasible [3]. Similarly shaped curves are found for all pure β-emitters.

An important aspect of the TDCR technique is the ability to take account directly of chemical quenching [21]. This is because any change in efficiency due to such quenching will manifest itself in the measured triple and double count rates and result in a new value for R. The figure-of-merit extracted will thus automatically compensate for effects due to chemical quenching and the method derives the activity directly irrespective of the source quench state. From this point of view the technique is absolute, requiring neither quench correction curves nor calibration standards.

An alternative implementation of the TDCR technique [20] accounts for asymmetry in the detection system [22]. In this approach, in a three-phototube detection system, the single-phototube detection efficiency is defined as

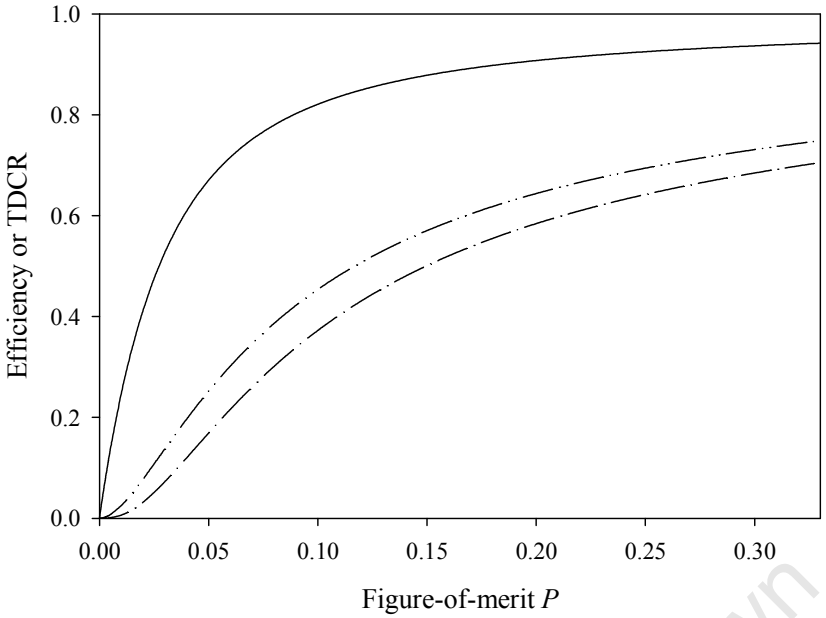

Fig. 2.4 Curves of ε_d (dash-dot-dot), ε_t (dash-dot) and $\varepsilon_t/\varepsilon_d$ (solid) vs. P for ^{63}Ni.

$$\varepsilon_s = \int_0^{E_m} S(E)\left[1-\exp(-\omega N/3)\right]dE\,, \tag{2.21}$$

where

$$N = \int_0^{E} \frac{A\,dE}{1+kB(dE/dx)} \tag{2.22}$$

is the mean number of photons produced in the liquid scintillator, taking into account the scintillator non-linearity, and ω is the quantum efficiency of the phototube. The floating parameter solved to determine the efficiency of a system is ωA, with A defined as the figure-of-merit expressing the number of photons emitted per unit energy released in the scintillator.* The double-coincidence detection efficiency for each pair of phototubes $[AB, BC, AC]$ is given by

$$\varepsilon_{dXY} = \int_0^{E_m} S(E)\left[1-\exp(-\omega_X N/3)\right]\left[1-\exp(-\omega_Y N/3)\right]dE\,,\ XY = AB, BC, AC \tag{2.23}$$

and the triple-coincidence detection efficiency by

$$\varepsilon_t = \int_0^{E_m} S(E)\left[1-\exp(-\omega_A N/3)\right]\left[1-\exp(-\omega_B N/3)\right]\left[1-\exp(-\omega_C N/3)\right]dE\,. \tag{2.24}$$

* At a first glance the expressions given in Refs. [20] and [22] appear to differ from those given earlier in this thesis. However, substitution of Eqs. (2.8) and (2.22) into Eq. (2.21) and comparison with Eq. (2.11) makes it clear that the expressions are equivalent, with $P=\omega A/3$. This agrees with the definitions given for the figures-of-merit where P describes the number of electrons at the first dynode of a single phototube, and A describes the total number of photons emitted from the scintillator, both per keV deposited in the scintillator.

The experimental double- and triple-coincidence count rates N_{dAB}, N_{dBC}, N_{dAC} and N_t are recorded simultaneously. Values for the set of free parameters ω_A, ω_B, ω_C and A used in the calculation of the efficiencies ε_{dAB}, ε_{dBC}, ε_{dAC} and ε_t are found for which the expression

$$\left(\frac{\varepsilon_t}{\varepsilon_{dAB}}-\frac{N_t}{N_{dAB}}\right)^2+\left(\frac{\varepsilon_t}{\varepsilon_{dBC}}-\frac{N_t}{N_{dBC}}\right)^2+\left(\frac{\varepsilon_t}{\varepsilon_{dAC}}-\frac{N_t}{N_{dAC}}\right)^2 \tag{2.25}$$

is minimised. From these efficiencies, the source activity N_0 can be extracted by dividing the measured coincidence count rates with the corresponding efficiencies, i.e.

$$N_0 \cong \frac{N_{dAB}}{\varepsilon_{dAB}} \cong \frac{N_{dBC}}{\varepsilon_{dBC}} \cong \frac{N_{dAC}}{\varepsilon_{dAC}} \cong \frac{N_t}{\varepsilon_t}. \tag{2.26}$$

2.5 The CIEMAT/NIST method

The CIEMAT/NIST efficiency tracing method grew from a model developed to make it possible to measure any radionuclide in any scintillation cocktail and with any liquid scintillation analyser [23]. The method makes use of measurements of a reference radionuclide and compares the experimental detection efficiency with the theoretical one to fix the figure-of-merit of the detection system. The detection efficiencies for different radionuclides can be calculated from this figure-of-merit [5].

^{3}H is generally used as the tracer for the measurement of other pure β-emitters. This radionuclide was selected as the tracer of choice because organic solution standards with well-characterised activities are available and for its low β-decay energy. The deduced efficiencies of higher energy emitters are less sensitive to the specific value used for the figure-of-merit and the propagated uncertainties become smaller [4].

The basic method is described with reference to Fig. 2.5 for a two-phototube liquid scintillation analyser used to measure ^{14}C with ^{3}H as the tracer [4,24]. Starting with ^{3}H, the double-coincidence count rate N_d and the quench indication parameter QP^* are measured for a

* Most automatic liquid scintillation analysers have a built-in facility to measure the efficiency of the source/detector combination in terms of a quench indicating parameter QP. An external γ-ray source is moved into close proximity of the scintillation source and the resultant Compton spectrum used to determine the QP index [25]. Beforehand, the scintillation source is measured with the γ-ray source moved away and well shielded. Various approaches, making use of different γ-emitters, have been developed to transform the measured Compton spectrum to a QP index.

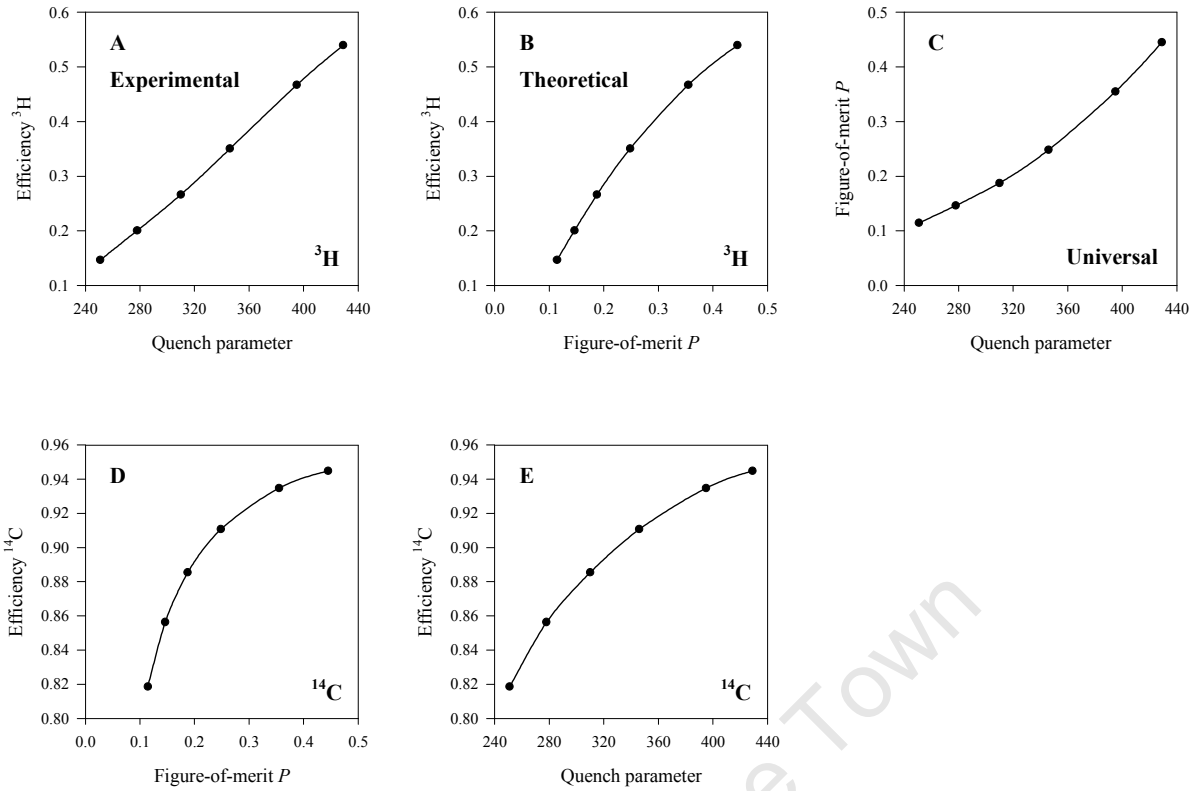

Fig. 2.5 Calibration of a liquid scintillation analyser for ^{14}C using ^{3}H standard sources [24].

set of differently quenched standard sources. For each quench state, the double-coincidence efficiency $\varepsilon_d = N_d / N_0$ is experimentally determined, with N_0 being the known source activity, and a curve of ε_d vs. QP generated (Fig. 2.5A). For each ε_d value the corresponding figure-of-merit P can be calculated from Eq. (2.12), from which the relationship between ε_d and P for ^{3}H can be determined (curve of ε_d vs. P in Fig. 2.5B). These two curves are combined to give the relationship between P and QP (Fig. 2.5C), which is universally applicable to any radionuclide measured in the same detection system with the same scintillator. The curve of efficiency vs. QP for any radionuclide of interest (e.g. ^{14}C in Fig. 2.5E) can then be obtained from the ε_d vs. P curve calculated from Eq. (2.12) for the specific radionuclide (Fig. 2.5D) and the universal curve (Fig. 2.5C). The activity of a source is obtained by measuring the quench indicating parameter and the double-coincidence count rate and dividing N_d by ε_d obtained from Fig. 2.5E for the specific quench state.

2.6 References

[1] J.A.B. Gibson, H.J. Gale, Absolute standardization with liquid scintillation counters, J. Phys. E. 1, ser. 2 (1968) 99.

[2] B.R.S. Simpson, B.R. Meyer, Direct determination of the activity of non-gamma-emitting radionuclides by the TDCR efficiency calculation technique: a review of the present status, NAC Report NAC/92-02 (1992).

[3] B.R.S. Simpson, B.R. Meyer, Direct activity measurement of pure beta-emitting radionuclides by the TDCR efficiency calculation technique, Nucl. Instr. and Meth. A 339 (1994) 14.

[4] A. Grau Malonda, E. Garcia-Toraño, Evaluation of counting efficiency in liquid scintillation counting by pure β-ray emitters, Int. J. Appl. Radiat. Isot. 33 (1982) 249.

[5] B.M. Coursey, A. Grau Malonda, E. Garcia-Toraño, J.M. Los Arcos, The standardization of pure-beta-particle-emitting radionuclides, Trans. Amer. Nucl. Soc. 50 (1985) 13.

[6] M.F. L'Annunziata, M.J. Kessler, Liquid scintillation analysis: principles and practice, in: M.F. L'Annunziata (Ed.), Handbook of radioactivity analysis, second ed., Academic Press, New York, 2003, pp. 347 – 352.

[7] J.B. Birks, The theory and practice of scintillation counting, Pergamon Press, Oxford, 1965, pp. 39 – 67.

[8] J.B. Birks, An introduction to liquid scintillation counting, Koch-Light Laboratories Ltd., pp. 4 – 5.

[9] J.B. Birks, The theory and practice of scintillation counting, Pergamon Press, Oxford, 1965, pp. 11 – 12.

[10] G.F. Knoll, Radiation detection and measurement, third ed., John Wiley & Sons, Inc., New York, 2000, pp. 265 – 266.

[11] R. Broda, K. Pochwalski, T. Radoszewski, Calculation of liquid-scintillation detector efficiency, Appl. Radiat. Isot. 39 (1988) 159.

[12] I. Salma, É. Zemplén-Papp, Experimental investigation of statistical models describing distribution of counts, Nucl. Instr. and Meth. A 312 (1992) 591.

[13] H.J. Larson, Introduction to probability theory and statistical inference, John Wiley & Sons, Inc., New York, 1969, pp. 106 – 129.

[14] G.F. Knoll, Radiation detection and measurement, third ed., John Wiley & Sons, Inc., New York, 2000, pp. 70 –75.

[15] J. Foster, K. Kouris, I.P. Matthews, N.M. Spyrou, Binomial vs Poisson statistics in radiation studies, Nucl. Instr. and Meth. 212 (1983) 301.

[16] Grau Carles [sic], E. Gunther, G. García, A. Grau Malonda, Ionization quenching in LSC, Appl. Radiat. Isot. 60 (2004) 447.

[17] J.B. Birks, The theory and practice of scintillation counting, Pergamon Press, Oxford, 1965, pp. 185 – 192.

[18] P. Cassette, Evaluation of the influence of wall effects on the liquid scintillation counting detection efficiency for the standardisation of high-energy beta and alpha radionuclides, Proc. LSC2001, Advances in liquid scintillation spectrometry, Radiocarbon (2002) 45.

[19] A. Grau Malonda, B.M. Coursey, Calculation of beta-particle counting efficiency for liquid-scintillation systems with three phototubes, Appl. Radiat. Isot. 39 (1988) 1191.

[20] P. Cassette, M.M. Bé, F. Jaubert, M.C. Lépy, Measurement of a ^{103}Pd solution using the TDCR method by LSC, Appl. Radiat. Isot. 60 (2004) 439.

[21] B.R.S. Simpson, B.R. Meyer, Further investigations of the TDCR efficiency calculation technique for the direct determination of activity, Nucl. Instr. and Meth. A 312 (1992) 90.

[22] P. Arenillas, P. Cassette, Implementation of the TDCR liquid scintillation method at CNEA-LMR, Argentina, Appl. Radiat. Isot. 64 (2006) 1500.

[23] A. Grau Malonda, Free parameter models in liquid scintillation counting, Editorial Ciemat, Madrid, 1999, pp. 7 – 11.

[24] A. Grau Malonda, Free parameter models in liquid scintillation counting, Editorial Ciemat, Madrid, 1999, pp. 112 – 114.

[25] M.F. L'Annunziata, M.J. Kessler, Liquid scintillation analysis: principles and practice, in: M.F. L'Annunziata (Ed.), Handbook of radioactivity analysis, second ed., Academic Press, New York, 2003, pp. 360 – 388.

CHAPTER 3 The basic principles and a simulation of the method

3.1 Introduction

This chapter describes the simple liquid scintillation counting technique that was developed to measure mixtures of two pure β-emitting radionuclides [1]. To reiterate, the method is based on elements of two techniques that are widely used to measure single radionuclide solutions, namely the triple-to-double coincidence ratio (TDCR) efficiency calculation technique and the CIEMAT/NIST efficiency tracing method. As described earlier, the TDCR technique makes use of the measured triple-to-double coincidence ratio to extract the figure-of-merit of a counting system, from which the detection efficiency and activity of a source can be calculated. When measuring a source of unknown mixture composition, this added parameter makes the TDCR approach unfeasible. An external tracer standard provides the additional information required to determine the figure-of-merit, as is done in the CIEMAT/NIST method. This, together with the measured source triple- and double-coincidence count rates, allows the individual radionuclide activities to be extracted.

3.2 The basic method

To determine the activity of each radionuclide in a source containing a mixture of two known pure β-emitting radionuclides, the source is viewed by a matched three-phototube detection system and both the double-coincidence count rate, N_d, and the triple-coincidence rate, N_t, are recorded simultaneously. If the activities of the radionuclides in the mixture are given by N_0 and N_0' respectively, then

$$N_d = N_0\varepsilon_d + N_0'\varepsilon_d' \tag{3.1}$$

and

$$N_t = N_0\varepsilon_t + N_0'\varepsilon_t', \tag{3.2}$$

where $\varepsilon_d, \varepsilon_d', \varepsilon_t$ and ε_t' are the double- and triple-coincidence detection efficiencies for the respective radionuclides. These efficiencies can be expressed theoretically in terms of the figure-of-merit, P, that characterises the liquid scintillation counting system, as was described

in Section 2.3. P is obtained from a pure β-emitting tracer standard of similar quench to the prepared source, as is done in the CIEMAT/NIST method reviewed in Section 2.5. The required radionuclide activities can be calculated from the determined efficiencies and measured count rates in various ways, the most obvious being to solve Eqs. (3.1) and (3.2) simultaneously for N_0, and similarly for N_0', to give

$$N_0 = \frac{N_t\varepsilon_d' - N_d\varepsilon_t'}{\varepsilon_t\varepsilon_d' - \varepsilon_d\varepsilon_t'} \tag{3.3}$$

and

$$N_0' = \frac{N_d\varepsilon_t - N_t\varepsilon_d}{\varepsilon_t\varepsilon_d' - \varepsilon_d\varepsilon_t'}. \tag{3.4}$$

3.3 An alternative approach providing insight

An alternative approach to solving for N_0 and N_0' provides insight into the method. Eqs. (3.1) and (3.2) are divided by the sum of the activities, $N_S = N_0 + N_0'$, such that

$$N_d/N_S = r\varepsilon_d + (1-r)\varepsilon_d' \tag{3.5}$$

and

$$N_t/N_S = r\varepsilon_t + (1-r)\varepsilon_t', \tag{3.6}$$

where

$$r = N_0/N_S \text{ and } (1-r) = N_0'/N_S\,. \tag{3.7}$$

Taking the ratio of Eqs. (3.5) and (3.6) eliminates the unknown quantity N_S and gives the TDCR indicator

$$\frac{N_t}{N_d} = \frac{r\varepsilon_t + (1-r)\varepsilon_t'}{r\varepsilon_d + (1-r)\varepsilon_d'}, \tag{3.8}$$

which is effectively the weighted triple-coincidence efficiency divided by the weighted double-coincidence efficiency. It is of interest to note that the intuitive assumption that the TDCR indicator is simply the weighted sum of each radionuclide's individual TDCR value is not correct, i.e. $\frac{N_t}{N_d} \neq r\frac{\varepsilon_t}{\varepsilon_d} + (1-r)\frac{\varepsilon_t'}{\varepsilon_d'}$.

The concept of the method is demonstrated in Fig. 3.1. The curves were generated by theoretically calculating the double- and triple-coincidence detection efficiencies of ^{14}C and

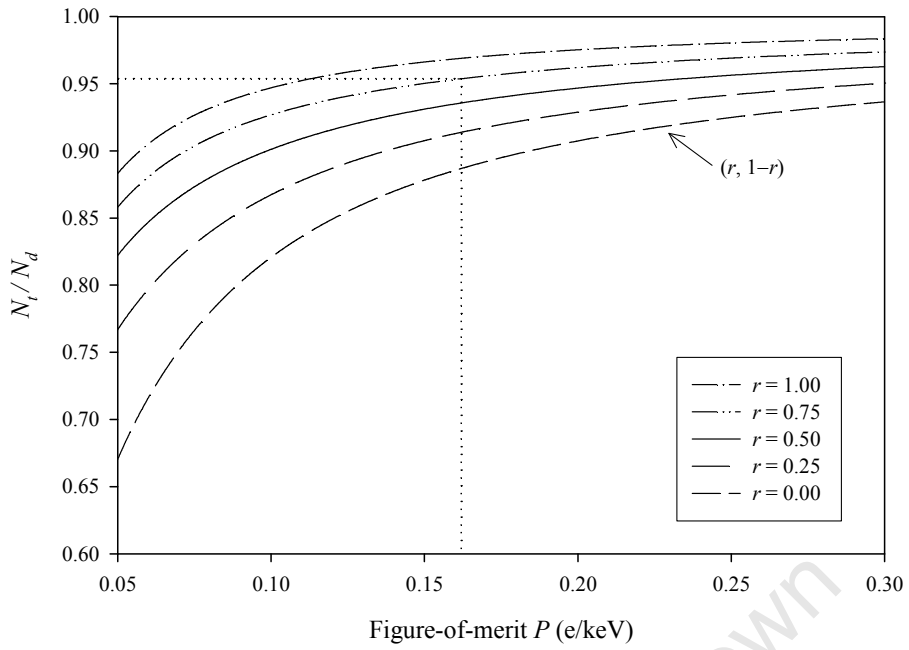

Fig. 3.1 Curves demonstrating the relationship between N_t/N_d and P for various mixtures of ^{14}C and ^{63}Ni are shown. The fraction of ^{14}C in each mixture is indicated by r and the ^{63}Ni fraction by $(1 - r)$. The shapes of the curves will generally be similar for any combination of two pure β-emitting radionuclides.
The dotted lines give an example illustrating the application of the method in practice. If it is assumed that N_t/N_d was measured to be 0.954 and P determined as 0.162 e/keV using an external standard, the intercept of the lines indicates that the measured sample comprised a fractional composition of ^{14}C ($r = 0.75$) and ^{63}Ni ($1 - r = 0.25$). The activities of each component can then be obtained from r as explained in the text.

^{63}Ni for various figures-of-merit from 0.05 to 0.3 e/keV and, for each value of P, calculating the corresponding N_t/N_d values from Eq. (3.8). Curves were generated for five different mixture compositions, but in reality a continuum of lines is possible as the activity fraction, r, varies from 1 to 0. Measuring a mixed source then entails determining N_t/N_d and P experimentally and the curve corresponding to the intersection of the two values indicates the fractional composition. Once r is known, the required activities, N_0 and N_0', can be easily obtained.

N_0 and N_0' are obtained mathematically by rearranging Eq. (3.8) to solve for r such that

$$r = \frac{\varepsilon_t' - (N_t/N_d)\varepsilon_d'}{(N_t/N_d)(\varepsilon_d - \varepsilon_d') - (\varepsilon_t - \varepsilon_t')} \tag{3.9}$$

and inserting the experimentally determined N_t/N_d values and efficiencies. Inserting the value calculated for r into Eq. (3.5) or (3.6) allows the determination of the total source activity, N_S. Thereafter, the respective radionuclide activities are calculated from Eq. (3.7). The results obtained when analysing data with the more lengthy conceptual approach are identical to those given by the direct calculation.

3.4 Counting statistics simulation

A simulation was performed to gauge the effect of counting statistics on the method's ability to extract a mixture composition under typical counting conditions and to validate derived uncertainty formulae based on counting statistics.

3.4.1 The simulation and effect of counting statistics

Eleven hypothetical sources containing ^{14}C and/or ^{63}Ni were considered for the simulation. To replicate usual counting conditions, each source was assigned a total activity, N_S, of 2 000 Bq. The ^{14}C content decreased in steps of 200 Bq, from N_0 = 2 000 Bq in source 1 to 0 Bq in source 11, with the remainder of the activity, N_0', made up by ^{63}Ni. The simulation mimicked the counting of an actual source by a matched three-phototube detection system, where three separate double-coincidence counts, D_1, D_2 and D_3, and a single triple-coincidence count, T, are collected simultaneously in a time interval t. Each double count is made up of the triple count and a portion exclusive to the double count, X_1, X_2 and X_3, such that

$$D_i = X_i + T \text{, for } i = 1 \text{ to } 3 . \tag{3.10}$$

The average of the three double-coincidence counts, D, was used for data analysis.

The double- and triple-coincidence detection efficiencies for the respective radionuclides were calculated using a locally modified version of the computer program EFFY 2 [2], imposing that measurements with a similarly quenched tracer standard had given the figure-of-merit of the system to be 0.1621 e/keV. The efficiencies calculated were, for ^{14}C (ε_d = 0.8678, ε_t = 0.8409) and ^{63}Ni (ε_d' = 0.5910, ε_t' = 0.5242), in units of $s^{-1}Bq^{-1}$.

Exact double-, triple- and exclusive double-coincidence counts (free of statistical variation), D_0, T_0 and X_0, were calculated for each source for a typical counting time of t = 300 seconds, assuming that all three double-coincidence counts were the same:

$$D_0 = N_0\varepsilon_d t + N_0'\varepsilon_d' t\,, \tag{3.11}$$

$$T_0 = N_0\varepsilon_t t + N_0'\varepsilon_t' t\,, \tag{3.12}$$

$$X_0 = D_0 - T_0\,. \tag{3.13}$$

The values determined for a 50:50 activity mixture are given in Table 3.1 (a).

To simulate experimental double- and triple-coincidence counts, D and T, each independent component was varied separately according to square root statistics:*

$$T = T_0 + f\sqrt{T_0}\,, \tag{3.14}$$

$$X_i = X_0 + g_i\sqrt{X_0} \quad \text{for } i = 1 \text{ to } 3\,, \tag{3.15}$$

$$D = T + \tfrac{1}{3}\sum_{i=1}^{3} X_i\,, \tag{3.16}$$

with f and g_i being numbers, essentially between –3 and +3, randomly selected from a Gaussian (or normal) distribution. Square root statistics, where the standard deviation of the number of counts, σ, is given by the square root of the counts, are applicable since the measurement of radioactivity here follows Poisson statistics [3]. This is elaborated on in Appendix A.2.

For each hypothetical source, double-, triple- and exclusive double-coincidence counts, D, T and X_i, were simulated for six separate measurements. A computer program based on the random number generator routines given in the International Mathematical and Statistical Library [4] was used to generate 264 normally distributed numbers for f and g_i. A histogram of the numbers used is given in Fig. 3.2 and the data simulated for one of the sources in Table 3.1 (b).

* The approach used in Ref. [1] allows for some mismatch over and above counting statistics with $D = T_0 + f\sqrt{T_0} + \frac{1}{3}\sum_{i=1}^{3}\left(X_i + g_i\sqrt{X_i}\right)$. For the perfectly matched system described in this thesis, all $X_i = X_0$.

Table 3.1 The simulated counting data for hypothetical source six (a 50:50 activity mixture) with assigned activities N_0 and N_0' are given firstly without and then with statistical variation. The exact double-, triple- and exclusive double-coincidence counts, D_0, T_0 and X_0, were calculated from Eqs. (3.11), (3.12) and (3.13) and the simulated counts, T, X_i and D, from Eqs. (3.14), (3.15) and (3.16) respectively. Values for f and g_i, i = 1 to 3, were extracted from a generated series of normally distributed numbers with $\sigma = 1$. The activities extracted by the method, N_0^* and $N_0'^*$, were calculated from Eqs. (3.3) and (3.4) after converting the counts to rates. N_S^* gives the sum of the extracted activities.

(a)

No statistical variation	f	g_1	g_2	g_3	D_0	X_0	X_0	X_0	T_0	N_0 (Bq)	N_0' (Bq)	N_S (Bq)
Deduced values	-	-	-	-	437 650	28 117	28 117	28 117	409 533	1 000.00	1 000.00	2 000.00

(b)

With statistical variation	f	g_1	g_2	g_3	D	X_1	X_2	X_3	T	N_0^* (Bq)	$N_0'^*$ (Bq)	N_S^* (Bq)
Simulation 1	– 0.16663	– 0.95346	– 1.40083	– 1.19186	437 345	27 957	27 882	27 917	409 426	1 007.67	987.02	1 994.69
Simulation 2	0.62502	– 1.66668	3.16664	2.11780	438 252	27 837	28 648	28 472	409 933	993.72	1 012.62	2 006.34
Simulation 3	1.17104	– 0.82885	– 1.18903	0.44271	438 311	27 978	27 917	28 191	410 282	1 007.63	992.53	2 000.16
Simulation 4	– 2.22213	– 0.05845	0.10546	– 0.56955	436 198	28 107	28 134	28 021	408 111	993.68	1 001.09	1 994.77
Simulation 5	– 0.82399	1.13291	1.01253	1.34296	437 317	28 307	28 286	28 342	409 006	989.11	1 014.12	2 003.23
Simulation 6	0.36456	– 0.20269	0.14924	– 1.28412	437 808	28 083	28 142	27 901	409 766	1 004.34	994.52	1 998.86
Ave (Sim 1-6)										999.36	1 000.32	1 999.67

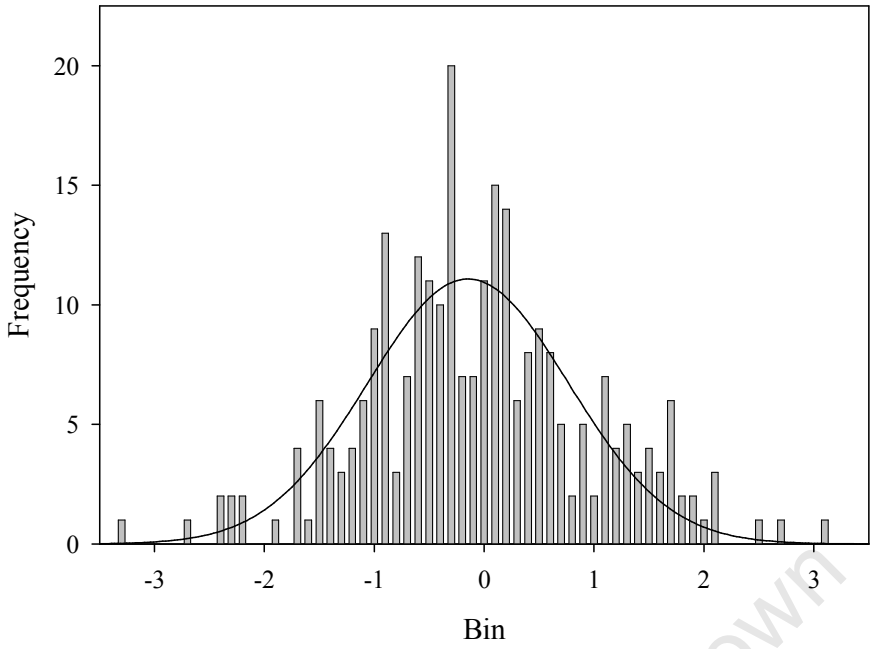

Fig. 3.2 Histogram of the random numbers used in the simulation. The curve shows a Gaussian fit to the data with $\sigma = 1$. Approximately 68 % of the counts are expected to be within $\pm 1\sigma$, 95 % within $\pm 2\sigma$ and 99.7 % within $\pm 3\sigma$ of the mean.

The ^{14}C and ^{63}Ni activities were calculated from Eqs. (3.3) and (3.4) after converting the counts to rates. The results were averaged for each source and are given in Table 3.2, together with the statistical uncertainties. Here σ_m is the standard deviation of the mean $\left(\sigma/\sqrt{n}\right)$, where σ is the standard uncertainty given by a statistical analysis and n the number of repeat measurements. The effect of statistical variation of the double- and triple-coincidence counts on the extracted activities is indicated in more detail in Fig. 3.3. Normal statistical variation was observed throughout. The simulation clearly demonstrates that counting statistics' effects does not impede the method's ability to extract reliably the activities of each component over a wide range of mixture compositions.

Table 3.2 The activities assigned to each hypothetical source, N_0 and N_0', are given together with the averaged activities, N_0^* and $N_0'^*$, extracted from Eqs. (3.3) and (3.4) for each simulated measurement. N_S^* is the sum of the extracted individual activities. For each source, the standard deviations of the mean, $\sigma_m(N_0^*)$, $\sigma_m(N_0'^*)$ and $\sigma_m(N_S^*)$, were derived from a statistical analysis of the counting data.

Source	N_0 (Bq)	N_0^* (Bq)	$\sigma_m(N_0^*)$ (Bq)	N_0' (Bq)	$N_0'^*$ (Bq)	$\sigma_m(N_0'^*)$ (Bq)	N_S^* (Bq)	$\sigma_m(N_S^*)$ (Bq)
1	2 000.00	2 000.47	3.23	0.00	1.99	2.51	2 002.46	1.48
2	1 800.00	1 800.71	1.61	200.00	197.04	1.01	1 997.75	0.78
3	1 600.00	1 599.00	1.94	400.00	401.55	2.82	2 000.55	0.93
4	1 400.00	1 403.69	2.74	600.00	597.40	3.26	2 001.09	1.63
5	1 200.00	1 199.52	2.16	800.00	800.90	2.33	2 000.43	1.07
6	1 000.00	999.36	3.32	1 000.00	1 000.32	4.52	1 999.67	1.89
7	800.00	799.19	0.84	1 200.00	1 200.83	1.67	2 000.02	1.16
8	600.00	598.36	1.95	1 400.00	1 402.41	2.33	2 000.77	1.24
9	400.00	401.75	1.96	1 600.00	1 598.13	1.64	1 999.87	0.77
10	200.00	200.07	2.02	1 800.00	1 797.34	2.72	1 997.41	1.34
11	0.00	1.93	1.83	2 000.00	1 997.88	2.36	1 999.81	1.07

3.4.2 The derivation and validation of uncertainty formulae

To derive a formula to estimate the uncertainty of the extracted activity, N_0, due to counting statistics, the count rates in Eq. (3.3) are converted to counts and time and the two resulting dependent variables, D and T, are re-written in terms of independent variables T, X_1, X_2 and X_3

$$N_0 = \frac{\frac{T}{t}\varepsilon_d' - \left(\frac{3T + X_1 + X_2 + X_3}{3t}\right)\varepsilon_t'}{\varepsilon_t\varepsilon_d' - \varepsilon_d\varepsilon_t'}\,, \tag{3.17}$$

where t is the counting time in seconds. Applying the uncertainty propagation formula [5]

$$\sigma(N_0) = \sqrt{\left(\frac{\partial N_0}{\partial T}\right)^2 \sigma_T^2 + \sum_{i=1}^{3}\left[\left(\frac{\partial N_0}{\partial X_i}\right)^2 \sigma_{X_i}^2\right]} \tag{3.18}$$

to Eq. (3.17) gives the predicted uncertainty as

$$\sigma(N_0) = \sqrt{\left(\frac{\varepsilon_d' - \varepsilon_t'}{t(\varepsilon_t\varepsilon_d' - \varepsilon_d\varepsilon_t')}\right)^2 T + \left(\frac{\varepsilon_t'}{3t(\varepsilon_t\varepsilon_d' - \varepsilon_d\varepsilon_t')}\right)^2 (X_1 + X_2 + X_3)}\,, \tag{3.19}$$

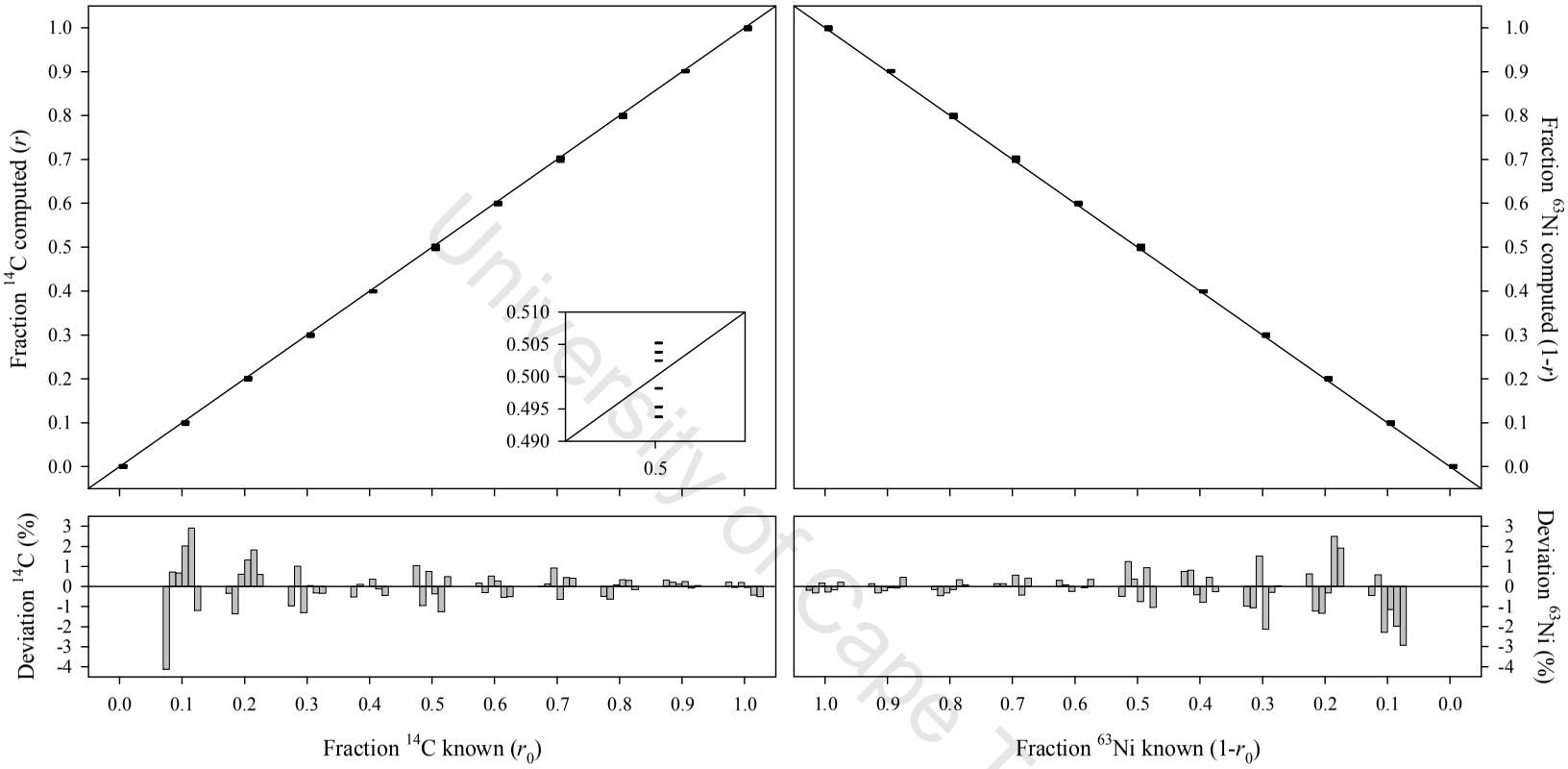

Fig. 3.3 In the scatter plots, the source compositions computed by the method $(r, 1-r)$ are compared with the known compositions $(r_0, 1-r_0)$, with the ^{14}C plot on the left-hand side and ^{63}Ni on the right. The diagonal lines indicate the expected ^{14}C and ^{63}Ni fractions respectively and the black markers are horizontal lines indicating the values extracted from each simulated data set. The inset shows an expanded view of one of the ^{14}C source fractions to emphasise the spread in the extracted values.

The bar diagrams below the scatter plots indicate the percentage deviations (given by $\frac{\text{fraction computed} - \text{fraction known}}{\text{fraction known}} \times 100$) for the ^{14}C and ^{63}Ni fractions respectively. Normal statistical variation is observed, with the relative deviations increasing as the composition fractions decrease.

where square root statistics are used to estimate the standard deviation of the number of counts. Similarly, the statistical uncertainty of N_0' is given by

$$\sigma(N_0') = \sqrt{\left(\frac{\varepsilon_d - \varepsilon_t}{t(\varepsilon_t\varepsilon_d' - \varepsilon_d\varepsilon_t')}\right)^2 T + \left(\frac{\varepsilon_t}{3t(\varepsilon_t\varepsilon_d' - \varepsilon_d\varepsilon_t')}\right)^2 (X_1 + X_2 + X_3)}. \qquad (3.20)$$

The uncertainties predicted for our simulation are given in Table 3.3 as standard deviations of the mean, σ_m, which can be compared with the statistical uncertainties given in Table 3.2. The good agreement obtained indicates consistency within the model. The equations derived to predict the uncertainty can be used to determine how many sources and repeat measurements are required in the practical situation to achieve reliable results.

Table 3.3 The predicted uncertainties, $\sigma_m(N_0)$, $\sigma_m(N_0')$ and $\sigma_m(N_S)$, given by Eqs. (3.19), (3.20) and (3.21), averaged per source and divided by $\sqrt{n}$ (where n = number of repeat measurements), can be compared with the corresponding statistical uncertainties shown in Table 3.2. For the prediction of $\sigma_m(N_S)$, the correlation coefficient, $r(N_0^*, N_0'^*) = -0.89$, was used. This was the average of the correlation coefficients calculated from Eq. (3.22) using the extracted variances, $\mathrm{Var}(N_0^*)$ and $\mathrm{Var}(N_0'^*)$, and the covariance, $\mathrm{Cov}(N_0^*, N_0'^*)$, for each hypothetical source.

Source	$\sigma_m(N_0)$ (Bq)	$\sigma_m(N_0')$ (Bq)	$\sigma_m(N_S)$ (Bq)	$\mathrm{Var}(N_0^*)$ (Bq^2)	$\mathrm{Var}(N_0'^*)$ (Bq^2)	$\mathrm{Cov}(N_0^*, N_0'^*)$ (Bq^2)	$r(N_0^*, N_0'^*)$
1	1.98	2.09	0.95	62.68	37.92	– 43.73	– 0.90
2	2.01	2.22	1.00	15.52	6.10	– 8.97	– 0.92
3	2.05	2.35	1.06	22.53	47.55	– 32.45	– 0.99
4	2.08	2.47	1.12	45.03	63.96	– 46.57	– 0.87
5	2.11	2.58	1.18	28.04	32.48	– 26.81	– 0.89
6	2.15	2.69	1.24	66.29	122.75	– 83.84	– 0.93
7	2.18	2.80	1.30	4.23	16.70	– 6.42	– 0.76
8	2.21	2.90	1.36	22.85	32.46	– 23.07	– 0.85
9	2.24	3.00	1.42	23.05	16.19	– 17.83	– 0.92
10	2.27	3.09	1.48	24.38	44.41	– 29.03	– 0.88
11	2.30	3.18	1.53	20.14	33.53	– 23.40	– 0.90

Because the two activities, N_0 and N_0', are extracted from the same set of counting data, the values are correlated and the uncertainty of the sum, $\sigma(N_S)$, is not simply the square root of the sum of the individual squared uncertainties. An additional parameter is required to account for the correlation, so that [6,7]

$$\sigma(N_S) = \sqrt{\sigma^2(N_0) + \sigma^2(N_0') + 2\sigma(N_0)\sigma(N_0')r(N_0, N_0')}, \tag{3.21}$$

where $r(N_0, N_0')$ is the correlation coefficient of the two activities. This can be determined experimentally from [6,7]

$$r(N_0, N_0') = \frac{\mathrm{Cov}(N_0, N_0')}{\sqrt{\mathrm{Var}(N_0)}\sqrt{\mathrm{Var}(N_0')}}, \tag{3.22}$$

where the variances, $\mathrm{Var}(N_0)$ and $\mathrm{Var}(N_0')$, quantify the amount of internal fluctuation in each data set and per definition, $\sigma(N_0) = \sqrt{\mathrm{Var}(N_0)}$; and the covariance, $\mathrm{Cov}(N_0, N_0')$, indicates the amount of correlation between the two quantities. The "experimental" variances were calculated from a statistical analysis [6,8]

$$\mathrm{Var}(N_0) = \frac{1}{n-1}\sum_{i=1}^{n}\left(N_{0i} - \overline{N_0}\right)^2 \text{ and } \mathrm{Var}(N_0') = \frac{1}{n-1}\sum_{i=1}^{n}\left(N_{0i}' - \overline{N_0'}\right)^2, \tag{3.23}$$

where the simulation gave rise to a set of extracted activity values, (N_{0i}, N_{0i}') for i = 1 to n, for each hypothetical source and $\overline{N_0}$ and $\overline{N_0'}$ were the arithmetic means of the activities obtained for each source. The experimental covariance was similarly calculated from [6,8]

$$\mathrm{Cov}(N_0, N_0') = \frac{1}{n-1}\sum_{i=1}^{n}\left(N_{0i} - \overline{N_0}\right)\left(N_{0i}' - \overline{N_0'}\right). \tag{3.24}$$

The results, summarised for each source, are given in Table 3.3. The correlation coefficients obtained showed no systematic trend to correspond with the imposed changes in radionuclide composition. The eleven values obtained were thus averaged to give $r(N_0, N_0') = -0.89 \pm 0.02$. The value being close to -1 indicates a strong degree of anti-correlation so that the uncertainty of the sum is predicted to be less than the sum in quadrature of the individual activities.

3.5 References

[1] W.M. van Wyngaardt, B.R.S. Simpson, A simple counting technique for measuring mixtures of two pure β-emitting radionuclides, Nucl. Instr. and Meth. A 564 (2006) 339.

[2] E. García-Toraño, A. Grau Malonda, EFFY, a new program to compute the counting efficiency of beta particles in liquid scintillators, Comp. Phys. Commun. 36 (1985) 307.

[3] G.F. Knoll, Radiation detection and measurement, third ed., John Wiley & Sons, Inc., New York, 2000, pp. 70 – 79.

[4] Generation and testing of random numbers, in: IMSL (International Mathematical and Statistical Library) user's manual, Vol. 2, ed. 9.2, IMSL Inc., November 1984, pp. G-1.

[5] Guide to the expression of uncertainty in measurement, first ed., first printing, International Organization for Standardization, Geneva, 1993, pp. 19 – 20.

[6] Guide to the expression of uncertainty in measurement, first ed., first printing, International Organization for Standardization, Geneva, 1993, pp. 10 – 11, 20 – 22.

[7] W. Kessel, Measurement uncertainty according to ISO/BIPM-GUM, Termochimica Acta 382 (2002) 1.

[8] A. Allisy, J.W. Müller, Assessment of uncertainties in measurements, ICRU News December (1994) 4.

CHAPTER 4 Experimental – measuring mixtures of ^{14}C and ^{63}Ni

4.1 Introduction

The radionuclides ^{14}C and ^{63}Ni were selected to demonstrate experimentally the feasibility of the technique to resolve mixtures of two pure β-emitting radionuclides. The experimental work was simplified by also using ^{63}Ni as the external tracer standard instead of ^{3}H. In the CIEMAT/NIST method ^{3}H is used to determine the efficiencies of more energetic radionuclides because the propagated uncertainties in the efficiencies are reduced considerably [1]. This reduction in uncertainty will be smaller when ^{63}Ni is used as a tracer due to its higher energy (E_{max} = 66.945 keV as opposed to E_{max} = 18.56 keV for ^{3}H) [2], but this will be offset by the smaller uncertainty achievable in the standardisation of ^{63}Ni compared to ^{3}H, particularly when using the TDCR technique. Thus, ^{63}Ni is an acceptable substitution for accurately tracing counting efficiencies.

4.2 Source preparation

Stock solutions of ^{14}C-labelled Na_2CO_3 in an aqueous solution of 486 mg/l Na_2CO_3 and ^{63}Ni-labelled $NiCl_2$ in a solution of 508 mg/l $NiCl_2{\cdot}6H_20$ in 0.21 M HCl were utilised in the source preparation. The nominal activity concentrations of the solutions were 19.5 Bq/mg for ^{14}C and 26.8 Bq/mg for ^{63}Ni at the time of source preparation. The liquid scintillation cocktail used was Insta-Gel Plus from Packard Bioscience to which 1.7 % (V/V) Carbo-Sorb II from Packard had been added to prevent the loss of ^{14}C due to the reaction of Na_2CO_3 with acid. Ten sources with different ^{14}C / ^{63}Ni ratios and count rates of around 2 000 s^{-1} were prepared by adding accurately weighed aliquots of the stock solutions to 12 ml scintillator cocktail in Wheaton scintillation vials. Sources were labelled M1 to M10, with source M1 containing only ^{14}C, source M10 only ^{63}Ni and the sources in-between being the mixed radionuclide sources with the ^{14}C fractions decreasing as the source numbers increased. The mass compositions are given in Table 4.1.

The pure ^{63}Ni source was used as the tracer standard for the whole experiment. It was

Table 4.1 Mass and activity compositions of the prepared sources.

Source	Mass ^{14}C (mg)	Mass ^{63}Ni (mg)	Total mass (mg)	Activity ^{14}C (Bq)	Activity ^{63}Ni (Bq)
M1	112.347	0.000	112.347	2190.22	0.00
M2	104.711	16.151	120.862	2041.36	432.09
M3	91.916	18.379	110.295	1791.91	491.69
M4	88.100	31.845	119.945	1717.52	851.95
M5	68.638	48.198	116.836	1338.11	1289.44
M6	51.713	61.694	113.407	1008.15	1650.50
M7	47.034	68.853	115.887	916.93	1842.02
M8	27.800	92.345	120.145	541.96	2470.50
M9	15.665	102.140	117.805	305.39	2732.55
M10	0.000	118.046	118.046	0.00	3158.08

therefore important to prepare the sources to match their quench states as closely as practically possible. This was done by adding essentially the same total mass of radionuclide solution to each source, using the identical liquid scintillation cocktail for all sources (although the pure ^{63}Ni source would not normally require the addition of Carbo-Sorb), and using the same volume of scintillator cocktail for each source. Thus, it was assumed (as a first approximation) that the ^{63}Ni standard could be used to represent reliably the quench state of all the prepared mixed sources, and the extracted figure-of-merit, *P*, from this source was used throughout.

4.3 Collection of data

The sources were counted using the NMISA three-phototube detection system [3] comprising three RCA 8850 high-gain phototubes (PM_1, PM_2, PM_3) in a non-symmetrical arrangement (Fig. 4.1). Outputs from the phototubes, after being fed through the usual pre-amplifiers (PA), amplifiers (AMP) and timing single-channel analysers (TSCA), were mixed in a locally designed and built two- and three-fold coincidence unit [4]. Three single-channel outputs (S_1, S_2, S_3), three double-coincidence outputs (D_{12}, D_{23}, D_{13}) and a single triple-coincidence output (T) were each registered separately.

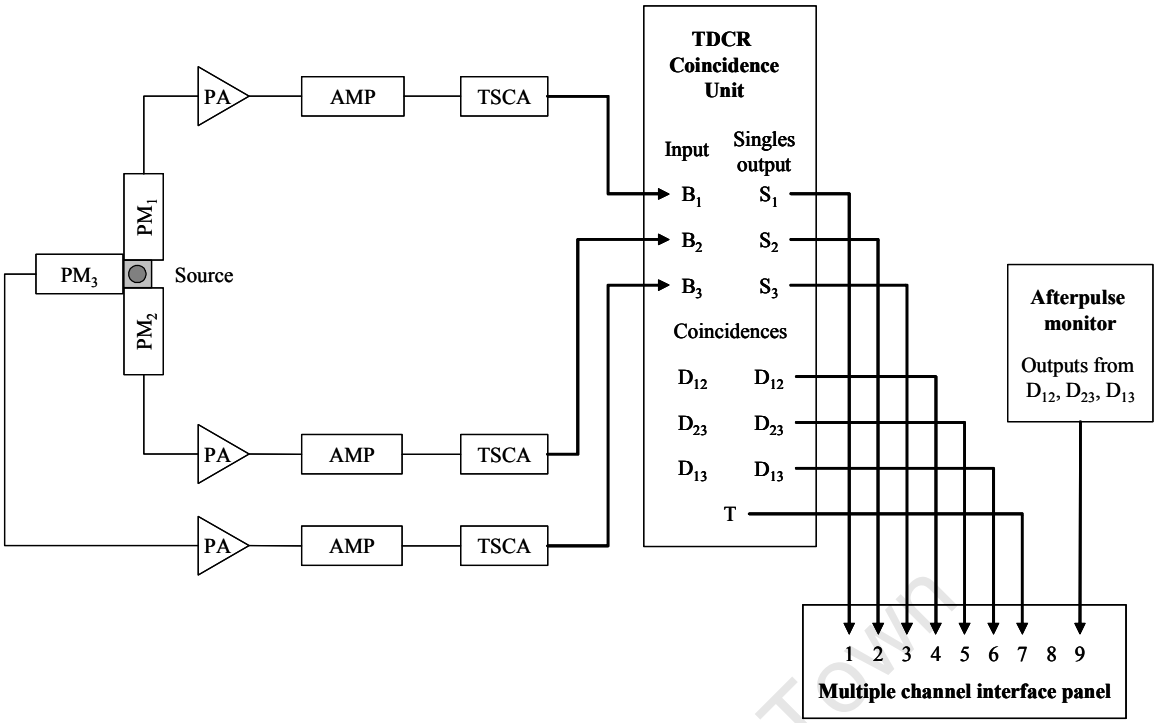

Fig. 4.1 Schematic diagram of the NMISA three-phototube detection system. Afterpulsing was monitored and recorded simultaneously with counting for each of the three double-coincidence channels in turn.

The experimental set-up was simple, with only one threshold being set for each channel and counting integrally from just below the single electron peak (a representative pulse-height spectrum is given in Fig. 4.2). To satisfy the criterion that each phototube should have the same figure-of-merit, the efficiencies were matched by positioning the counting vial relative to the phototubes so that the three double-coincidence count rates were as similar as possible after accounting for background and afterpulsing effects. The phototubes were typically matched to within 0.5 % or better. To reduce potential systematic effects due to phototube mismatch, not more than three measurements of the same source were made concurrently, with a total of six measurements of 300 seconds each collected per source.

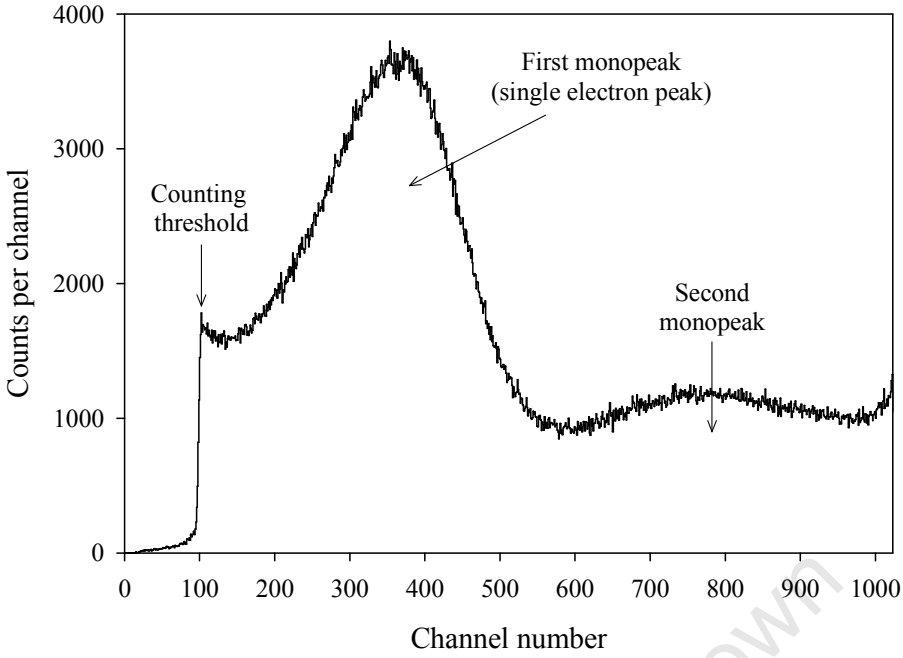

Fig. 4.2 Pulse-height spectrum for source M1 collected with phototube 2.

4.4 Programs used for computation and analysis

The program EFFY 2, developed by researchers at CIEMAT in Spain, was modified locally and used for data analysis. EFFY 2 was adapted to determine counting efficiencies specifically for Insta-Gel Plus and the program INPLUSF set up to determine ε_d and ε_t as a function of the figure-of-merit P for this scintillation cocktail. Another version, INPDATH, incorporates the same changes and is used specifically for the data analysis of single-radionuclide solutions of pure β-emitters by the TDCR technique. The routines for the correction of counting data were extracted from INPDATH and incorporated into the program TDRAW which was used for data pre-processing for the resolution of mixtures.

4.4.1 EFFY 2

EFFY 2 [5] was developed to compute the counting efficiency of β particles in a *double* phototube liquid scintillation counter, expressed as a function of the system figure-of-merit, M [*]. The program calculates the efficiency for a single phototube and for two phototubes in

[*] Refer to Appendix B for a description of the system figure-of-merit M and the single phototube figure-of-merit P.

coincidence, based on the theory detailed in Chapter 2, specifically by utilising Eqs. (2.11 and 2.12) with P effectively replaced by $1/2M$. Beta spectra are calculated from the Fermi theory of β decay, taking into account shape factors. The total detection probability is obtained by dividing the spectrum into weighted bands, calculating the detection probability for each of them and summing. The average and mean energies of the spectra are also obtained. Energy-dependent ionisation quenching is accounted for by the rational expression [6,7]

$$Q(E) = \frac{A + B\log E + C(\log E)^2}{1 + D\log E + F(\log E)^2}, \tag{4.1}$$

where $\log E$ is the decimal logarithm of the energy in units of keV. The coefficients A = 0.357478, B = 0.459577, C = 0.159905, D = 0.0977557 and F = 0.215852 were determined for a toluene-based scintillator with $kB = 0.0075\ \mathrm{g/(cm^2 MeV)}$.

4.4.2 TDCR data analysis

A locally modified version of EFFY 2, given the name INPDATH, was used to analyse the data collected from the two single-radionuclide sources measured by the TDCR efficiency calculation technique. The counts were corrected for background, deadtime [8] (τ_D = 1.0 μs), coincidence resolving time (τ_R = 0.47 μs) and afterpulsing [9] (up to a maximum of θ = 0.62 %, depending on the source and phototube channel) to give the corrected double- and triple-coincidence count rates, N_d and N_t. The methods used to determine the correction factors are described in Appendix C and the formulae used to correct the counting data are given in Section 4.4.4.

For the program INPDATH, EFFY 2 was extended to calculate efficiencies for a three-phototube detection system [10]. The program was adapted to calculate both the double- and triple-coincidence efficiencies as a function of the individual phototube figure-of-merit, P, where $P = 1/3M$, as detailed in Ref. [11]. INPDATH also produces the ratio of the triple-to-double efficiencies as a function of P, $\varepsilon_t(P)/\varepsilon_d(P)$. The program varies the figure-of-merit incrementally to determine the value of P that solves

$$\frac{N_t}{N_d} = \frac{\varepsilon_t(P)}{\varepsilon_d(P)}, \tag{4.2}$$

from which the source activity is calculated.

An additional change within INPDATH was that the coefficients of the rational expression used to correct for ionisation quenching were modified to account for the different scintillator composition, namely Insta-Gel Plus ($C_{18.6}H_{30.9}O_{3.9}N_{0.006}$) [12], for which a Birks constant of $kB = 0.008\,\mathrm{g}/(\mathrm{cm}^2\mathrm{MeV})$ was assumed. The local NMISA program IONQUEN was used to achieve this by determining the ionisation quenching function, $Q(E)$, for a range of energies between 0.01 and 2000 keV. The program assumes that the stopping power, (dE/dx), is proportional to $1/\sqrt{E}$ for energies below 0.4 keV [13] and makes use of the Bethe formula for the specific energy loss due to ionisation and excitation of fast electrons [14] to calculate the stopping power for energies ≥ 0.4 keV. Finally, numerical integration of the Birks formula [15],

$$Q(E) = \frac{1}{E}\int_0^E \frac{dE}{1 + kB(dE/dx)}, \tag{4.3}$$

by means of the Simpson method [16] gave values for $Q(E)$ that were fitted with a rational function of the same form as Eq. (4.1) over the energy range 0 to 100 keV (Fig. 4.3). Fitting only over this limited energy range was adequate since the exponential terms in the efficiency formulae (Eqs. 2.11, 2.12, 2.13) become negligible at higher energies and an imperfect estimate of $Q(E)$ in this region (E > 100 keV) does not affect the efficiency calculation.

The TDCR data analysis provided the activities of sources M10 = 3158 ± 16 Bq of ^{63}Ni and M1 = 2190 ± 11 Bq of ^{14}C on 1 February 2005, from which the activity compositions of the mixed-radionuclide sources were determined gravimetrically (Table 4.1). The figures-of-merit that solved Eq. (4.2) were P = 0.1621 e/keV for the ^{63}Ni source and P = 0.1562 e/keV for the ^{14}C source.

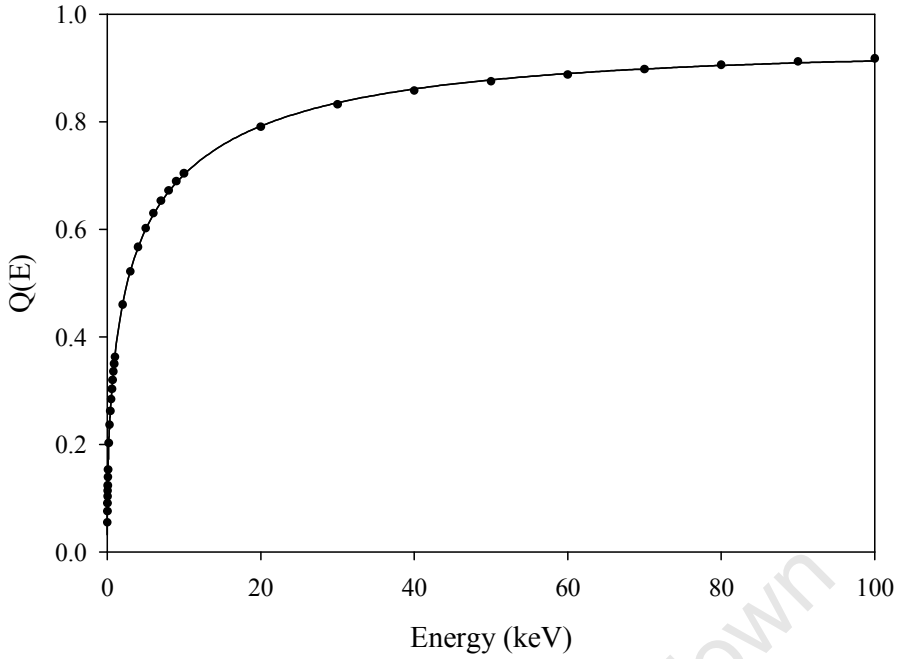

Fig. 4.3 Values determined for the energy-dependent ionisation quenching function, $Q(E)$, for Insta-Gel Plus (solid circles), were fitted with a rational function of the form $Q(E) = A + B\log E + C(\log E)^2 / 1 + D\log E + F(\log E)^2$ up to an energy of 100 keV to give the coefficients A = 0.366526, B = 0.172749, C = 0.0276717, D = – 0.334959 and F = 0.142684 (continuous curve).

4.4.3 The calculation of detection efficiencies i.t.o. the figure-of-merit P

The program INPLUSF was used to calculate the double- and triple-coincidence detection efficiencies of ^{14}C and ^{63}Ni in terms of the figure-of-merit, P, using the same routines as those in INPDATH. Efficiencies for a range of P values are given in Table 4.2. Since the ^{63}Ni source was used as the tracer for all the mixed sources, the double- and triple-coincidence detection efficiencies were determined for P = 0.1621 e/keV. The efficiencies obtained were: for ^{14}C (ε_d = 0.8678, ε_t = 0.8409) and for ^{63}Ni (ε_d = 0.5910, ε_t = 0.5242), all given in units of $s^{-1}Bq^{-1}$.

Table 4.2 Efficiencies determined for Insta-Gel Plus.

	^{14}C			^{63}Ni		
P	ε_t (%)	ε_t (%)	$\varepsilon_t/\varepsilon_d$	ε_d (%)	ε_t (%)	$\varepsilon_t/\varepsilon_d$
0.2222	90.0335	88.0336	0.97779	66.8355	61.2326	0.91617
0.2151	89.7380	87.6754	0.97702	66.0862	60.3724	0.91354
0.2083	89.4431	87.3179	0.97624	65.3483	59.5265	0.91091
0.2020	89.1487	86.9609	0.97546	64.6216	58.6947	0.90828
0.1961	88.8548	86.6046	0.97468	63.9058	57.8765	0.90565
0.1905	88.5615	86.2489	0.97389	63.2007	57.0718	0.90302
0.1852	88.2686	85.8938	0.97310	62.5061	56.2801	0.90039
0.1802	87.9762	85.5393	0.97230	61.8217	55.5014	0.89777
0.1754	87.6844	85.1854	0.97150	61.1473	54.7352	0.89514
0.1709	87.3931	84.8322	0.97070	60.4827	53.9813	0.89251
0.1667	87.1022	84.4795	0.96989	59.8278	53.2396	0.88988
0.1626	86.8119	84.1275	0.96908	59.1823	52.5097	0.88725
0.1587	86.5220	83.7762	0.96826	58.5460	51.7914	0.88463
0.1550	86.2327	83.4255	0.96745	57.9188	51.0846	0.88200
0.1515	85.9439	83.0754	0.96662	57.3006	50.3890	0.87938
0.1481	85.6555	82.7260	0.96580	56.6911	49.7044	0.87676
0.1449	85.3677	82.3773	0.96497	56.0902	49.0307	0.87414
0.1418	85.0804	82.0292	0.96414	55.4978	48.3675	0.87152
0.1389	84.7937	81.6818	0.96330	54.9136	47.7149	0.86891
0.1361	84.5074	81.3352	0.96246	54.3376	47.0724	0.86630

4.4.4 Data pre-processing

The program TDRAW was used to perform corrections to the measurement data. The counts collected simultaneously for each source were the singles (S_1, S_2, S_3), the doubles (D_{xy}, with xy = 12, 23, 13 indicating coincidences between the three pairs of phototubes) and the triple-coincidence counts (T), all in a counting time t. Background count rates were also collected for each observable (bs_1, bs_2, bs_3, bd_{12}, bd_{23}, bd_{13}, bt). If the background corrected singles rates are Ns_1, Ns_2 and Ns_3 and the double and triple rates (not corrected for background) are ND_{12}, ND_{23}, ND_{13} and NT respectively, then the double-coincidence count rate corrected for background, deadtime (τ_D = 1.0 μs) and coincidence resolving time (τ_R = 0.47 μs) for channel

D_{xy} was in this study given by the Bryant formula [17]

$$\mathrm{Nd}_{xy} = \frac{\left(\mathrm{ND}_{xy} - 2\tau_R \mathrm{Ns}_x \mathrm{Ns}_y\right)\left[1 - \left(\mathrm{Ns}_x + \mathrm{Ns}_y\right)\tau_D/2\right]}{\left(1 - \mathrm{Ns}_x\tau_D\right)\left(1 - \mathrm{Ns}_y\tau_D\right)\left[1 - \left(\mathrm{Ns}_x + \mathrm{Ns}_y\right)\left(\tau_D + 2\tau_R\right)/2 + \mathrm{Nd}_{xy}\tau_D\right]} - \mathrm{bd}_{xy} \qquad (4.4)$$

with xy = 12, 23 and 13. The triple-coincidence rate with the same corrections is given approximately by an analogous formula

$$\mathrm{Nt} = \frac{\left(\mathrm{NT} - 2\tau_R \mathrm{ND}_{12}\mathrm{ND}_{23}\right)\left[1 - \left(\mathrm{ND}_{12} + \mathrm{ND}_{23}\right)\tau_D/2\right]}{\left(1 - \mathrm{ND}_{12}\tau_D\right)\left(1 - \mathrm{ND}_{23}\tau_D\right)\left[1 - \left(\mathrm{ND}_{12} + \mathrm{ND}_{23}\right)\left(\tau_D + 2\tau_R\right)/2 + \mathrm{NT}\tau_D\right]} - \mathrm{bt}\,. \qquad (4.5)$$

A similar corrected triple rate is obtained if other combinations of the doubles rates (e.g. ND_{12} and ND_{13} or ND_{23} and ND_{13}) are used. Accounting for afterpulses as well (θ_{xy} up to a maximum of 0.0026 in this experiment), the corrected double-coincidence count rates become

$$Nd_{xy} = \mathrm{Nd}_{xy}/\left(1 + \theta_{xy}\right), \qquad (4.6)$$

with *xy* = 12, 23 and 13. No afterpulse correction was required for the triple counts.

The average double-coincidence count rate, N_d, was utilised in the data analysis of Section 4.5 and is calculated in the usual way

$$N_d = 1/3\left(Nd_{12} + Nd_{23} + Nd_{13}\right). \qquad (4.7)$$

The standard uncertainty due to counting statistics, $\sigma\left(N_d\right)$, is approximated by

$$\sigma\left(N_d\right) = \frac{1}{3}\sqrt{\frac{Nd_{12} + Nd_{23} + Nd_{13}}{t}}\,, \qquad (4.8)$$

where Eq. (4.8) was derived by applying the uncertainty propagation formula [18] to Eq. (4.7) after converting the rates to counts and time and assuming that the uncertainty of the counts is given by the square root of the number of counts. This uncertainty estimate is a useful indicator of the amount of data to collect. The usual aim is to limit the total statistical uncertainty for a measurement to 0.15 %.

The corrected triple-coincidence count rate was used for further data analysis without additional modifications, i.e., N_t used in Section 4.5 was that given by Eq. (4.5). The standard uncertainty was given by $\sigma\left(N_t\right) = \sqrt{N_t/t}$.

4.5 Analysis, results and data evaluation

Eqs. (3.3) and (3.4) from Section 3.2

$$N_0 = \frac{N_t\varepsilon'_d - N_d\varepsilon'_t}{\varepsilon_t\varepsilon'_d - \varepsilon_d\varepsilon'_t} \tag{3.3}$$

$$N'_0 = \frac{N_d\varepsilon_t - N_t\varepsilon_d}{\varepsilon_t\varepsilon'_d - \varepsilon_d\varepsilon'_t} \tag{3.4}$$

were used to extract the radionuclide activities, N_0 and N'_0, for each ^{14}C / ^{63}Ni mixture. The corrected double- and triple-coincidence count rates, N_d and N_t, for each source measurement were substituted into Eqs. (3.3) and (3.4), together with the efficiencies calculated for the figure-of-merit P = 0.1621 e/keV determined from the tracer (source M10 containing only ^{63}Ni). The efficiencies as given in Section 4.4.3 for ^{14}C (ε_d = 0.8678, ε_t = 0.8409) and for ^{63}Ni (ε_d = 0.5910, ε_t = 0.5242), in units of $s^{-1}Bq^{-1}$, were used. The extracted activities were decay corrected to the same reference date (1 February 2005) by multiplying with the decay correction factor, $Z = \exp(-\lambda t')$, where $\lambda = \ln 2 / T_{½}$ is the decay constant of the radionuclide, $T_{½}$ is the radionuclide's half-life ($T_{½}(^{14}\mathrm{C}) = 5700$ years and $T_{½}(^{63}\mathrm{Ni}) = 100.6$ years) [2] and t' is the time interval between the measurement and reference date. The activities thus determined were summed to give the total activity, N_S, for each measurement. A full set of data for one of the sources (M5) is shown in Table 4.3 (a).

The uncertainties due to counting statistics were estimated from Eqs. (3.19), (3.20) and (3.21) from Section 3.4

$$\sigma(N_0) = \sqrt{\left(\frac{\varepsilon'_d - \varepsilon'_t}{t(\varepsilon_t\varepsilon'_d - \varepsilon_d\varepsilon'_t)}\right)^2 T + \left(\frac{\varepsilon'_t}{3t(\varepsilon_t\varepsilon'_d - \varepsilon_d\varepsilon'_t)}\right)^2 (X_1 + X_2 + X_3)} \tag{3.19}$$

$$\sigma(N'_0) = \sqrt{\left(\frac{\varepsilon_d - \varepsilon_t}{t(\varepsilon_t\varepsilon'_d - \varepsilon_d\varepsilon'_t)}\right)^2 T + \left(\frac{\varepsilon_t}{3t(\varepsilon_t\varepsilon'_d - \varepsilon_d\varepsilon'_t)}\right)^2 (X_1 + X_2 + X_3)} \tag{3.20}$$

$$\sigma(N_S) = \sqrt{\sigma^2(N_0) + \sigma^2(N'_0) + 2\sigma(N_0)\sigma(N'_0)r(N_0, N'_0)}, \tag{3.21}$$

where $r(N_0, N'_0) = -0.89$ from the simulation was used in the estimate for $\sigma(N_S)$. Also, an equation to predict the statistical uncertainty in the N_t/N_d ratio,

$$\sigma(N_t/N_d) = \frac{3\sqrt{(X_1 + X_2 + X_3)^2 T + (X_1 + X_2 + X_3)T^2}}{(3T + X_1 + X_2 + X_3)^2}, \tag{4.9}$$

is derived in Appendix D. T and X_i (i = 1 to 3) are the triple- and exclusive double-coincidence counts collected in a counting time t. The introduction of X_i is necessary to account for the correlation between the double- and triple-coincidence counts D_i and T, where

$D_i = X_i + T$. The counts and predicted statistical uncertainties are given for six repeat measurements of source M5 in Table 4.3 (b).

Table 4.3 (a) Source M5 was measured twice on each of three days (28 and 31 January; 1 February 2005). The corrected count rates for each of the six repeat measurements are given, with Nd_{12}, Nd_{23} and Nd_{13} the rates for each of the three double-coincidence channels, N_d the average double-coincidence rate, N_t the triple-coincidence count rate and N_t/N_d the TDCR value. The activities extracted by Eqs. (3.3) and (3.4) were multiplied with the appropriate, small decay correction factor, to give the radionuclide activities, $N_0(^{14}\mathrm{C})$ and $N_0'(^{63}\mathrm{Ni})$, which were summed to give the total source activity, N_S. The average activity values obtained for each of the measured sources are given in Table 4.4.

Run	Nd_{12} (s^{-1})	Nd_{23} (s^{-1})	Nd_{13} (s^{-1})	N_d (s^{-1})	N_t (s^{-1})	N_t/N_d	$N_0(^{14}\mathrm{C})$ (Bq)	$N_0'(^{63}\mathrm{Ni})$ (Bq)	N_S (Bq)
1	1923.45	1930.18	1928.10	1927.24	1806.47	0.93733	1363.84	1258.20	2622.05
2	1919.82	1926.63	1925.61	1924.02	1802.95	0.93707	1354.54	1266.41	2620.95
3	1924.75	1919.00	1927.32	1923.69	1801.90	0.93669	1343.99	1281.41	2625.40
4	1922.39	1917.97	1922.49	1920.95	1798.81	0.93642	1334.71	1290.41	2625.12
5	1932.69	1930.01	1922.03	1928.24	1806.08	0.93664	1345.84	1286.43	2632.27
6	1929.94	1925.87	1917.78	1924.53	1802.60	0.93664	1343.26	1283.95	2627.20

Table 4.3 (b) The triple-coincidence counts, T, and the exclusive double-coincidence counts, X_{12}, X_{23} and X_{13}, recorded for six repeat measurements of source M5 in a counting time of $t = 300$ seconds, were used to predict statistical uncertainties in the TDCR value, $\sigma(N_t/N_d)$, in the extracted activities, $\sigma(N_0)$ and $\sigma(N_0')$, and in the total activity, $\sigma(N_S)$. Because the two activities are anti-correlated, $\sigma(N_S)$ is smaller than either of $\sigma(N_0)$ and $\sigma(N_0')$. The predicted statistical standard deviation of the mean for each activity value (i.e. $\sigma/\sqrt{6}$ expressed as a fraction of the activity) is given in Table 4.5 for the eight mixed radionuclide sources.

Run	X_{12}	X_{23}	X_{13}	T	$\sigma(N_t/N_d)$	$\sigma(N_0)$ (Bq)	$\sigma(N_0')$ (Bq)	$\sigma(N_S)$ (Bq)
1	35094	37112	36490	541941	0.000195	6.00	7.49	3.48
2	35062	37104	36797	540885	0.000196	6.01	7.50	3.48
3	36853	35128	37624	540571	0.000196	6.02	7.52	3.50
4	37072	35748	37101	539644	0.000197	6.02	7.53	3.50
5	37984	37180	34787	541823	0.000196	6.02	7.53	3.50
6	38203	36980	34555	540780	0.000196	6.02	7.53	3.50

The final results, averaged for each source, are given in Table 4.4, together with the relative deviations from the gravimetric activity compositions (also given in Table 4.1). In Fig. 4.4, the measured activity fractions are compared with the expected values for each individual measurement. The extracted activities of each component compare well with the prepared activities over a wide fractional range, although the deviations display a systematic trend for each radionuclide, changing from positive to negative as the fraction increases.

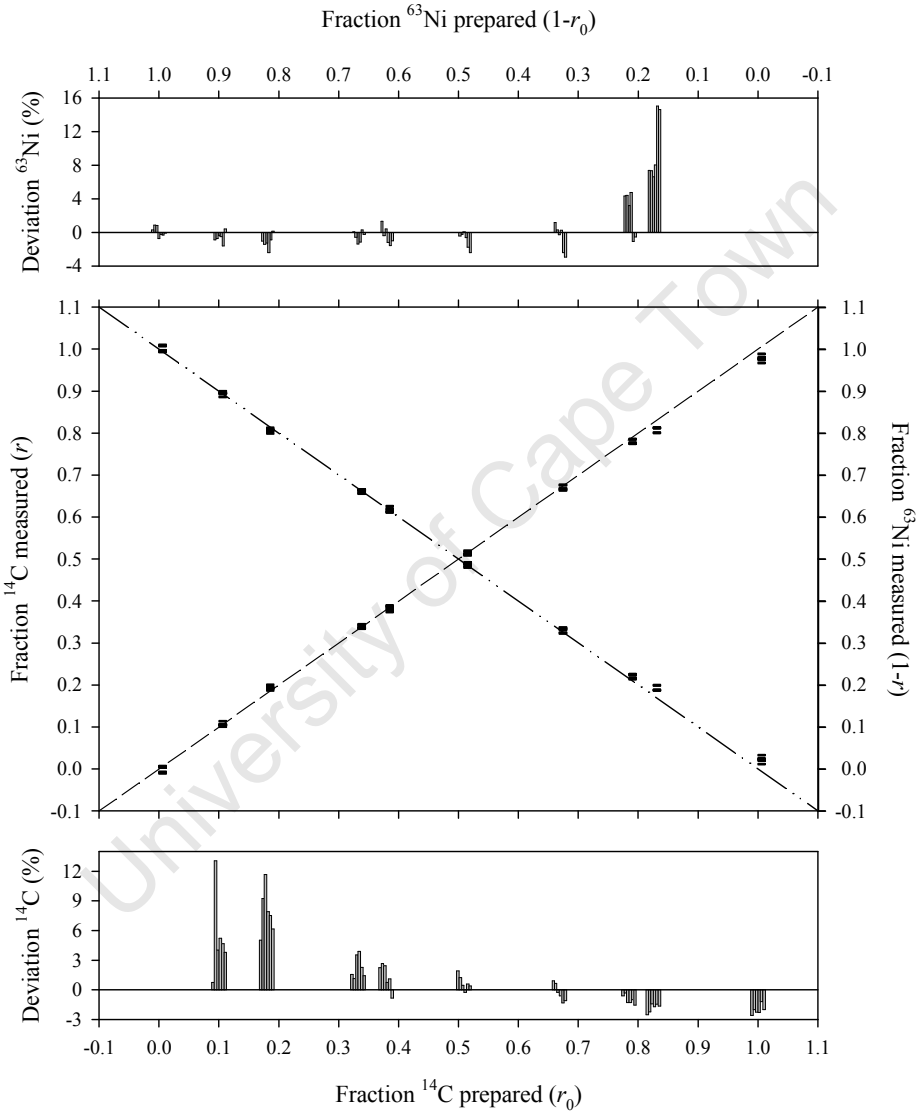

Fig. 4.4 In the scatter plot, the source compositions extracted by the method (r,1 − r) are compared with the gravimetric compositions (r_0,1 − r_0). The diagonal lines indicate the expected compositions (^{14}C broken line, ^{63}Ni dash-dot-dot). The markers are horizontal lines indicating ^{63}Ni and ^{14}C compositions calculated by the method for each measurement. The bar diagrams above and below the scatter plot indicate the percentage deviations (given by $\frac{\text{fraction measured - fraction prepared}}{\text{fraction prepared}} \times 100$) for the ^{63}Ni and ^{14}C components, respectively, for each repeated measurement of a given source. As is expected, the relative deviations increase as the activities decrease.

Table 4.4 The gravimetric activity composition of each source, $N_G(^{14}\mathrm{C})$, $N_G(^{63}\mathrm{Ni})$ and $N_G(\mathrm{Total})$, is given together with the averaged activities extracted by the method for each source, $N_0(^{14}\mathrm{C})$, $N_0'(^{63}\mathrm{Ni})$ and $N_S(\mathrm{Total})$. The deviations of the averaged measured activities from the gravimetric compositions are given relative to the radionuclide activities ($\%\,\mathrm{deviation} = \frac{\text{fraction measured - fraction prepared}}{\text{fraction prepared}} \times 100$). Because N_0 and N_0' are correlated, the deviations for the total activities, N_S, are small. The ratios r_0 and r indicate the gravimetric and measured activity fractions, respectively, of ^{14}C.

Source	$N_G(^{14}\mathrm{C})$ (Bq)	$N_0(^{14}\mathrm{C})$ (Bq)	Dev(^{14}C) (%)	$N_G(^{63}\mathrm{Ni})$ (Bq)	$N_0'(^{63}\mathrm{Ni})$ (Bq)	Dev(^{63}Ni) (%)	$N_G(\mathrm{Total})$ (Bq)	$N_S(\mathrm{Total})$ (Bq)	Dev(Total) (%)	r_0	r
M1	2190.22	2145.05	– 2.06	0.00	49.43	-	2190.22	2194.48	0.19	1.0000	0.9775
M2	2041.36	2004.00	– 1.83	432.09	474.60	9.84	2473.44	2478.60	0.21	0.8253	0.8085
M3	1791.91	1773.84	– 1.01	491.69	504.00	2.50	2283.61	2277.84	– 0.25	0.7847	0.7787
M4	1717.52	1712.70	– 0.28	851.95	846.39	– 0.65	2569.47	2559.09	– 0.40	0.6684	0.6693
M5	1338.11	1347.70	0.72	1289.44	1277.80	– 0.90	2627.55	2625.50	– 0.08	0.5093	0.5133
M6	1008.15	1022.19	1.39	1650.50	1643.97	– 0.40	2658.65	2666.16	0.28	0.3792	0.3834
M7	916.93	938.08	2.31	1842.02	1832.76	– 0.50	2758.96	2770.84	0.43	0.3323	0.3386
M8	541.96	584.89	7.92	2470.50	2442.03	– 1.15	3012.47	3026.93	0.48	0.1799	0.1932
M9	305.39	321.41	5.24	2732.55	2715.86	– 0.61	3037.94	3037.26	– 0.02	0.1005	0.1058
M10	0.00	– 1.97	-	3158.08	3160.78	0.09	3158.08	3158.81	0.02	0.0000	– 0.0006

4.6 Discussion of errors and uncertainties

The errors and uncertainties observed for the extracted activities are most clearly explained with reference to Fig. 3.1.

4.6.1 Effect due to counting statistics:

Since radioactive decay is by nature a random process, N_t/N_d will vary from measurement to measurement so that a different (r,1 − r) curve is selected each time, giving rise to statistically varying, anti-correlated extracted activities. The ratio can be measured with a very small statistical uncertainty, predicted by Eq. (4.9) and given in Table 4.3 (b) and Table 4.5. The resultant uncertainties in the extracted activities due to the statistical variation in N_t and N_d can be estimated from Eqs. (3.19) and (3.20). The statistical uncertainties are given in Table 4.5, expressed as a fraction of the individual activities, for the measurements of the mixed radionuclide sources.

4.6.2 Other effects affecting the counts and hence N_t/N_d :

Afterpulsing could only be measured for one of the double-coincidence channels at a time and the afterpulse correction for each measurement was thus determined from data collected during three separate measurements of the same source. The resultant uncertainty in the N_t/N_d ratio can lead to the selection of an incorrect (r,1 − r) curve. This is probably a random effect increasing the spread of measured activities, but it could also be responsible for a systematic trend.

The corrections made for deadtime, coincidence resolving time and background each has a small uncertainty and could thus also affect N_t/N_d , resulting in the selection of a somewhat incorrect curve.

These random effects all contribute to the additional uncertainties given in Table 4.5.

Table 4.5 The second column of this table shows the small statistical uncertainty obtained for N_t/N_d. The remainder of the table shows the additional spread in results from repeat measurements of the same source, given by the difference (in quadrature) between the uncertainty contribution due to measured statistical variation and that calculated for counting statistics from Eqs. (3.19) and (3.20). Contributors to this additional spread are uncertainty in the correction for afterpulses, deadtime, coincidence resolving time and background and also phototube mismatch. The uncertainty contributions are given relative to the specific radionuclide activities at 1σ. The values given for the uncertainty in counting statistics and the additional spread for ^{14}C differ slightly from those given in Ref. [19] due to an error made in the calculation of $\sigma(N_0)$ for the publication.

	N_t/N_d	^{14}C			^{63}Ni		
source	counting statistics (%)	measured statistical variation (%)	counting statistics (%)	additional statistical spread (%)	measured statistical variation (%)	counting statistics (%)	additional statistical spread (%)
M2	0.007	0.19	0.11	0.15	1.44	0.55	1.34
M3	0.007	0.19	0.12	0.14	1.05	0.50	0.92
M4	0.007	0.37	0.14	0.34	0.68	0.33	0.59
M5	0.009	0.31	0.18	0.25	0.40	0.24	0.32
M6	0.010	0.54	0.25	0.48	0.45	0.20	0.40
M7	0.010	0.46	0.28	0.37	0.28	0.18	0.21
M8	0.011	0.88	0.47	0.75	0.34	0.15	0.31
M9	0.012	1.60	0.87	1.34	0.27	0.14	0.24

4.6.3 Effects due to variation in P:

(a) Non-reproducible placement of a counting vial leads to asymmetry in the phototube efficiencies. This variation in phototube matching leads to an actual net figure-of-merit different from the P value used and the incorrect (r,1 − r) curve is selected. This effect probably averages out between repeat placements of the same source giving close to the "true" activity values, but it spreads out the results giving a larger standard deviation. This effect also contributed to the additional uncertainties given in Table 4.5.

(b) If the value of P used (as given by the tracer standard) does not properly correspond to the actual quench state of the mixture source, the incorrect (r,1 − r) curve will be selected, leading to systematically higher or lower extracted activity values. The assumption that the quench states of all sources used in the experiment were the same was not strictly correct. This is

demonstrated by TDCR analysis of the measurement data for the pure ^{14}C source M1 that gave $P = 0.1562$, as opposed to $P = 0.1621$ that was given by the tracer. The differences between the figures-of-merit are likely due to differences in the total amount of radionuclide solution added per source, differences in the chemical compositions of the two radionuclide stock solutions used (Na_2CO_3 in H_2O vs. $NiCl_2$ in HCl), different proportions of the stock solutions used and chemical reactions between Carbo-Sorb and HCl altering chemical quenching.

The deviation of P from the value used is expected to decrease as the fraction of ^{14}C in each mixed source decreases and would account for the systematic trend observed in the data (Fig. 4.4). To assess this effect, the measurement data were analysed with P varying between 0.1562 and 0.1621 according to the mass fraction compositions of the respective sources. The results of this analysis are shown in Table 4.6 and indicate that the accuracy of the extracted activities for the two sources with the highest ^{14}C contents (M1, M2) improved, but those of the other sources worsened somewhat.

(c) In this method, all efficiencies are deduced from a model that calculates the efficiency as a function of the figure-of-merit P. These are estimates of the true efficiencies, which are given by $\varepsilon_{\text{true}} = \text{count rate}/\text{activity}$, where the true activity must be obtained by a method other than the CIEMAT/NIST or TDCR methods to be independent of the model. Any deficiencies in the model (e.g. theoretical spectra, kB value, $Q(E)$ determination, the model itself) could lead to a somewhat different P value for each radionuclide dissolved in the same liquid scintillation cocktail since there are differences in the energies of particles emitted. The somewhat different figures-of-merit that were obtained for the two single radionuclide sources indicate possible imperfections in some aspects of the model used. The method may require better theory to give reliable results for all situations.

Table 4.6 *P* was varied between 0.1562 and 0.1621 according to the mass fraction compositions of the respective sources. The resultant efficiencies and the activities extracted from Eqs. (3.3) and (3.4) are given, together with the deviations from the gravimetric compositions. These can be compared with the deviations given in Table 4.4.

Source	Mass fraction	*P* graded	ε_d		ε_t		Activities extracted (Bq)		Deviation (%)	
	^{14}C		^{14}C	^{63}Ni	^{14}C	^{63}Ni	^{14}C	^{63}Ni	^{14}C	^{63}Ni
M1	1.0000	0.1562	0.8633	0.5812	0.8354	0.5132	2190.16	– 0.20	0.00	-
M2	0.8664	0.1570	0.8639	0.5825	0.8361	0.5146	2053.10	422.34	0.58	– 2.25
M3	0.8334	0.1572	0.8640	0.5828	0.8363	0.5149	1817.98	457.24	1.45	– 7.01
M4	0.7345	0.1578	0.8645	0.5840	0.8369	0.5162	1758.20	798.89	2.37	– 6.23
M5	0.5875	0.1586	0.8651	0.5853	0.8377	0.5177	1389.11	1235.32	3.81	– 4.20
M6	0.4560	0.1594	0.8657	0.5866	0.8384	0.5192	1057.01	1608.63	4.85	– 2.54
M7	0.4059	0.1597	0.8660	0.5871	0.8387	0.5197	971.04	1799.40	5.90	– 2.31
M8	0.2314	0.1607	0.8667	0.5887	0.8396	0.5216	607.80	2418.92	12.15	– 2.09
M9	0.1330	0.1613	0.8672	0.5897	0.8401	0.5227	335.53	2701.43	9.87	– 1.14
M10	0.0000	0.1621	0.8678	0.5910	0.8409	0.5242	– 1.97	3160.78	-	0.09

4.7 References

[1] A. Grau Malonda, E. García-Toraño, Evaluation of counting efficiency in liquid scintillation counting by pure β-ray emitters, Int. J. Appl. Radiat. Isot. 33 (1982) 249.

[2] M.-M. Bé, B. Duchemin, C. Morillon, E. Browne, V. Chechev, A. Egorov, R. Helmer, E. Schönfeld, Nucleide 2000. Nuclear and atomic decay data, Version 2-2004. BNM-CEA/DTA/LPRI, Saclay, France, 2004.

[3] B.R. Meyer, B.R.S. Simpson, A direct method for ^{55}Fe activity measurement, Appl. Radiat. Isot. 41 (1990) 375.

[4] B.R.S. Simpson, W.M. Morris, The standardization of ^{33}P by the TDCR efficiency calculation technique, Appl. Radiat. Isot. 60 (2004) 465.

[5] E. García-Toraño, A. Grau Malonda, EFFY, a new program to compute the counting efficiency of beta particles in liquid scintillators, Comp. Phys. Commun. 36 (1985) 307.

[6] A. Grau Malonda, Free parameter models in liquid scintillation counting, Editorial Ciemat, Madrid, Spain, 1999, pp. 20 – 29.

[7] F. Ortiz, J.M. Los Arcos, A. Grau, L. Rodríguez, Monte Carlo simulation of the spectral response of beta-particle emitters in LSC systems, Nucl. Instr. and Meth. A 312 (1992) 109.

[8] B.R.S. Simpson, Deadtime measurement and associated statistical uncertainty by means of a two-detector paired-source method, Appl. Radiat, Isot. 42 (1991) 811.

[9] B.R.S. Simpson, Radioactivity standardization in South Africa, Appl. Radiat. Isot. 56 (2002) 301.

[10] B.R.S. Simpson, B.R. Meyer, Direct activity measurement of pure beta-emitting radionuclides by the TDCR efficiency calculation technique, Nucl. Instr. and Meth. A 339 (1994) 14.

[11] A. Grau Malonda, B.M. Coursey, Calculation of beta-particle counting efficiency for liquid-scintillation systems with three phototubes, Appl. Radiat. Isot. 39 (1988) 1191.

[12] A. Grau Malonda, A. Grau Carles, Standardization of electron-capture radionuclides by liquid scintillation counting, Appl. Radiat. Isot. 52 (2000) 657.

[13] J.A.B. Gibson, The Statistics of the scintillation process and determination of the counting efficiency, in: The application of liquid scintillation counting to radionuclide metrology, Monographie BIPM-3, Bureau International des Poids et Mesures, Sevres, 1980, pp. 36 – 55.

[14] G.F. Knoll, Radiation detection and measurement, third ed., John Wiley & Sons, Inc., New York, 2000, pp. 43 – 44.

[15] J.A.B. Gibson, H.J. Gale, Absolute standardization with liquid scintillation counters, J. Phys. E. 1, ser. 2 (1968) 99.

[16] M.R. Spiegel, Mathematical handbook of formulas and tables, McGraw-Hill, New York, 1968, p. 95.

[17] NCRP Report No. 58, A handbook of radioactivity measurements procedures, second ed., National Council on Radiation Protection and Measurements, Bethesda, 1985, pp. 85 – 86.

[18] Guide to the expression of uncertainty in measurement, first ed., first printing, International Organization for Standardization, Geneva, 1993, pp. 19 – 20.

[19] W.M. van Wyngaardt, B.R.S. Simpson, A simple counting technique for measuring mixtures of two pure β-emitting radionuclides, Nucl. Instr. and Meth. A 564 (2006) 339.

CHAPTER 5 Experimental – measuring mixtures of ^{32}P, ^{33}P and ^{35}S

5.1 Introduction

The simulation given in Chapter 3 and the measurement of mixtures of ^{14}C and ^{63}Ni described in Chapter 4 served as proof-of-principle for the new method. For the latest experiment, the effect of spectral energy differences on the method's ability to extract the individual activities was investigated. For small energy differences, various mixtures of the low energy β-emitters ^{33}P (E_{max} = 248.50 keV) and ^{35}S (E_{max} = 167.14 keV) [1] were measured. The applicability of the method for radionuclide pairs with large energy differences was investigated by measuring mixtures of ^{32}P (E_{max} = 1 710.66 keV) [1] with both ^{33}P and ^{35}S. The experiments were facilitated by the ready availability of stock solutions of these radionuclides in chemically compatible form. The approach used in these experiments differed somewhat from that used for the mixtures of ^{14}C and ^{63}Ni, where mixed radionuclide sources were prepared from singe-radionuclide stock solutions. In the latest experiment, series of mixture solutions were prepared for each radionuclide pair and two counting sources prepared from each mixture solution. The compositions were expressed as activity concentrations rather than as activities for easy comparison of results obtained from different sources of the same mixture solution.

5.2 Stock solutions and the preparation of dilutions, mixtures and counting sources

The approach followed in the experiment is summarised in Fig. 5.1. Stock solutions of ^{32}P, ^{33}P and ^{35}S were purchased from AEC-Amersham and diluted in two steps to give solutions which were suitable for further work. Mixtures with different activity ratios were prepared from each pair of radionuclides by combining masses of the dilutions as summarised in Table 5.1. Liquid scintillation (LS) counting sources were prepared from each dilution and mixture solution. The activity concentration of each dilution was determined by conventional means as described in Section 5.4. The mixed radionuclide solutions were measured with the new method, mainly using appropriate sources of ^{33}P and ^{35}S as tracers, as described in Section 5.6.

The liquid scintillation cocktail to be used in the entire experiment was made up in a single batch to minimise differences in quenching due to variation in the cocktail composition. The cocktail consisted of 3 ml of 3 M HCl added to 1 litre of Quicksafe A from Zinsser Analytic. Counting sources were prepared by adding accurately weighed aliquots of the dilutions or mixtures to 12 ml liquid scintillation cocktail in Wheaton scintillation vials and mixing thoroughly. Sources were stored in the dark, at least overnight, before measurement. $CHCl_3$ was added as a quenching agent to some of the sources to reduce afterpulsing and to study the effect of the reduction of the counting efficiency on mixture resolution.

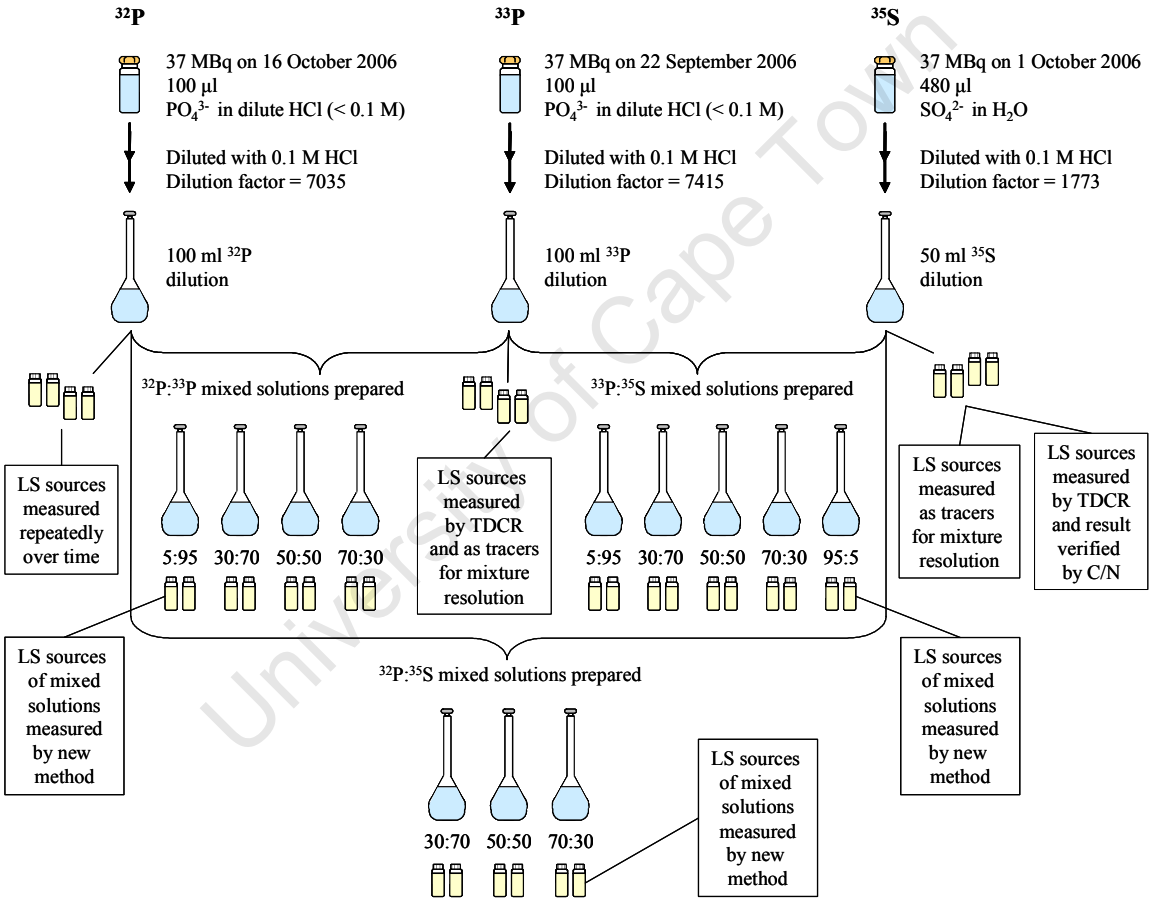

Fig. 5.1 Flow diagram summarising the experimental procedure followed. The numbers given with the mixture solutions indicate the approximate activity compositions at the measurement reference date.

Table 5.1 Mixtures prepared using the dilutions of ^{32}P, ^{33}P and ^{35}S.

Source	Mass ^{32}P (g)	Mass ^{33}P (g)	Mass ^{35}S (g)	Total mass (g)
^{33}P:^{35}S (5:95)		0.19172	3.26483	3.45655
^{33}P:^{35}S (30:70)		0.90680	2.22347	3.13027
^{33}P:^{35}S (50:50)		1.55496	1.62933	3.18429
^{33}P:^{35}S (70:30)		2.01415	0.90378	2.91793
^{33}P:^{35}S (95:5)		3.31048	0.16069	3.47117
^{32}P:^{33}P (5:95)	0.11197	2.75313		2.86510
^{32}P:^{33}P (30:70)	0.70123	2.95257		3.65380
^{32}P:^{33}P (50:50)	1.20367	2.07502		3.27869
^{32}P:^{33}P (70:30)	1.70636	1.22080		2.92716
^{32}P:^{35}S (30:70)	0.72566		1.89821	2.62387
^{32}P:^{35}S (50:50)	1.16679		1.40846	2.57525
^{32}P:^{35}S (70:30)	1.77248		0.84352	2.61601

5.3 Computer programs used for data processing

The scintillator Quicksafe A was used in this series of measurements instead of Insta-Gel Plus that was used in the previous experiment. It was thus necessary to use data analysis programs which account for the ionisation quenching effect of this specific scintillator rather than INPDATH and INPLUSF, which were developed for Insta-Gel Plus and were described in Sections 4.4.2 and 4.4.3.

The mass composition of Quicksafe A was determined by C, H, N & S analysis by means of a Carlo Erba NA 1500 C/N/S analyser, which makes use of gas chromatography to separate the gases produced on total combustion of a sample. The instrument in the C and N configuration was modified to determine H as well, while S was determined a few days later in the C, N and S configuration. The mass composition obtained was 77.3 % carbon, 10.08 % hydrogen, 0.53 % nitrogen and 0 % sulphur, with the remainder (12.09 %) taken to be oxygen. The mass composition translates to an atomic composition of $C_{37.4}H_{58.0}N_{0.2}O_{4.4}$. This agrees quite well with the atomic composition estimated previously for Insta-Gel from Packard, $C_{38.4}H_{56.7}O_{4.9}$, for the development of the programs BETINST (for TDCR data analysis) and BETATDI (for the calculation of double- and triple-coincidence detection efficiencies in terms of the figure-

of-merit, P). The latter atomic composition was obtained [2] from an estimate based on densities for Insta-Gel ($\rho = 0.9440$ g/ml) to be made up of 52.04 % per mass of the solvent *p*-xylene (C_8H_{10}, $\rho = 0.8541$ g/ml) and 47.96 % of the surfactant Triton X-100 ($C_{34}H_{62}O_{11}$, $\rho = 1.065$ g/ml). The ionisation quenching function, $Q(E)$, was calculated for the molecular formula of Insta-Gel and $kB = 0.0100\,\mathrm{g/(cm^2 MeV)}$ using a locally developed program IONQUEN. The values obtained for different energies were fitted with the rational function

$$Q(E) = \frac{A + B\log E + C(\log E)^2}{1 + D\log E + F(\log E)^2} \tag{5.1}$$

to give the coefficients A = 0.317425, B = 0.129990, C = 0.0155697, D = – 0.463361 and F = 0.164501, with $\log E$ the decimal logarithm of the energy in units of keV. The programs BETINST and BETATDI were used for Quicksafe A without any modification.

5.4 Measurement of the individual radionuclide solutions

All sources were measured in the NMISA three-phototube detection system described in Section 4.3 and shown schematically in Fig. 4.1, with a few modifications. The RCA 8850 phototube number 3 was replaced by a new BURLE 8850 high-gain phototube. In addition, an attenuator was placed at the input to the TSCA of channel 3 to reduce noise. Before each series of measurements, the detection system was reproducibly set up in terms of phototube efficiency matching using a source of the low-energy β-emitter ^{63}Ni. This entailed adjusting the electronics so that the maximum of the single electron peak was at channel 430 out of 1024 on the multichannel analyser for all three phototube channels and setting the counting thresholds just below the single electron peak. For counting, sources were placed into the detection system in the dark, illumination provided only by red light, to prevent the phototubes and sources from being exposed to white light. The positions of the sources of interest were adjusted relative to the phototubes to match the double-coincidence count rates to within 0.5 % after correcting for the background and afterpulses when present. A typical pulse height spectrum obtained from a ^{33}P source is given in Fig. 5.2.

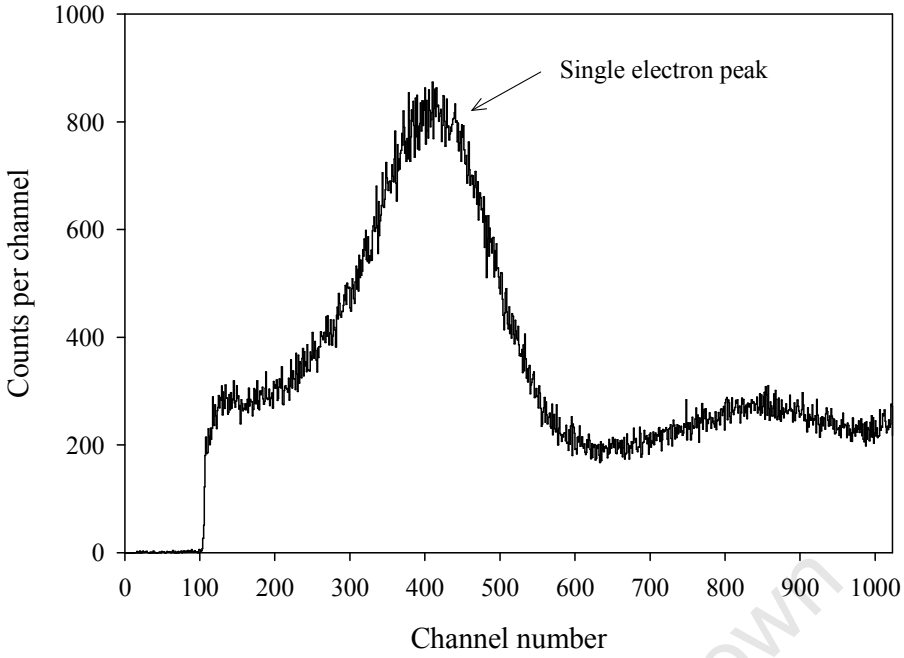

Fig. 5.2 β spectrum of ^{33}P collected with phototube 1 showing the first few monopeaks.

5.4.1 The activity measurement of ^{33}P and ^{35}S

The ^{33}P and ^{35}S solutions were expected to be free of impurities and the activities of the solutions were measured by the TDCR efficiency calculation technique to establish the activities. This method had been previously used and verified for ^{33}P [3].

For the measurement of ^{33}P, three sources containing between 41.4 and 62.1 mg of the dilution were prepared, giving count rates of 1 800 to 2 800 s^{-1}. Each source was counted for six intervals of 300 seconds each. The counting data was analysed with the program BETINST. As before, the counts were corrected for background, deadtime (τ_D = 1.0 μs) and coincidence resolving time (τ_R = 0.47 μs). Afterpulsing was measured simultaneously with the data collection and was found to be essentially zero. The activity concentration of the solution was determined as 46.67 ± 0.23 kBq/g at 12h00 on 29 September 2006. The uncertainty specified is the standard combined uncertainty. Data analysis gave the figure-of-merit as P = 0.1459 e/keV.

^{35}S was measured in the same way as ^{33}P. Three sources were prepared, containing between 54.3 and 58.7 mg of the dilution and giving count rates of 1 900 to 2 100 s^{-1}. Data analysis gave the activity concentration of the solution as 43.23 ± 0.22 kBq/g at 12h00 on 29 September 2006, with the uncertainty specified being the standard combined uncertainty. The figure-of-merit extracted by the analysis was P = 0.1507 e/keV.

Since this was the first time that ^{35}S had been measured by the TDCR technique in this laboratory, the result obtained was verified by using a variation of the CIEMAT/NIST method. The sources measured for the ^{33}P standardisation were treated as external tracer standards of similar quench to the ^{35}S sources of interest. In addition, two ^{63}Ni tracer standards were prepared and measured in between the ^{35}S and ^{33}P sources. TDCR analysis of the data collected for the ^{63}Ni sources provided an activity concentration for the solution that agreed with a previous measurement to within 0.7 % and gave the figure-of-merit as P = 0.1623 e/keV. The double-coincidence detection efficiencies of ^{35}S were calculated for the values of P determined from the ^{33}P and ^{63}Ni sources, using the program BETATDI. The ^{35}S activity concentrations, A, were then calculated from

$$A = N_d / (\varepsilon_d m), \tag{5.2}$$

where N_d is the double-coincidence count rate measured for ^{35}S, ε_d is the double-coincidence detection efficiency calculated from the tracer and m is the source mass. The results obtained by this exercise are summarised in Table 5.2 and show that the activity concentrations obtained agree with the TDCR result to within the experimental uncertainty.

Table 5.2 Sources of ^{63}Ni and ^{33}P were used as tracers to verify the activity concentration of ^{35}S obtained by the TDCR method. For each tracer standard the figure-of-merit, P, was obtained from TDCR measurements and the ^{35}S detection efficiency calculated for this value of P.

Tracer	P (e/keV)	ε_d ($s^{-1}Bq^{-1}$)	^{35}S activity concentration (kBq/g)	Deviation (%)
^{63}Ni	0.1623	0.8310	43.03	– 0.46
^{33}P	0.1459	0.8227	43.47	0.55

5.4.2 The activity measurement of ^{32}P

Since the ^{32}P solution contained possible impurities of ^{33}P and ^{35}S, the solution was measured repeatedly over an extended period of time taking advantage of the differences in the decay rates ($T_{½}$ = 14.284 days, 25.383 days and 87.320 days respectively for ^{32}P, ^{33}P and ^{35}S [1]) to extract the individual activities. The method [4], summarised below, was the one implemented by the NMISA laboratory in the international key comparison of ^{32}P activity measurements organised by the International Bureau of Weights and Measures (BIPM) in 2005.

If C_1, C_2 and C_3 are the count rates per unit mass of the three components of the solution at a given reference date, then the count rate concentration of the solution at a time t after the reference date, $C(t)$, can be expressed as

$$C(t) = C_1 e^{-\lambda_1 t} + C_2 e^{-\lambda_2 t} + C_3 e^{-\lambda_3 t}. \tag{5.3}$$

The decay correction factors, $e^{-\lambda_i t}$, account for the decay of each component to the specific measurement date, with $\lambda_i = \ln(2)/T_{½}$ the respective decay constants. The individual reference count rate concentrations are given by

$$C_i = A_i \varepsilon_i / m \text{, for } i = 1 \text{ to } 3, \tag{5.4}$$

where A_i represents the disintegration rate of each component on the reference date, ε_i the detection efficiency for each radionuclide and m the specific source mass. The method assumes that the detection efficiencies are the same for all sources over the complete measurement time. Although this is difficult to achieve in practice, variation of the efficiency was minimised by duplicating source preparation and counting conditions as closely as possible.

^{32}P counting sources were prepared from the masses of the dilution given in Table 5.3, with 1 ml of $CHCl_3$ added to each source to reduce the production of afterpulses. The sources were prepared and measured on the dates given in Table 5.3 so that 108 repeat measurements of the solution were made over a decay time of 46 days. Afterpulsing was measured simultaneously with the counting for each of the three double-coincidence channels in turn. Fewer afterpulses were recorded for the new phototube (with an attenuator) so that the afterpulse corrections for channels 2 and 3 (coincidences between $\beta_2 - \beta_3$ and $\beta_1 - \beta_3$) were lower than those of channel 1 (coincidences between $\beta_1 - \beta_2$). The corrections applied were approximately (0.8, 0.3 and 0.2) % for channels (1, 2 and 3) respectively. The program TDRAW was used to correct

Table 5.3 Eight sources were prepared and measured to determine the activity concentration of the ^{32}P solution with impurities of ^{33}P and ^{35}S. Sources 1 to 3 were prepared on 18 October 2006 and each of the remaining sources was prepared on the day before the first measurement of the specific source. The measurements of the sources on the different days are summarised in the table. For the first six measurement days, each measurement consisted of a count collected in 300 seconds with the count rates varying between 1 700 and 3 700 s^{-1}. Thereafter, sources were measured for intervals of 900 seconds each, with count rates between 360 and 1 600 s^{-1}, to ensure good counting statistics.

Source number	1	2	3	4	5	6	7	8
Source mass (mg)	42.141	39.960	49.680	71.046	94.309	75.453	83.274	91.022
Measurement date	Number of repeat measurements per day							
23 October 2006	4	3	5					
25 October 2006				3	3			
27 October 2006				3	3			
30 October 2006				3	3			
1 November 2006				3	3			
3 November 2006				3	3	3		
7 November 2006				3		3		
10 November 2006				3		3		
13 November 2006				3		3		
17 November 2006				3		3	3	
20 November 2006				3		3	3	
24 November 2006						3	3	3
1 December 2006						3	3	3
8 December 2006						3	3	3

the counting data for background, deadtime (τ_D = 1.0 μs), coincidence resolving time (τ_R = 0.47 μs) and afterpulsing and gave the corrected average double- and triple-coincidence count rates and the respective statistical uncertainties as output.

For both the double- and triple-coincidence count rates, sets of paired data comprising the corrected count rate concentrations, $C(t_i)$, and the times, t_i, between the reference and measurement dates for each measurement were fitted to Eq. (5.3) by means of a weighted least-squares fitting procedure whereby

$$Q = \sum_{i=1}^{108} w_i \left[C(t_i) - C_1 e^{-\lambda_1 t_i} - C_2 e^{-\lambda_2 t_i} - C_3 e^{-\lambda_3 t_i} \right]^2 \qquad (5.5)$$

was minimised [4]. The weights, $w_i = 1/\sigma_i^2$, were obtained from the statistical uncertainties, σ_i, of the measured count rate concentrations. The fitting was performed by a Fortran program EXP3FIT that determined the coefficients, C_1, C_2 and C_3, for which Q was minimised. These coefficients estimated the count rate concentrations of each component of the solution. The two data sets were similarly fitted with a function of the form

$$C(t) = C_1 e^{-\lambda_1 t} + C_2 e^{-\lambda_2 t}, \qquad (5.6)$$

i.e., a mixture containing only ^{32}P and ^{33}P, by means of the program EXP2FIT.

The coefficient count rate concentrations were converted to activities by comparison with ^{33}P standard sources which were measured in between the ^{32}P sources. In all, fourteen measurements were made of four different ^{33}P sources. The average figure-of-merit obtained for the system was P = 0.0655 e/keV. Double- and triple-coincidence detection efficiencies were calculated for this value of P for all three component radionuclides using the program BETATDI and gave: for ^{32}P (ε_d = 0.9911, ε_t = 0.9892), for ^{33}P (ε_d = 0.7878, ε_t = 0.7460) and for ^{35}S (ε_d = 0.6679, ε_t = 0.6070), in units of $s^{-1}Bq^{-1}$. Dividing the coefficients by the respective efficiencies gave the activity concentration compositions of the solution for the four data analysis sets. The results are given in Table 5.4.

Table 5.4 The ^{32}P compositions obtained from four different fits to the experimental data are given on the reference date of 23 October 2006, 12h00. The uncertainties shown are statistical only.

Radionuclide	Activity concentration from double-coincidence data (kBq/g)		Activity concentration from triple-coincidence data (kBq/g)	
	2-component fit	3-component fit	2-component fit	3-component fit
^{32}P	43.07 ± 0.01	43.16 ± 0.04	42.74 ± 0.02	42.67 ± 0.06
^{33}P	0.58 ± 0.01	0.43 ± 0.06	0.70 ± 0.01	0.82 ± 0.11
^{35}S		0.06 ± 0.02		− 0.05 ± 0.04

The reduced chi-square values for the fits to the double-coincidence data were 7.8 and for the fits to the triple-coincidence data the reduced chi-square values were 2.7. The smaller values indicated that the triple-coincidence data fit the decay curve better. The additional variation

observed for the double-coincidence counts is probably due to uncertainty in the relatively large afterpulse corrections, which were not required for the triple-coincidence data. The fit to the triple-coincidence data was not as good as the one obtained in Ref. [4], where a reduced chi-square value of 1.28 indicated an excellent fit to the double-coincidence data. The additional variation observed in the present counting data could be due to gradual adsorption taking place in the counting sources which were measured repeatedly over a longer time period (up to 5 weeks), larger differences in phototube matching and variation in the amount of solution used to prepare the respective sources. Because the impurity content of the solution was low, the decay curve deviated only slightly from the decay of pure ^{32}P and it was difficult to determine the impurity concentrations with great accuracy. The results obtained were nevertheless more than adequate for the present demonstration.

Since the ^{35}S content given by both 3-component fits were essentially zero and the fits to the triple-coincidence count rates were better, the result of the two-component fit to the triple-coincidence data was used as a reference composition and the remaining values were used to estimate the uncertainty due to the fit. This gave the activity concentration of the solution as 42.74 ± 0.30 kBq/g ^{32}P and 0.70 ± 0.23 kBq/g ^{33}P on 23 October 2006, 12h00. The uncertainties specified are the standard combined uncertainties.

5.5 Preamble to mixture resolution

5.5.1 Summary of the gravimetric activity concentrations of the mixed radionuclide solutions

The activity concentrations of the mixture solutions were calculated algebraically from those determined for the original dilutions by taking into account the mass portions weighed out, as detailed further. The results obtained from the measurement of the mixed solutions were subsequently compared against these gravimetrically determined activity compositions (i.e. gravimetric compositions), which are summarised in Table 5.5.

For the ^{33}P:^{35}S mixtures the activity concentrations of the dilutions used were $A(^{33}\mathrm{P}) = 46.67$ kBq/g and $A(^{35}\mathrm{S}) = 43.23$ kBq/g on the reference date of 12h00 on 29 September 2006. For the ^{32}P-containing mixtures the reference date of 12h00 on 23 October 2006 was used so that $A(^{33}\mathrm{P}) = 24.23$ kBq/g, $A(^{35}\mathrm{S}) = 35.73$ kBq/g and $A(^{32}\mathrm{P}) = 42.74$ KBq/g, with the activity

Table 5.5 The gravimetric compositions of the ^{33}P:^{35}S mixed radionuclide solutions are given on the reference date of 29 September 2006 and the gravimetric compositions of the ^{32}P:^{33}P and ^{32}P:^{35}S mixed radionuclide solutions on the reference date of 23 October 2006. For the calculation of the total activity and the % activity compositions of the ^{32}P:^{35}S mixtures the ^{33}P impurity was ignored so that a two-component mixture could be assumed. For these mixtures the impurity was accounted for in the counting data.

Source	$A_G(^{32}\mathrm{P})$ (kBq/g)	$A_G(^{33}\mathrm{P})$ (kBq/g)	$A_G(^{35}\mathrm{S})$ (kBq/g)	$A_G(\mathrm{Total})$ (kBq/g)	^{32}P (%)	^{33}P (%)	^{35}S (%)
^{33}P:^{35}S (5:95)		2.59	40.84	43.42		5.96	94.04
^{33}P:^{35}S (30:70)		13.52	30.71	44.23		30.57	69.43
^{33}P:^{35}S (50:50)		22.79	22.12	44.91		50.74	49.26
^{33}P:^{35}S (70:30)		32.22	13.39	45.61		70.64	29.36
^{33}P:^{35}S (95:5)		44.51	2.00	46.51		95.70	4.30
^{32}P:^{33}P (5:95)	1.67	23.31		24.98	6.68	93.32	
^{32}P:^{33}P (30:70)	8.20	19.72		27.92	29.38	70.62	
^{32}P:^{33}P (50:50)	15.69	15.59		31.28	50.15	49.85	
^{32}P:^{33}P (70:30)	24.91	10.51		35.43	70.32	29.68	
^{32}P:^{35}S (30:70)	11.82	0.19	25.85	37.67	31.37		68.63
^{32}P:^{35}S (50:50)	19.36	0.32	19.54	38.91	49.77		50.23
^{32}P:^{35}S (70:30)	28.96	0.47	11.52	40.48	71.53		28.47

concentration of the impurity in the ^{32}P solution being $A'(^{33}\mathrm{P}) = 0.70$ kBq/g. For each mixture solution a mass m_1 of the higher energy emitter was mixed with a mass m_2 of the lower energy emitter to prepare a mass $m_{\mathrm{total}} = m_1 + m_2$ of the mixture. The masses used are given in Table 5.1. The gravimetric activity concentrations, $A_G(^{33}\mathrm{P})$ and $A_G(^{35}\mathrm{S})$, were calculated for the ^{33}P:^{35}S mixtures from

$$A_G(^{33}\mathrm{P}) = A(^{33}\mathrm{P})m_1/m_{\mathrm{total}} \text{ and } A_G(^{35}\mathrm{S}) = A(^{35}\mathrm{S})m_2/m_{\mathrm{total}}\,. \tag{5.7}$$

For the ^{32}P:^{33}P mixtures, the gravimetric activity concentrations, $A_G(^{32}\mathrm{P})$ and $A_G(^{33}\mathrm{P})$, were calculated from

$$A_G(^{32}\mathrm{P}) = A(^{32}\mathrm{P})m_1/m_{\mathrm{total}} \text{ and } A_G(^{33}\mathrm{P}) = \left[A(^{33}\mathrm{P})m_2 + A'(^{33}\mathrm{P})m_1\right]/m_{\mathrm{total}}\,, \tag{5.8}$$

where the ^{33}P impurity from the ^{32}P solution was simply added to the ^{33}P activity from the ^{33}P solution. For the ^{32}P:^{35}S mixtures, the gravimetric activity concentrations were calculated from

$$A_G(^{32}\mathrm{P}) = A(^{32}\mathrm{P})m_1/m_{\mathrm{total}} \text{ and } A_G(^{35}\mathrm{S}) = A(^{35}\mathrm{S})m_2/m_{\mathrm{total}}\,, \tag{5.9}$$

with the ^{33}P impurity being given by

$$A_G\left(^{33}\mathrm{P}\right) = A'\left(^{33}\mathrm{P}\right) m_1 / m_{\text{total}} \,. \tag{5.10}$$

The latter activity concentration was used to correct the acquired ^{32}P:^{35}S count rates for the contribution of the ^{33}P impurity so that a two-component system could be assumed.

5.5.2 Notation used

Throughout this chapter, the convention adopted when referring to characteristics of two-radionuclide mixtures in terms of symbols is that unprimed symbols are used for the higher energy radionuclide and the same symbols primed are used for the lower energy radionuclide. For example, A_0, ε_d, ε_t and λ refer to the activity concentration, double- and triple-coincidence detection efficiencies and decay constant of the higher energy component and A_0', ε_d', ε_t' and λ' refer to the same characteristics of the lower energy component. Where compositions are expressed as fractions, $r = A_0/\left(A_0 + A_0'\right)$ and $\left(1-r\right) = A_0'/\left(A_0 + A_0'\right)$.

5.5.3 TDCR parameter computation

To aid in the visualisation of the concept of the method for mixtures of β-emitters with different spectral energies, plots of N_t/N_d vs. P were generated for the three pure components ^{32}P, ^{33}P and ^{35}S (Fig. 5.3A) as well as for various mixtures of the three radionuclide pairs (Fig. 5.3B-D) as described in Section 3.3. It can be seen from Fig. 5.3A that the line for the high-energy β-emitter ^{32}P is almost straight and horizontal, curving slightly downwards at a very low figure-of-merit. The ratio N_t/N_d reaches a minimum of 0.99 at P = 0.02 e/keV. As the β energy of the radionuclide decreases, the slope of the line at high P and the downward curvature at lower P increases so that N_t/N_d = 0.80 for ^{33}P and N_t/N_d = 0.70 for ^{35}S at 0.02 e/keV. For Plots 5.3B, C and D, continua of lines are in fact possible, as the fractional compositions change from r = 0 to r = 1, i.e., incrementally from one pure component to the other.

A
Curves for pure ^{32}P, ^{33}P and ^{35}S

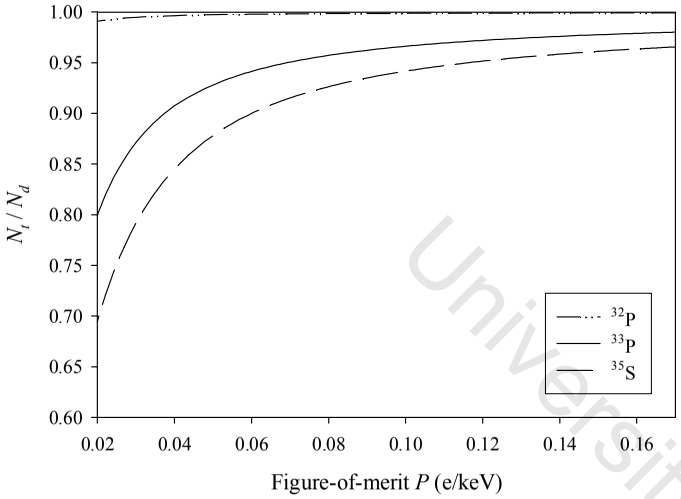

B
^{33}P:^{35}S mixtures

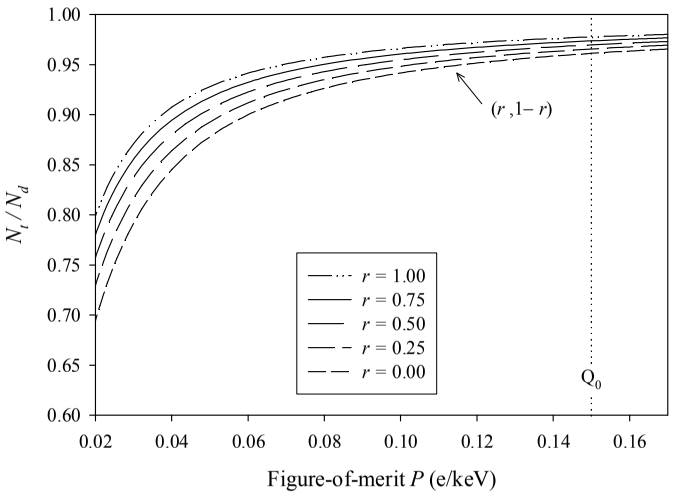

C
^{32}P:^{33}P mixtures

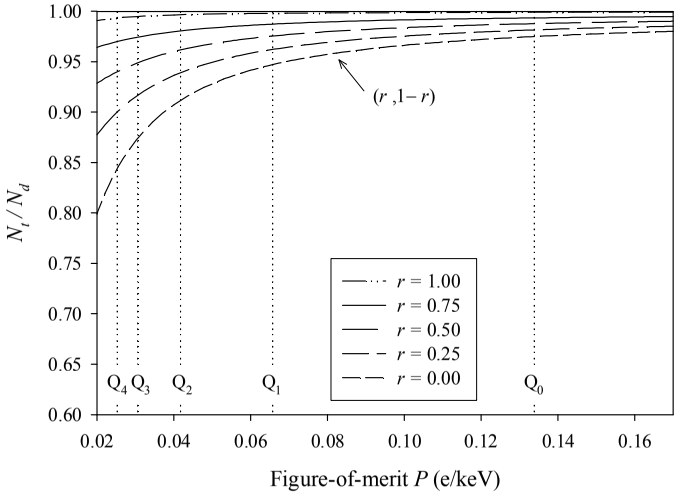

D
^{32}P:^{35}S mixtures

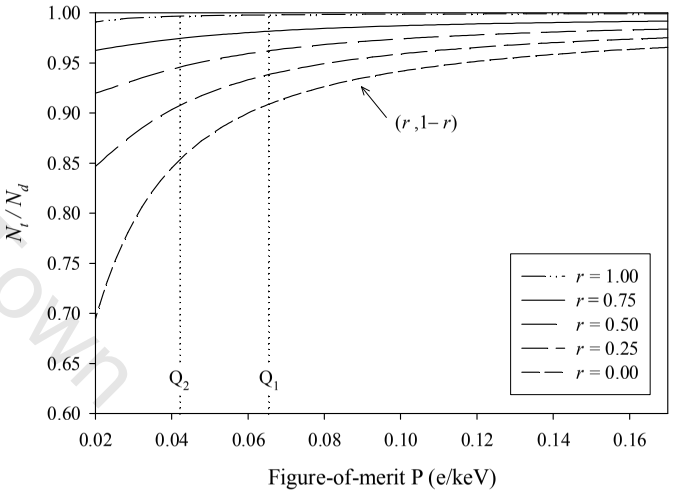

Fig. 5.3 The curves demonstrating the relationship between N_t/N_d and P for ^{32}P, ^{33}P, ^{35}S and various two-component mixtures of these radionuclides. On Plots B – D, r indicates the activity fraction of the high energy component and Q_i the quench state where measurements were undertaken, with Q_i indicating that "i" ml of $CHCl_3$ was added to the sources.

5.6 The measurement of mixtures

5.6.1 The measurement of mixtures of ^{33}P and ^{35}S

Two sources were prepared from each of the five ^{33}P:^{35}S mixture solutions. Each source contained between 38.3 and 65.0 mg of mixed radionuclide solution so that the double-coincidence count rates varied between 1 000 and 2 000 s^{-1}. The sources prepared from the^{33}P:^{35}S (70:30) mixture were selected for a preliminary, detailed investigation, and were measured together with pure sources of ^{63}Ni, ^{35}S and ^{33}P as tracers to estimate the figure-of-merit of the mixture sources. The sources were measured on two separate days and for each day the figure-of-merit was determined from each of the three tracers by analysing the individual radionuclide counting data with the program BETINST. For all measurements the afterpulse correction was consistent with zero. The data collected for the mixed radionuclide sources were corrected for background, deadtime (τ_D = 1.0 μs) and coincidence resolving time (τ_R = 0.47 μs) using the program TDRAW, which provided the double- and triple-coincidence count rates, N_d and N_t, required for further analysis. The program BETATDI was used to calculate the double- and triple-coincidence detection efficiencies for ^{33}P and ^{35}S for each value of P extracted from the tracer measurements. The efficiencies obtained are given in Table 5.6.

The activity concentrations on the reference date, A_0 and A_0', were calculated from

$$A_0 = N_0\left(\frac{e^{-\lambda t'}}{m}\right) = \left(\frac{N_t\varepsilon_d' - N_d\varepsilon_t'}{\varepsilon_t\varepsilon_d' - \varepsilon_d\varepsilon_t'}\right)\left(\frac{e^{-\lambda t'}}{m}\right) \tag{5.11}$$

and

$$A_0' = N_0'\left(\frac{e^{-\lambda' t'}}{m}\right) = \left(\frac{N_d\varepsilon_t - N_t\varepsilon_d}{\varepsilon_t\varepsilon_d' - \varepsilon_d\varepsilon_t'}\right)\left(\frac{e^{-\lambda' t'}}{m}\right), \tag{5.12}$$

where the source activities N_0 and N_0' are given by Eqs. (3.3) and (3.4) from Chapter 3 and the second term transforms activities to activity concentrations on a specific reference date. This facilitates the comparison of results from sources prepared from the same solution but measured at times t' after the reference date. For the calculation of statistical uncertainties, Eqs. (3.19) and (3.20) from Chapter 3 were similarly adapted to give the statistical uncertainties of the extracted activity concentrations on the reference date:

Table 5.6 The figure-of-merit and double- and triple-coincidence detection efficiencies used to resolve mixtures of ^{33}P:^{35}S. The ^{33}P:^{35}S (70:30) sources were measured on 29 September and 6 October using ^{63}Ni, ^{35}S and ^{33}P as tracers. The remaining mixtures were measured on 10 – 12 October using ^{35}S as a tracer.

Measurement date	Tracer	P (e/keV)	$\varepsilon_d(^{33}\mathrm{P})$ ($s^{-1}Bq^{-1}$)	$\varepsilon_t(^{33}\mathrm{P})$ ($s^{-1}Bq^{-1}$)	$\varepsilon_d(^{35}\mathrm{S})$ ($s^{-1}Bq^{-1}$)	$\varepsilon_t(^{35}\mathrm{S})$ ($s^{-1}Bq^{-1}$)
29 September 2006	^{36}Ni	0.1623	0.9018	0.8831	0.8370	0.8069
29 September 2006	^{35}S	0.1512	0.8958	0.8759	0.8276	0.7957
29 September 2006	^{33}P	0.1474	0.8936	0.8733	0.8241	0.7915
6 October 2006	^{36}Ni	0.1619	0.9017	0.8829	0.8367	0.8066
6 October 2006	^{35}S	0.1536	0.8972	0.8776	0.8298	0.7983
6 October 2006	^{33}P	0.1513	0.8959	0.8760	0.8277	0.7958
10 October 2006	^{35}S	0.1477	0.8938	0.8735	0.8244	0.7918
11 & 12 October 2006	^{35}S	0.1487	0.8944	0.8742	0.8253	0.7930

$$\sigma(A_0)=\sqrt{\left(\frac{\varepsilon_d'-\varepsilon_t'}{t\left(\varepsilon_t\varepsilon_d'-\varepsilon_d\varepsilon_t'\right)}\right)^2 T+\left(\frac{\varepsilon_t'}{t\left(\varepsilon_t\varepsilon_d'-\varepsilon_d\varepsilon_t'\right)}\right)^2\left(\frac{X}{3}\right)}\times\left(\frac{e^{-\lambda t'}}{m}\right), \tag{5.13}$$

$$\sigma(A_0')=\sqrt{\left(\frac{\varepsilon_d-\varepsilon_t}{t\left(\varepsilon_t'\varepsilon_d-\varepsilon_d'\varepsilon_t\right)}\right)^2 T+\left(\frac{\varepsilon_t}{t\left(\varepsilon_t'\varepsilon_d-\varepsilon_d'\varepsilon_t\right)}\right)^2\left(\frac{X}{3}\right)}\times\left(\frac{e^{-\lambda' t'}}{m}\right). \tag{5.14}$$

The triple-coincidence counts, T, and the average exclusive double-coincidence counts, X, collected in a counting time t are used, where

$$X=\left(X_1+X_2+X_3\right)/3=\left[\left(D_1+D_2+D_3\right)/3\right]-T, \tag{5.15}$$

with D_i being the double-coincidence counts collected for each channel and X_i the corresponding exclusive double-coincidence counts per channel.

The average of 13 measurements made on 29 September 2006 and the average of 12 measurements made on 6 October 2006 are summarised in Table 5.7 for the three different tracers used to determine the figure-of-merit. The various tracers gave results that varied from one another, particularly those from ^{63}Ni, with those from ^{35}S giving excellent agreement between the gravimetric source composition and the activity concentrations extracted by the method. The variation obtained with the different tracers indicates a possible deficiency in one or other aspect of the model used to calculate the efficiencies, although small differences in chemical quenching between the various sources could also have contributed to the variation. The effect of these inconsistencies is minimised when the tracer

Table 5.7 Activity concentrations, A_0 and A_0', extracted for the mixture solution ^{33}P:^{35}S (70:30) are compared for different tracer standards used. The gravimetrically determined composition of the solution is $A_G(^{33}\mathrm{P}) = 32.22$ kBq/g and $A_G(^{35}\mathrm{S}) = 13.39$ kBq/g. All concentrations are given on the reference date of 29 September 2006, 12h00.

Measure-ment date	29 September 2006			6 October 2006		
Tracer	P (e/keV)	$A_0(^{33}\mathrm{P})$ (kBq/g)	$A_0'(^{35}\mathrm{S})$ (kBq/g)	P (e/keV)	$A_0(^{33}\mathrm{P})$ (kBq/g)	$A_0'(^{35}\mathrm{S})$ (kBq/g)
^{63}Ni	0.1623	26.73	18.89	0.1619	28.23	16.78
^{35}S	0.1512	32.12	13.45	0.1536	32.42	13.11
^{33}P	0.1474	33.99	11.57	0.1513	33.60	12.07

standard used is the same as the low energy component of the mixture. The results extracted from the individual (70:30) source measurements, using ^{35}S as a tracer, are given together with the predicted statistical uncertainties in the fourth row of plots in Fig. 5.4.

The remaining ^{33}P:^{35}S mixed sources were measured over three days using two ^{35}S sources as tracers. For each mixture, one source was measured thrice for three intervals of 300 seconds each and the other source twice for three intervals of 300 seconds each so that each mixture was measured 15 times. The data were analysed in the same way as the ^{33}P:^{35}S (70:30) data. The result of each individual measurement is displayed in Fig. 5.4. For each solution the average measured values can be compared with the prepared gravimetric activity concentrations in Fig. 5.4 and in Table 5.8. The table also gives uncertainty estimates that are primarily due to counting statistics (shown in Fig. 5.4) and possible differences in quenching between the mixture and tracer sources leading to variation in the actual figure-of-merit used. For this mixture combination, the deviations from the prepared activities were not significantly different from those expected based on uncertainties. The results show excellent agreement between the prepared and extracted activity concentrations for all mixtures except for the mixture containing only 5% ^{35}S, where the deviations are nevertheless still less than 2 kBq/g.

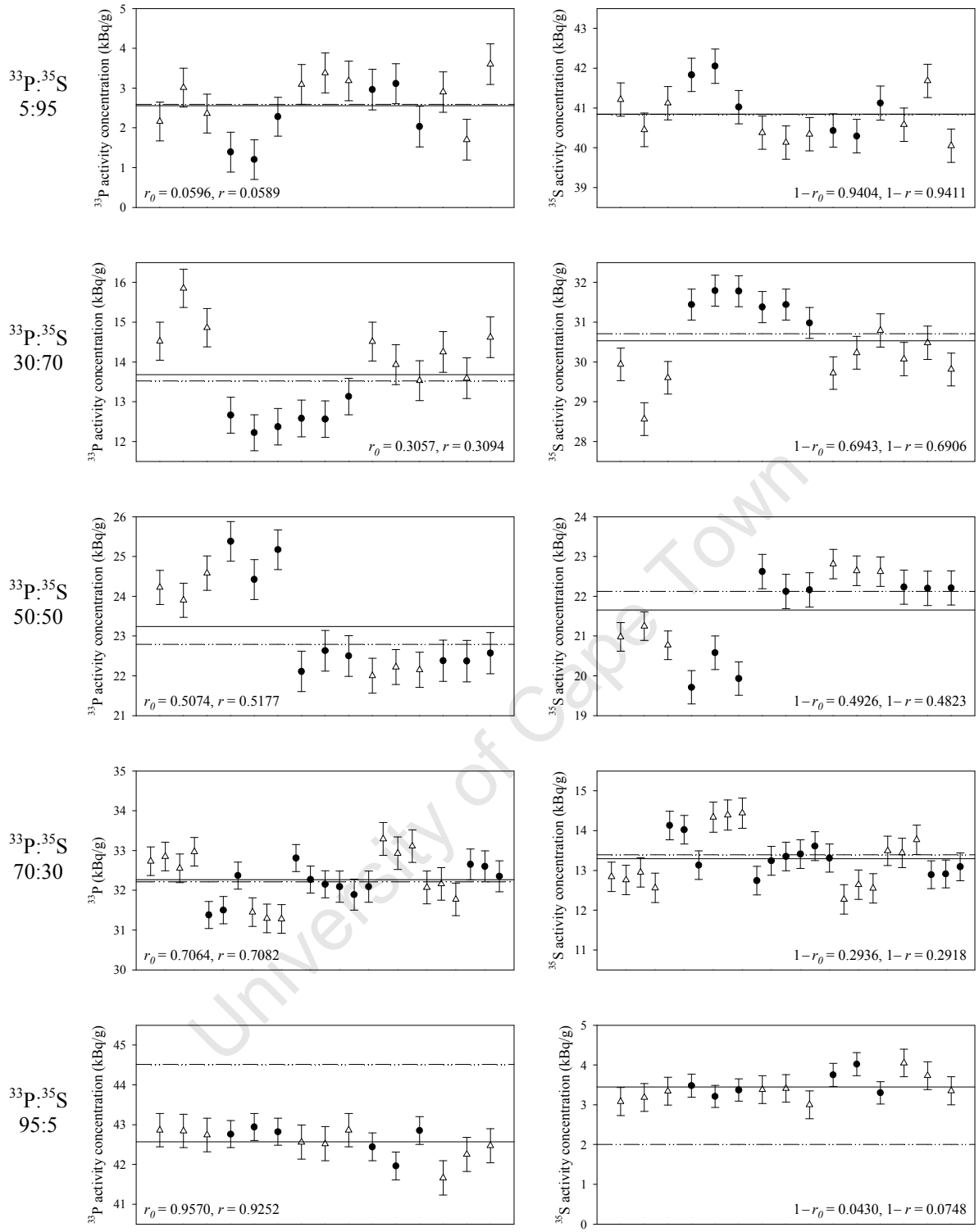

Fig. 5.4 The plots show the activity concentration and statistical uncertainty obtained from each individual measurement of the ^{33}P:^{35}S mixture solutions using ^{35}S as the tracer. Results from two different sources in each case are indicated by unfilled triangles and filled circles respectively. The ^{33}P components are given on the left and the ^{35}S components on the right-hand side. The dash-dot-dotted lines give the gravimetric concentrations and the solid lines the average value of all measurements of the same solution. The ratios, r_0 and r, given on each ^{33}P plot, and the ratios, $(1 - r_0)$ and $(1 - r)$, given on each ^{35}S plot, indicate the gravimetric and measured activity fractions determined for each solution.

Table 5.8 The averaged results of measurements of the ^{33}P:^{35}S mixtures are given, with A_G the gravimetrically determined activity concentrations and A_0 and A_0' the values extracted from measurement using ^{35}S as the tracer. Uncertainty estimates for the extracted activities are indicated by $\Delta(^{33}\mathrm{P})$ and $\Delta(^{35}\mathrm{S})$. The deviations were calculated from $\mathrm{Dev} = [(A_0 - A_G)/A_G] \times 100$.*

Mixture	$A_G(^{33}\mathrm{P})$ (kBq/g)	$A_0(^{33}\mathrm{P})$ (kBq/g)	$\Delta(^{33}\mathrm{P})$ (%)	$\mathrm{Dev}(^{33}\mathrm{P})$ (%)	$A_G(^{35}\mathrm{S})$ (kBq/g)	$A_0'(^{35}\mathrm{S})$ (kBq/g)	$\Delta(^{35}\mathrm{S})$ (%)	$\mathrm{Dev}(^{35}\mathrm{S})$ (%)
5:95	2.59	2.56	11	– 1.18	40.84	40.84	0.52	0.02
30:70	13.52	13.68	1.6	1.17	30.71	30.53	0.62	– 0.57
50:50	22.79	23.24	0.91	1.97	22.12	21.65	0.81	– 2.11
70:30	32.22	32.26	0.55	0.15	13.39	13.29	1.4	– 0.75
95:5	44.51	42.57	0.37	– 4.36	2.00	3.44	5.4	72.03

* A_0 is replaced by A_0' as appropriate.

5.6.2 The measurement of mixtures of ^{32}P and ^{33}P

5.6.2 (a) The measurement of ^{32}P as received

Because it was known from following the decay (see Section 5.4.2) that the ^{32}P solution contained about 1.6 % of ^{33}P as an impurity, the new method was applied to this *mixture* solution to assess its usefulness under these particularly stringent conditions. Previously, measurements of the high-energy β-emitters ^{89}Sr and ^{90}Y [5] had shown that the TDCR method was particularly sensitive to inexact corrections in the flat region of N_t/N_d vs. P curves. This sensitivity was expected to be even more so for mixtures. Since the curve for ^{32}P (r = 1 in Fig. 5.3C) is quite flat, the strategy applied was to quench sources, particularly if afterpulsing was high, to undertake measurements in a more favourable efficiency region.

Three sources containing between 40.0 and 49.7 mg of the ^{32}P dilution were prepared giving double-coincidence count rates of between 1 350 and 2 200 s^{-1}. Source 1 was measured without quenching for four repeats of 300 seconds each, with afterpulsing being monitored simultaneously with the counting for each of the three double-coincidence and triple-coincidence channels in turn. The afterpulse correction for channel 1 was found to be high, with the values measured being (1.71 ± 0.08, 0.19 ± 0.07, 0.19 ± 0.07) % for the double-

coincidence channels (1, 2, 3) and consistent with zero for the triple-coincidences. $CHCl_3$ was then added to all three sources as a quenching agent in increments of 1 ml from 1 ml to 4 ml to reduce the detection efficiency and so also the afterpulsing. The sources were measured in each of the different quench states for 3 to 5 repeats of 300 seconds each. For sources containing 1 ml of $CHCl_3$, the afterpulse corrections applied were (0.69, 0.25, 0.30) % and the corrections reduced to (0.09, 0.07, 0.09) % for sources containing 4 ml of $CHCl_3$. ^{33}P sources, filled with $CHCl_3$ to the same volume as the ^{32}P sources, were measured as well in the role as tracers. For these sources the afterpulse corrections were generally below 0.10 %.

The data analysis was performed as described in Section 5.6.1. From the figures-of-merit determined from the tracer standards, the double- and triple-coincidence detection efficiencies for ^{32}P and ^{33}P were calculated. The values used are summarised in Table 5.9. The result of each individual measurement is given in Fig. 5.5. The results obtained from the unquenched source were particularly poor and showed significant variation between the repeat measurements. An insufficiently accurate afterpulse correction in this flat region (quench Q_0 in Fig. 5.3C) certainly contributed to the large deviations observed. To assess this, the data were re-analysed after increasing the afterpulse corrections by one, two and three times the measured statistical uncertainty. This increased the extracted average ^{32}P activity concentration from 33.49 kBq/g to 37.33 kBq/g and reduced the average extracted ^{33}P activity concentration from 12.52 kBq/g to 7.70 kBq/g. The results are indicated by the unfilled circles in Fig. 5.5.

Table 5.9 The figure-of-merit and double- and triple-coincidence detection efficiencies used to try to resolve the unmixed ^{32}P solution using different quench states.

Quench state	P (e/keV)	$\varepsilon_d\left(^{32}P\right)$ ($s^{-1}Bq^{-1}$)	$\varepsilon_t\left(^{32}P\right)$ ($s^{-1}Bq^{-1}$)	$\varepsilon_d\left(^{33}P\right)$ ($s^{-1}Bq^{-1}$)	$\varepsilon_t\left(^{33}P\right)$ ($s^{-1}Bq^{-1}$)
Q_0	0.1338	0.9956	0.9947	0.8846	0.8624
Q_1	0.0657	0.9912	0.9892	0.7883	0.7466
Q_2	0.0413	0.9855	0.9821	0.6867	0.6254
Q_3	0.0301	0.9790	0.9739	0.5963	0.5197
Q_4	0.0252	0.9741	0.9677	0.5408	0.4563

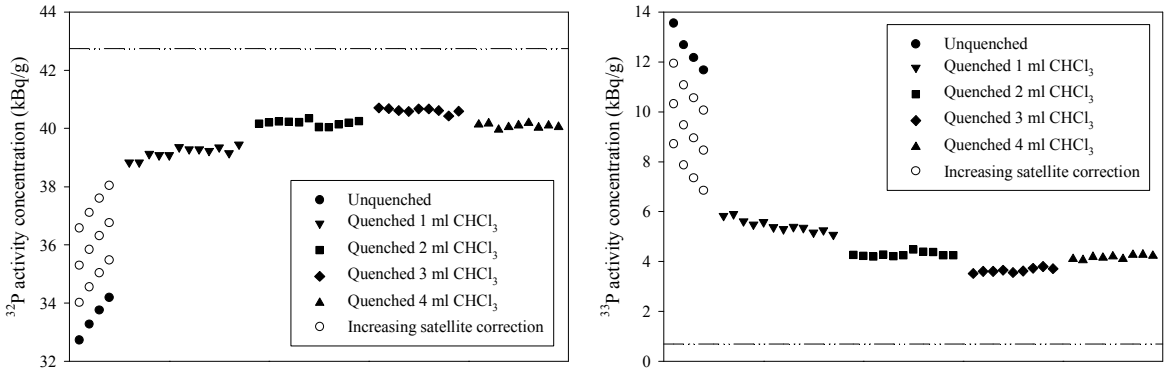

Fig. 5.5 The plots show the activity concentration obtained from each individual measurement of sources prepared from the original ^{32}P dilution in various quench states. The dash-dot-dotted lines show the gravimetric activity concentrations, $A_G\left(^{32}\mathrm{P}\right)$= 42.74 kBq/g, and the impurity $A_G\left(^{33}\mathrm{P}\right)$= 0.70 kBq/g. Black markers give the results with the satellites as measured and the unfilled circles give the results obtained when the satellite corrections were increased by 1 to 3 times the statistical uncertainty.

As can be seen, the results obtained improved with increased quenching, the best agreement with the gravimetric activity concentrations being obtained with the sources quenched with 3 ml of $CHCl_3$, where the ^{32}P activity concentration was under-estimated by 2.5 kBq/g and the ^{33}P activity concentration over-estimated by 3.1 kBq/g. These results are quite reasonable if it is considered that measurements were completed in only a few days, compared with the 46 days required to determine the solution composition by following the decay. With 4 ml of $CHCl_3$ the detection efficiency for the tracer became rather low and the uncertainty in the extracted figure-of-merit increased. In fact the uncertainty of P extracted from the tracer increased from about 0.2 % to about 0.5 % for quenching with up to 3 ml of $CHCl_3$ and increased to 2,5 % for sources containing 4 ml of $CHCl_3$.

5.6.2 (b) The measurement of mixtures of ^{32}P and ^{33}P

Two sources were prepared from each of the four ^{32}P:^{33}P mixture solutions with masses ranging between 59.2 and 101.3 mg of solution per source. Since the previous measurements had confirmed the expectation that better mixture resolution would be obtained by quenching, the sources from the 5:95 mixture were measured with 3 and 4 ml of $CHCl_3$ added and the sources with the more equal mixture fractions each with 2 and 3 ml of $CHCl_3$. Each source was counted for three repeat measurements of 300 seconds each for each quench state. The double-coincidence count rates varied between 1 000 and 1 750 s^{-1}. Afterpulses were again

measured simultaneously with the counting, for each of the three double-coincidence channels in turn. A significant afterpulse contribution was measured for channel 1 (coincidences between $\beta_1 - \beta_2$), with larger corrections generally required for mixtures with higher ^{32}P content and lower quench states. The corrections applied varied between (0.24, 0.13, 0.12) % and (0.06, 0.00, 0.00) % for channels (1, 2, 3). Two ^{33}P sources were prepared and measured in the same quench state as the mixture sources to serve as tracers to estimate the figure-of-merit of the system. The afterpulsing measured for the tracer standards were negligible. Singles spectra from β-channel 1 for each of the three ^{32}P:^{33}P mixtures and for the two pure components were collected from the sources quenched with 3 ml of $CHCl_3$. The spectra, normalised to a source count rate of 2 000 s^{-1}, are given in Fig. 5.6 and show how the single electron peak decreases as the fraction of the high energy radionuclide ^{32}P increases.

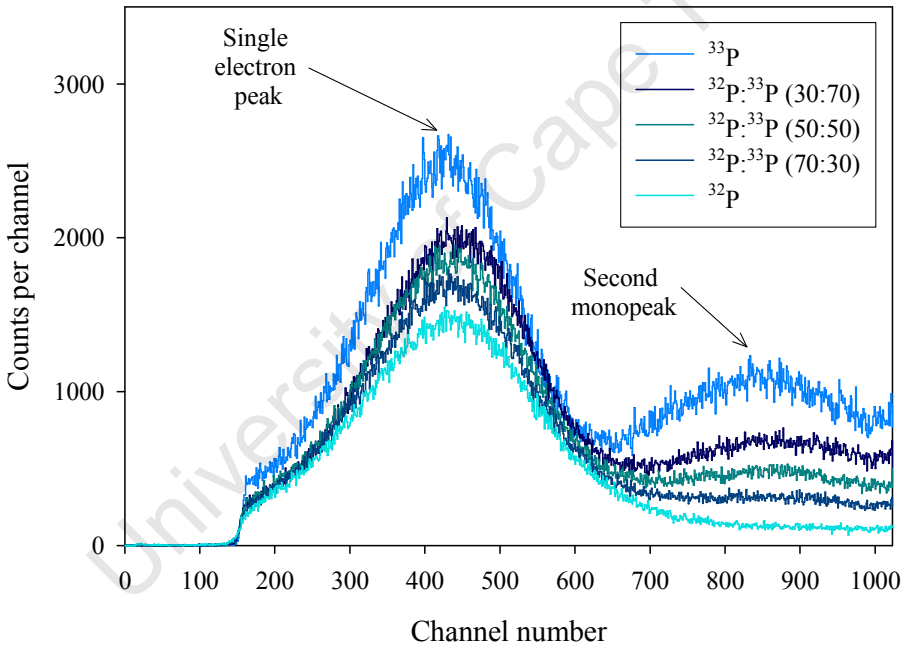

Fig. 5.6 Spectra of graduated mixtures of ^{32}P and ^{33}P for sources quenched with 3 ml $CHCl_3$. Each spectrum was normalised to a source count rate of 2 000 s^{-1}.

The figures-of-merit and efficiencies used to resolve the mixtures are given in Table 5.10. All data analysis was performed in the same way as described in Section 5.6.1. The result of each individual measurement (with its statistical uncertainty) is displayed in Fig. 5.7. For each solution the average measured values can be compared with the prepared gravimetric activity

Table 5.10 The figure-of-merit and double- and triple-coincidence detection efficiencies used to resolve the mixtures for the different quench states.

Quench state	P (e/keV)	$\varepsilon_d(^{32}\mathrm{P})$ ($s^{-1}Bq^{-1}$)	$\varepsilon_t(^{32}\mathrm{P})$ ($s^{-1}Bq^{-1}$)	$\varepsilon_d(^{33}\mathrm{P})$ ($s^{-1}Bq^{-1}$)	$\varepsilon_t(^{33}\mathrm{P})$ ($s^{-1}Bq^{-1}$)
Q_2	0.04214	0.9858	0.9825	0.6918	0.6314
Q_3	0.03114	0.9799	0.9750	0.6072	0.5323
Q_4	0.02525	0.9741	0.9677	0.5408	0.4563

concentrations calculated in Section 5.5.1, in Fig. 5.7 and in Table 5.11. The results show reasonable agreement between the prepared and measured activity concentrations, although not as good as that obtained for the ^{33}P:^{35}S mixtures. The estimated uncertainties are also given in Table 5.11 and are smaller than those obtained for the ^{33}P:^{35}S mixtures, as expected from the higher detection efficiencies and the larger differences between the energies of the component radionuclides. However, the relative deviations are generally significantly larger than the uncertainties, indicating a possible inconsistency in the model used for the efficiency calculation. The absolute deviations are below 2 kBq/g for all of the results but one.

Table 5.11 The averaged results of measurements of the ^{32}P:^{33}P mixtures are given, with A_G the gravimetric activity concentrations and A_0 and A_0' the measured values. The mass of $CHCl_3$ added per source is indicated as the quench state, with Q_3 indicating that 3 ml of $CHCl_3$ had been added, etc. Uncertainty estimated for the extracted activities are indicated by $\Delta(^{32}\mathrm{P})$ and $\Delta(^{33}\mathrm{P})$. The deviations were calculated from $\mathrm{Dev} = [(A_0 - A_G)/A_G] \times 100$. *

Mixture and quench state	$A_G(^{32}\mathrm{P})$ (kBq/g)	$A_0(^{32}\mathrm{P})$ (kBq/g)	$\Delta(^{32}\mathrm{P})$	$\mathrm{Dev}(^{32}\mathrm{P})$ (%)	$A_G(^{33}\mathrm{P})$ (kBq/g)	$A_0'(^{33}\mathrm{P})$ (kBq/g)	$\Delta(^{33}\mathrm{P})$	$\mathrm{Dev}(^{33}\mathrm{P})$ (%)
5:95 Q_3	1.67	0.93	11	– 44.27	23.31	23.81	0.39	2.14
5:95 Q_4	1.67	0.60	53	– 64.11	23.31	23.73	1.4	1.80
30:70 Q_2	8.20	7.73	0.50	– 5.76	19.72	20.32	0.19	3.06
30:70 Q_3	8.20	7.25	1.3	– 11.57	19.72	20.69	0.37	4.94
50:50 Q_2	15.69	14.94	0.21	– 4.75	15.59	16.65	0.23	6.76
50:50 Q_3	15.69	14.53	0.50	– 7.37	15.59	16.93	0.40	8.57
70:30 Q_2	24.91	23.33	0.14	– 6.33	10.51	12.66	0.32	20.36
70:30 Q_3	24.91	23.48	0.27	– 5.75	10.51	12.25	0.48	16.52

* A_0 is replaced by A_0' as appropriate.

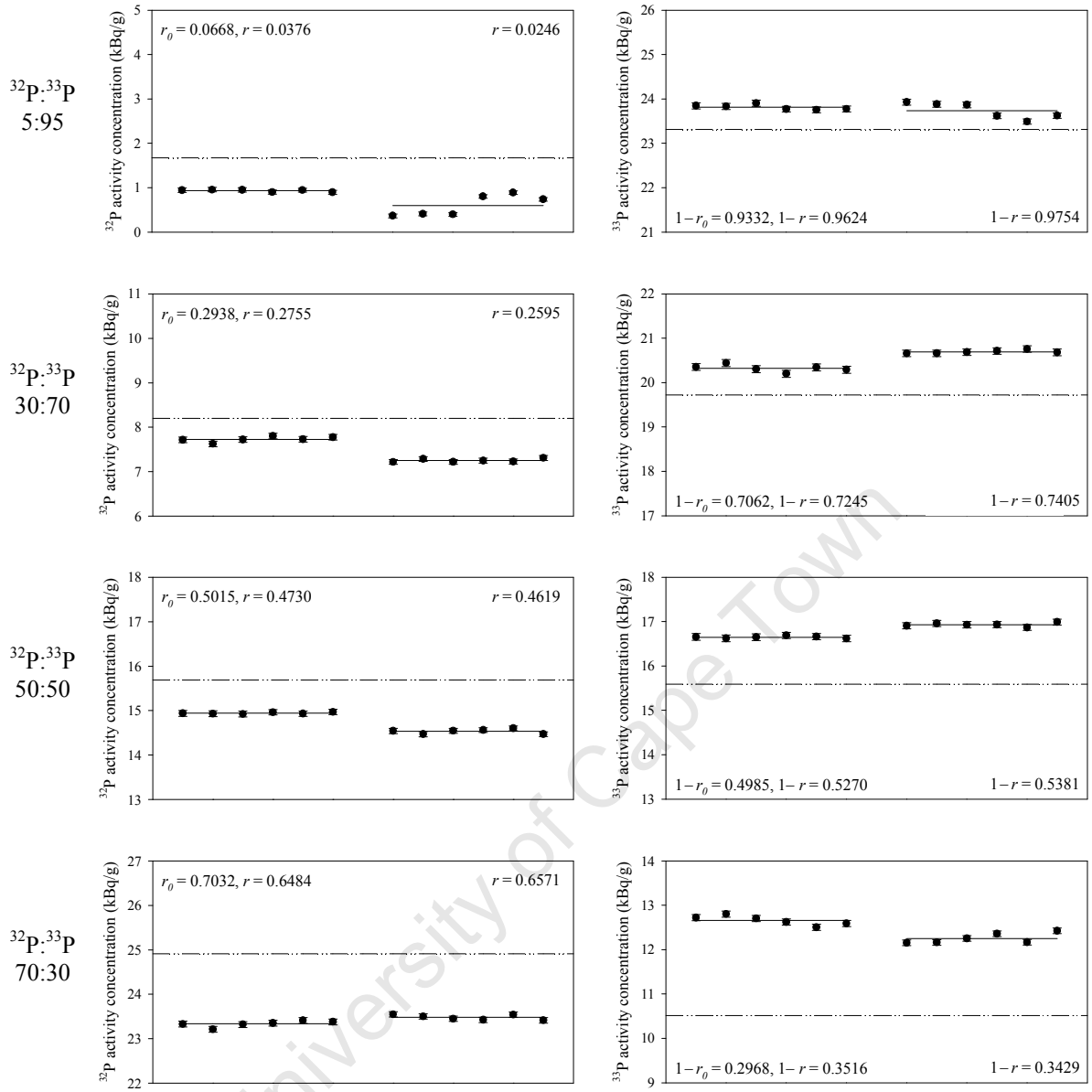

Fig. 5.7 The plots show the activity concentration obtained from each individual measurement of the ^{32}P:^{33}P mixture solutions with the ^{32}P components given on the left and the ^{33}P components on the right-hand side. The statistical uncertainties are given and are of the same size as the markers. In each plot, two sets of measurements are given, with the measurements from the less quenched source on the left and the more highly quenched source on the right. The dash-dot-dotted lines give the gravimetric concentrations and the solid lines the average value of each set of measurements of the same solution. The ratios, r_0 and r, given on each ^{32}P plot, and the ratios, $(1 - r_0)$ and $(1 - r)$, given on each ^{33}P plot, indicate the gravimetric and measured activity fractions determined for each solution.

5.6.3 The measurement of mixtures of ^{32}P and ^{35}S

Two sources were prepared for each of the three ^{32}P:^{35}S mixture solutions, with masses ranging between 59.7 and 81.3 mg per source. Each source was counted for three repeat measurements of 300 seconds each in two different quench states, with 1 ml and 2 ml of $CHCl_3$ added. The double-coincidence count rates varied between 1 300 and 1 900 s^{-1}. Afterpulses were measured simultaneously with the counting for each of the three double-coincidence channels in turn and showed the same trends observed for the other ^{32}P-containing mixtures. The afterpulse corrections applied varied between (0.39, 0.05, 0.09) % and (0.11, 0.03, 0.04) % for channels (1, 2, 3) for sources with varying amounts of ^{32}P and $CHCl_3$. One ^{33}P and one ^{35}S source were prepared and measured in the same quench state as the mixed sources as tracers to estimate the figure-of-merit of the system. The afterpulse contribution measured for the tracer standards was negligible. The figures-of-merit obtained from the tracers and the efficiencies used to resolve the mixtures are given in Table 5.12.

Table 5.12 The figure-of-merit and double- and triple-coincidence detection efficiencies used to resolve the ^{32}P:^{35}S mixtures for the different quench states. The ^{33}P efficiencies given were used to correct the counts for the ^{33}P impurity before data analysis, as detailed in the text.

Quench state	Tracer	P (e/keV)	$\varepsilon_d(^{32}P)$ ($s^{-1}Bq^{-1}$)	$\varepsilon_t(^{32}P)$ ($s^{-1}Bq^{-1}$)	$\varepsilon_d(^{33}P)$ ($s^{-1}Bq^{-1}$)	$\varepsilon_t(^{33}P)$ ($s^{-1}Bq^{-1}$)	$\varepsilon_d(^{35}S)$ ($s^{-1}Bq^{-1}$)	$\varepsilon_t(^{35}S)$ ($s^{-1}Bq^{-1}$)
Q_1	^{35}S	0.0654	0.9911	0.9892	0.7876	0.7457	0.6675	0.6066
Q_1	^{33}P	0.0656	0.9912	0.9892	0.7881	0.7463	0.6682	0.6074
Q_2	^{35}S	0.0422	0.9858	0.9825	0.6919	0.6316	0.5433	0.4638
Q_2	^{33}P	0.0429	0.9861	0.9829	0.6965	0.6369	0.5488	0.4700

Data analysis was performed in the same way as described in Section 5.6.1. Before determining the mixture activity concentrations A_0 and A_0' from Eqs. (5.11) and (5.12), the contributions of the contaminant ^{33}P to the measured count rates as given by

$$N_d(^{33}P) = A_G(^{33}P)\left[\varepsilon_d(^{33}P)\cdot\frac{m}{e^{-\lambda'' t'}}\right] \tag{5.16}$$

and

$$N_t\left(^{33}\mathrm{P}\right) = A_G\left(^{33}\mathrm{P}\right)\left[\varepsilon_t\left(^{33}\mathrm{P}\right)\cdot\frac{m}{e^{-\lambda'' t'}}\right], \tag{5.17}$$

were subtracted from the double- and triple-coincidence count rates N_d and N_t. $A_G\left(^{33}\mathrm{P}\right)$ gives the gravimetrically determined activity concentration of the contaminant calculated from Eq. (5.10) and given in Table 5.5. The efficiencies, $\varepsilon_d\left(^{33}\mathrm{P}\right)$ and $\varepsilon_t\left(^{33}\mathrm{P}\right)$, were determined from P as given by the respective tracer standards. The final term converts the contaminant activity concentrations on the reference date to the source count rates on the later measurement date. The source mass is given by m and λ'' is the decay constant for ^{33}P.

The result of each individual measurement, where ^{35}S was used as the tracer, is displayed in Fig. 5.8 for both quench states. In Table 5.13, the average measured values obtained with both ^{35}S and ^{33}P as tracers for each solution can be compared with the gravimetric activity concentrations calculated from Eq. (5.9), where a two-component mixture was assumed. The deviations were, on average, 1 % smaller when using ^{35}S as opposed to ^{33}P and lower for the sources quenched with 2 ml $CHCl_3$ than for those quenched with 1 ml $CHCl_3$. Again the results showed deviations greater than expected based on the uncertainty estimates, but showed better agreement between the prepared and measured activity concentrations than was obtained for the corresponding ^{32}P:^{33}P mixtures.

Table 5.13 (a) The averaged results of measurements of the ^{32}P:^{35}S mixtures are given for ^{35}S as the tracer, with A_G the gravimetric activity concentrations and A_0 and A_0' the measured values. The quantity of $CHCl_3$ added per source is indicated as the quench state with Q_1 indicating that 1 ml of $CHCl_3$ had been added, etc. Uncertainty estimates for the extracted activities are indicated by $\Delta(^{32}\mathrm{P})$ and $\Delta(^{35}\mathrm{S})$. The deviations were calculated from $\mathrm{Dev} = [(A_0 - A_G)/A_G] \times 100$.*

Mixture and quench state	$A_G(^{32}\mathrm{P})$ (kBq/g)	$A_0(^{32}\mathrm{P})$ (kBq/g)	$\Delta(^{32}\mathrm{P})$ (%)	$\mathrm{Dev}(^{32}\mathrm{P})$ (%)	$A_G(^{35}\mathrm{S})$ (kBq/g)	$A_0'(^{35}\mathrm{S})$ (kBq/g)	$\Delta(^{35}\mathrm{S})$ (%)	$\mathrm{Dev}(^{35}\mathrm{S})$ (%)
30:70 Q_1	11.82	11.11	0.62	– 5.99	25.85	26.59	0.20	2.87
30:70 Q_2	11.82	11.35	0.51	– 3.95	25.85	26.17	0.17	1.24
50:50 Q_1	19.36	18.43	0.28	– 4.80	19.54	20.39	0.22	4.31
50:50 Q_2	19.36	18.82	0.22	– 2.81	19.54	20.05	0.17	2.57
70:30 Q_1	28.96	27.56	0.16	– 4.80	11.52	13.18	0.28	14.39
70:30 Q_2	28.96	28.00	0.12	– 3.29	11.52	12.62	0.22	9.56

Table 5.13 (b) The averaged results of measurements of the ^{32}P:^{35}S mixtures are given for ^{33}P as the tracer.

Mixture and quench state	$A_G(^{32}\mathrm{P})$ (kBq/g)	$A_0(^{32}\mathrm{P})$ (kBq/g)	$\Delta(^{32}\mathrm{P})$ (%)	$\mathrm{Dev}(^{32}\mathrm{P})$ (%)	$A_G(^{35}\mathrm{S})$ (kBq/g)	$A_0'(^{35}\mathrm{S})$ (kBq/g)	$\Delta(^{35}\mathrm{S})$ (%)	$\mathrm{Dev}(^{35}\mathrm{S})$ (%)
30:70 Q_1	11.82	11.04	0.69	– 6.62	25.85	26.64	0.23	3.06
30:70 Q_2	11.82	10.91	0.53	– 7.65	25.85	26.43	0.17	2.23
50:50 Q_1	19.36	18.37	0.37	– 5.11	19.54	20.43	0.25	4.51
50:50 Q_2	19.36	18.47	0.26	– 4.60	19.54	20.25	0.17	3.61
70:30 Q_1	28.96	27.52	0.16	– 4.94	11.52	13.21	0.28	14.62
70:30 Q_2	28.96	27.77	0.15	– 4.11	11.52	12.76	0.22	10.78

* A_0 is replaced by A_0' as appropriate.

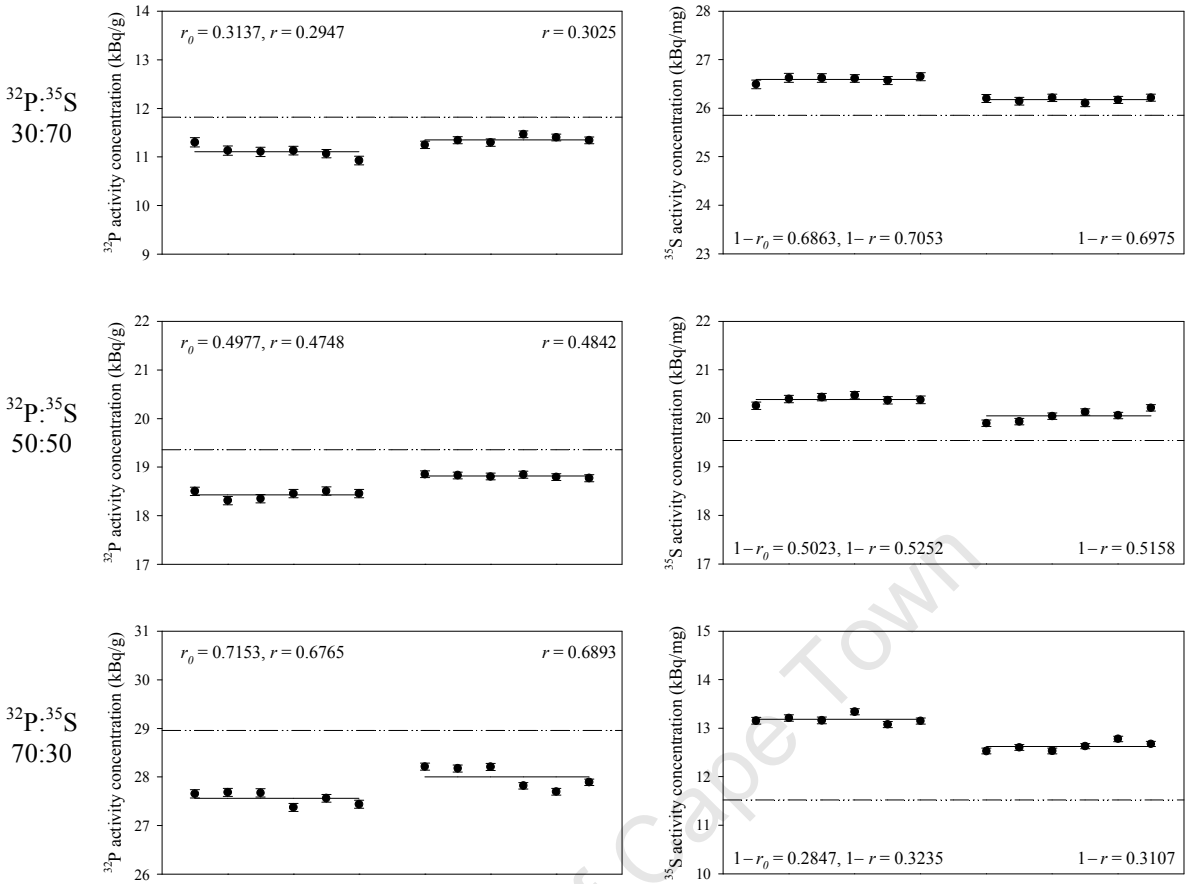

Fig. 5.8 The plots show the activity concentration obtained, when using ^{35}S as the tracer, for each individual measurement of the ^{32}P:^{35}S mixture solutions, with the ^{32}P components given on the left and the ^{35}S components on the right-hand side. The statistical uncertainties are given and are of the same size as the markers. In each plot, two sets of measurements are given, with the Q_1 series on the left and the Q_2 series on the right. The dash-dot-dotted lines give the gravimetric concentrations and the solid lines the average value of each set of measurements of the same solution. The ratios, r_0 and r, given on each ^{32}P plot, and the ratios, $(1 - r_0)$ and $(1 - r)$, given on each ^{35}S plot, indicate the gravimetric and measured activity fractions determined for each solution.

5.7 Discussion of results

Comparison of results from mixtures with similar fractional compositions showed that the smallest deviations from the gravimetric compositions were obtained for mixtures of the similar, low energy radionuclides ^{33}P and ^{35}S. For this radionuclide pair, the N_t/N_d vs. P curves (Fig. 5.3B) are somewhat sloped, even at a relatively high P value of 0.148 where measurements were undertaken. These mixtures also gave the largest predicted statistical uncertainties, which can be seen by comparing Figs. 5.4, 5.7 and 5.8 where all plots were

drawn so that the Y-axes spanned the same number of activity concentration units. The statistical uncertainties at one standard deviation are almost 5 times larger for the ^{33}P:^{35}S mixtures than for those of the ^{32}P:^{33}P and ^{32}P:^{35}S mixtures. This observation can be explained by rewriting Eqs. (5.13) and (5.14) in the following manner:

$$\sigma(A_0) = \left|\frac{\varepsilon_t}{\varepsilon_d} - \frac{\varepsilon_t'}{\varepsilon_d'}\right|^{-1} \sqrt{\left(1-\frac{\varepsilon_t'}{\varepsilon_d'}\right)^2 T + \left(\frac{\varepsilon_t'}{\varepsilon_d'}\right)^2 \frac{X}{3}} \times \left(\frac{e^{-\lambda t'}}{m\varepsilon_d t}\right), \tag{5.18}$$

$$\sigma(A_0') = \left|\frac{\varepsilon_t}{\varepsilon_d} - \frac{\varepsilon_t'}{\varepsilon_d'}\right|^{-1} \sqrt{\left(1-\frac{\varepsilon_t}{\varepsilon_d}\right)^2 T + \left(\frac{\varepsilon_t}{\varepsilon_d}\right)^2 \frac{X}{3}} \times \left(\frac{e^{-\lambda' t'}}{m\varepsilon_d' t}\right). \tag{5.19}$$

The main contributor to the statistical uncertainty is the first term, which becomes large when the difference between the triple-to-double efficiency ratios of the two components becomes small. This is demonstrated in Table 5.14, where values obtained from a single measurement of each 50:50 mixture solution are given for the various quench states used. The relative uncertainty, $\sigma(A_0)$, for the ^{33}P:^{35}S source is about four times larger than the uncertainties predicted for the other sources. This is brought about by the inverse absolute value term which is on average six times larger for the ^{33}P:^{35}S source than for the other mixtures. Since $N_t/N_d = \varepsilon_t/\varepsilon_d$ for a single radionuclide source, the relation between $\varepsilon_t/\varepsilon_d$ and $\varepsilon_t'/\varepsilon_d'$ in Eqs. 5.18 and 5.19 is the same as the relation between the N_t/N_d vs. P plots for the pure components in Fig. 5.3. Thus, the closer the N_t/N_d vs. P plots (as in Fig. 5.3) of the two pure components are to each other at the figure-of-merit used in the experiment, the more statistical variation is expected between repeat measurements of sources from the specific mixture.

The results obtained for the mixtures containing ^{32}P were somewhat worse than those for mixtures of ^{33}P and ^{35}S, but improved with increased quenching. Deviations from the gravimetric compositions were larger for mixtures of ^{32}P with ^{33}P (Fig. 5.3C) than with ^{35}S (Fig. 5.3D) where the N_t/N_d vs. P curves were further apart and more curved due to the lower β energy of ^{35}S. For higher values of P, the nearly horizontal curve increases the sensitivity of the method to small inconsistencies between N_t/N_d and the actual P value used. An extreme case was the measurement of the unquenched ^{32}P source (containing 1.6 % ^{33}P), where a small increase in the measured N_t/N_d ratio of 0.0008 (from 0.9930 to 0.9938) between the first and the last measurement translated to an increase in the extracted ^{32}P

Table 5.14 Values for the triple-to-double efficiency ratios, $\varepsilon_t/\varepsilon_d$ and $\varepsilon_t'/\varepsilon_d'$, and the triple- and exclusive double-coincidence counts, T and X collected in 300 seconds for one source of each 50:50 mixture solution, are given.

$|\ |^{-1}$ represents $\left|\frac{\varepsilon_t}{\varepsilon_d}-\frac{\varepsilon_t'}{\varepsilon_d'}\right|^{-1}$ and $\sqrt{\times(\ )}$ represents $\sqrt{\left(1-\frac{\varepsilon_t'}{\varepsilon_d'}\right)^2 T+\left(\frac{\varepsilon_t'}{\varepsilon_d'}\right)^2 \frac{X}{3}\times\left(\frac{1}{\varepsilon_d t}\right)}$.

For the final results, N_0 and $\sigma(N_0)$ are decay corrected and converted to activity concentrations by multiplying with the term $e^{-\lambda t'}/m$.

Mixture and quench state	$\varepsilon_t/\varepsilon_d$ *	$\varepsilon_t'/\varepsilon_d'$ *	T	X	$\|\ \|^{-1}$	$\sqrt{\times(\ )}$ (Bq)	N_0 (Bq)	$\sigma(N_0)$ (Bq)	$\sigma(A_0)$ (%)
^{33}P:^{35}S Q_0	0.9773	0.9606	490448	15706	59.79	0.2789	950.1	16.68	1.76
^{32}P:^{33}P Q_2	0.9967	0.9127	438448	18773	11.91	0.3127	851.5	3.724	0.44
^{32}P:^{33}P Q_3	0.9950	0.8766	385191	23042	8.44	0.3690	785.0	3.116	0.40
^{32}P:^{35}S Q_1	0.9980	0.9087	501434	25308	11.20	0.3550	858.4	3.975	0.46
^{32}P:^{35}S Q_2	0.9967	0.8537	431050	32400	6.99	0.4422	838.4	3.092	0.37

* See Tables 5.6, 5.10 and 5.12 for the efficiencies used.

activity concentration of 1.47 kBq/g and a decrease in the ^{33}P activity concentration of 1.87 kBq/g. By quenching the source with 1 ml of $CHCl_3$, the source was measured at an efficiency where the N_t/N_d vs. P curves are more sloped and curved, reducing the variation between repeat measurements to 0.60 kBq/g for a similar variation in N_t/N_d. However, it is noted that this improvement by quenching must be balanced by the increased uncertainty of the extracted figure-of-merit at lower efficiencies.

5.8 References

[1] M.-M. Bé, B. Duchemin, C. Morillon, E. Browne, V. Chechev, A. Egorov, R. Helmer, E. Schönfeld, Nucleide 2000. Nuclear and atomic decay data, Version 2-2004. BNM-CEA/DTA/LPRI, Saclay, France, 2004.

[2] B.R.S. Simpson, Monte Carlo calculation of the γ-ray interaction probability pertaining to liquid scintillator samples of cylindrically-based shape, NAC Report NAC/94-4 (1994).

[3] B.R.S. Simpson, W.M. Morris, The standardization of ^{33}P by the TDCR efficiency calculation technique, Appl. Radiat. Isot. 60 (2004) 465.

[4] B.R.S. Simpson, W.M. van Wyngaardt, Activity measurement of phosphorus-32 in the presence of pure beta-emitting impurities, S. Afr. J. Sci. 102 (2006) 361.

[5] B.R.S. Simpson, W.M. van Wyngaardt, Activity measurements of the high-energy pure β-emitters ^{89}Sr and ^{90}Y by the TDCR efficiency calculation technique, Appl. Radiat. Isot. 64 (2006) 1481.

CHAPTER 6 Conclusions

6.1 Evaluation of the new method in terms of the initial objectives

The goal of this thesis was to develop a simple liquid scintillation counting technique to determine the activities of two pure β-emitting radionuclides in the same sample. The intention was to avoid the inconveniences, conditions and/or complexities of other methods available to resolve such mixtures. The new method achieved this objective, as detailed below:

- Using high-gain phototubes, counting is carried out integrally above a threshold set just below the single-electron peak, so that the new method does not require the setting of counting windows or the associated tracking of the windows to account for quenching, as is done in the conventional Dual Label-DPM methods.

- The new method does not require use of quench correction curves for the pure components. This reduces the number of sources that need to be prepared and measured. It is additionally useful since pure solutions of the mixture components may be difficult to obtain, for example, mother-daughter pairs such as ^{90}Sr-^{90}Y, where the daughter grows in rapidly. The new method requires only a tracer standard (in this work the low energy component of the mixture was found to be preferable) of similar quench to the mixed radionuclide source. Under optimal conditions it should be possible to resolve mixtures of any two pure β-emitters using tracer standards of the low-energy β-emitters ^{3}H or ^{63}Ni.

- This is a straightforward *counting* technique that does not rely on the acquisition of multiple spectra and subsequent spectral deconvolution to resolve mixtures.

- No complex computer programs are needed. The programs normally used for CIEMAT/NIST data analysis can be easily adapted to calculate double- and triple-coincidence detection efficiencies in terms of the figure-of-merit, P, and a spreadsheet is used to resolve the collected count rates in terms of activities. This is more direct than other available methods where mixtures are resolved in terms of count rates and the rates are then converted to activities by either using quench curves prepared from standards of

the pure components or through efficiency calculation by the CIEMAT/NIST method.

- The method does not rely on lengthy counting times to follow differences in the decay of component radionuclides of a mixture. The new method can therefore be used to resolve mixtures of radionuclides with similar or long half-lives, which would make following the decay impracticable.

6.2 Evaluation of the new method in terms of results achieved

The new method was successfully applied to radionuclide pairs with maximum β-energy ratios of 1.5 (^{33}P:^{35}S), 2.3 (^{14}C:^{36}Ni), 6.9 (^{32}P:^{33}P) and 10.2 (^{32}P:^{35}S). Contrary to the spectroscopic methods applied for routine use (for example, the conventional Dual Label-DPM or Full Spectrum-DPM methods), where the general recommendation is only to apply the method when the β energies differ by a factor of 3 or more, better results were obtained for the mixtures with the lower β-energy ratios. The present results are summarised in Table 6.1 and can be compared with results obtained with the Spectral Deconvolution technique, given in Table 6.2. The comparison of results obtained for different radionuclide mixtures by different methods in different laboratories is not optimal, but this gives some measure of the capability of the new method in terms of accuracy currently attainable. Spectral Deconvolution was selected for this comparison as it is currently the most powerful and widely applicable method available. Generally, the results obtained with the two methods agree well, although at this stage the new method tends to give larger deviations for the mixtures at the outer edges of the composition ranges. The measurements for the new method were, however, completed without the need of quench correction curves for the pure components and data processing was simple and direct.

The results of the ^{14}C-containing mixtures given in Tables 6.1 and 6.2 compare quite well. The stock solutions used to prepare the ^{14}C:^{63}Ni mixture sources were chemically incompatible and this probably caused differences between the quench states of the tracer standards (^{63}Ni) and sources containing larger fractions of ^{14}C, leading to somewhat larger deviations for these mixtures. For the ^{35}S-containing mixtures, the results from the new method, given in Table 6.1, were excellent, matching the best achievable by other methods (Table 6.2). The results for mixtures containing the high-energy β-emitters (^{32}P or ^{90}Y) can

be compared between the two tables. The mixtures containing ^{32}P, with large differences in the β-energies of the components, gave discrepancies from the gravimetrically prepared activities which were somewhat larger than those obtained using Spectral Deconvolution. For this high-energy radionuclide, mixture resolution was improved by quenching the solutions by the addition of $CHCl_3$. The deviations obtained for the ^{32}P-containing mixtures were larger than expected from the estimated uncertainties, indicating a possible deficiency in some or other aspect of the model used to calculate the detection efficiency in terms of the figure-of-merit.

Table 6.1 Summary of results obtained for mixture resolution by the new method. For the mixtures containing ^{32}P, the results obtained with the optimal quench state are given. Where the relative deviations are expressed as "mostly < ", larger discrepancies were obtained for some mixtures, often at the outer edges of the composition ranges.

Mixture	Composition range	Dev. (high energy component) (%)	Dev. (low energy component) (%)	References
^{14}C:^{63}Ni	10:90 to 83:17	mostly < 5.5 %	mostly < 2.5 %	[1], Section 4.5
^{33}P:^{35}S	5:95 to 95:5	mostly < 2 %	mostly < 2 %	[2], Section 5.6.1
^{32}P:^{33}P	5:95 to 70:30	mostly < 6 %	mostly < 7 %	[2], Section 5.6.2 (b)
^{32}P:^{35}S	30:70 to 70:30	< 4 %	mostly < 3 %	[2], Section 5.6.3

Table 6.2 Summary of results obtained for mixture resolution by Spectral Deconvolution. One of the ^{14}C:^{3}H mixture solutions gave a relative deviation for ^{3}H of about 20 %. The remaining deviations were close to those specified in the summary table below.

Mixture	Composition range	Dev. (high energy component) (%)	Dev. (low energy component) (%)	References
^{14}C:^{3}H	9:91 to 98:2	< 3 %	mostly < 6 %	[3], Section 1.4.2
^{45}Ca:^{35}S	12:88 to 92:8	< 1.6 %	< 4 %	[3], Section 1.4.2
^{90}Y:^{90}Sr	11:89 to 45:55	mostly < 2 %	< 2 %	[4], Section 1.4.2

6.3 Further developments and applications

In this thesis a new method was developed for the measurement of mixtures of two pure β-emitting radionuclides. The method is easy to apply and generally gave good results for the various mixtures measured. The application of the TDCR method for direct activity

measurement of pure β-emitters is growing rapidly so that many national laboratories either have a three-phototube detection system, for example RC in Poland [5], LNHB in France [6], NMISA in South Africa [7], NIST in the USA [8], CNEA-LMR in Argentina [9], IFIN-HH in Romania [10], KRISS in Korea [11] and ANSTO in Australia [12], or are busy developing one. This new method can therefore easily be implemented by other laboratories and thereby extend the usefulness of this type of detection system.

If all data correction is performed optimally and the quench state of the tracer standard matches the mixture source adequately, a discrepancy between the prepared and measured composition outside the estimated uncertainty indicates possible shortcomings somewhere in the free parameter model used to calculate the liquid scintillation detection efficiencies. Inconsistencies are possibly due to the statistical model of light emission, the kB value applied, the ionisation quenching function, $Q(E)$, used, or inadequate shape factors used for the theoretical determination of the β-spectrum. Because of the new method's sensitivity to incorrectly determined efficiency values, a spin-off is that it could be applied as a useful tool to gauge the accuracy of the efficiency model by comparing the agreement between the prepared and measured compositions of mixture sources.

Refining the efficiency model would ultimately improve the accuracy of results achievable with this method for resolving the activities of mixtures of pure β-emitters. Finally, there is a possibility that the method can be extended to mixtures of three pure β-emitters in the same sample by performing measurements at two different quench states to facilitate the resolution.

6.4 References

[1] W.M. van Wyngaardt, B.R.S. Simpson, A simple counting technique for measuring mixtures of two pure β-emitting radionuclides, Nucl. Instr. and Meth. A 564 (2006) 339.

[2] W.M. van Wyngaardt, B.R.S. Simpson, G.E. Jackson, Further investigations of a simple counting technique for measuring mixtures of two pure β-emitting radionuclides, Appl. Radiat. Isot. 66 (2008) 1012.

[3] A. Grau Carles, A new linear spectrum unfolding method applied to radionuclide mixtures in liquid scintillation counting, Appl. Radiat. Isot. 45 (1994) 83.

[4] A. Grau Malonda, L. Rodriguez Barquero, A. Grau Carles, Radioactivity determination of ^{90}Y, ^{90}Sr and ^{89}Sr mixtures by spectral deconvolution, Nucl. Instr. and Meth. A 339 (1994) 31.

[5] R. Broda, K. Pochwalski, The enhanced triple to double coincidence ratio (ETDCR) method for standardization of radionuclides by liquid scintillation counting, Nucl. Instr. and Meth. A 312 (1992) 85.

[6] P. Cassette, R. Vatin, Experimental evaluation of TDCR models for the 3 PM liquid scintillation counter, Nucl. Instr. and Meth. A 312 (1992) 95.

[7] B.R.S. Simpson, B.R. Meyer, Direct activity measurement of pure beta-emitting radionuclides by the TDCR efficiency calculation technique, Nucl. Instr. and Meth. A 339 (1994) 14.

[8] B.E. Zimmerman, R. Collé, J.T. Cessna, Construction and implementation of the NIST triple-to-double coincidence ratio (TDCR) spectrometer, Appl. Radiat. Isot. 60 (2004) 433.

[9] P. Arenillas, P. Cassette, Implementation of the TDCR liquid scintillation method at CNEA-LMR, Argentina, Appl. Radiat. Isot. 64 (2006) 1500.

[10] A.C. Razdolescu, R. Broda, P. Cassette, B.R.S. Simpson, W.M. van Wyngaardt, The IFIN-HH triple coincidence liquid scintillation counter, Appl. Radiat. Isot. 64 (2006) 1510.

[11] K.B. Lee, J.M. Lee, T.S. Park, H.Y. Hwang, Implementation of TDCR method in KRISS, Nucl. Instr. and Meth. A 534 (2004) 496.

[12] M.J. Qin, L. Mo, D. Alexiev, P. Cassette, Construction and implementation of a TDCR system at ANSTO, Appl. Radiat. Isot. 66 (2008) 1033.

APPENDIX A Probability distributions

Random processes such as radioactive decay and the detection of radioactivity are often described by means of statistical models such as the binomial distribution or, under specific conditions, the Poisson distribution [1,2]. If a Bernoulli (or binary) trial is defined as an experiment with two possible outcomes, generally referred to as success and failure [3], then the random process under study can be viewed as a number of repeated, independent Bernoulli trials. The probability of success for each trial is the same and the outcome of one trial is not affected by the outcomes of previous trials.

Appendix A.1 The binomial distribution

The binomial distribution is a general model which is widely applicable to all processes with a constant success probability. The binomial probability distribution [4]

$$P(x) = \frac{n!}{x!(n-x)!} p^x (1-p)^{n-x}, \; x = 0,1,2,....n \tag{A.1}$$

computes the probability $P(x)$ of getting exactly x successes in n independent Bernoulli trials, where each trial has an individual success probability of p. The mean of the distribution $\bar{x} = np$ predicts the average number of successes and the variance $\sigma^2 = np(1-p)$ describes the amount of fluctuation in the data.

As an example analogous to the application in the main text, the decay of a radionuclide source in a specified time t is described by the binomial distribution. If the source contains n nuclei at the start of the experiment and each of these nuclei is viewed as a separate trial with decay of the nuclide in the time t counted as a success, then it follows from the fundamental law of radioactive decay [5] that the success probability p of each trial will be given by

$$p = 1 - e^{-\lambda t}, \tag{A.2}$$

where $\lambda = \ln 2 / T_{½}$ is the decay constant of the radionuclide and $T_{½}$ its half-life. The probability of exactly x nuclei decaying in the time t is given by

$$P(x) = \frac{n!}{x!(n-x)!}\left(1-e^{-\lambda t}\right)^{x}\left(e^{-\lambda t}\right)^{n-x},\ x = 0,1,2,....n\,. \tag{A.3}$$

Appendix A.2 The Poisson distribution

A Poisson process [3] consists of discrete events occurring in a continuous interval of time or space. The process is characterised by a parameter λ (which must not be confused with the radioactive decay constant), which describes the average number of events in an interval of unit length such that λs events occur on average in an interval of length s. The events are formed in such a way that the interval can, in effect, be divided into n trials of sufficiently short length h (i.e. $s = nh$) so that either 0 or 1 event occurs in any trial and the probability that two or more events occur is negligible. The probability for exactly one event occurring in any trial is given by $p = \lambda h$. This probability is constant and the outcome of one trial is not affected by the outcomes of previous trials. When $n \to \infty$ (i.e. $h \to 0$) the conditions for a Poisson random process are met and it can be shown that the probability distribution is given by [3]

$$P(x) = \frac{(\lambda s)^{x} e^{-\lambda s}}{x!},\ x = 0,1,2,....\ , \tag{A.4}$$

whereby the probability of x events occurring in a continuous interval s is computed.

The binomial distribution (Eq. (A.1)) tends to the Poisson distribution when the number of trials n is very large and p is close to zero so that np is finite and constant [1,2]. Because n is finite, an alternative expression for the Poisson distribution [4],

$$P(x) = \frac{(np)^{x} e^{-np}}{x!},\ x = 0,1,2,....n\,, \tag{A.5}$$

is required. This comes about since $\lambda = p/h$ and $s = nh$, so that $\lambda s = np$. The Poisson approximation results in a useful simplification because the Poisson distribution is a function of the average number of successes and it is not necessary to know n and p individually. Another useful property of the Poisson distribution is that the mean of the distribution $\bar{x}$ equals the variance σ^2, i.e. $\bar{x} = \sigma^2 = np$ and the predicted standard deviation $\sigma = \sqrt{\bar{x}}$.

In the counting of radioactivity, n is usually related to the number of nuclei and therefore large (on the order of Avogadro's number) so that the binomial distribution becomes

computationally cumbersome. When, in addition, the probability p for each nucleus to decay and be counted in the specified observation time is small, the Poisson distribution is a convenient but accurate approximation. From the definition of the Poisson distribution, it follows that square root statistics can be used to obtain an estimate of the measurement uncertainty, i.e. $\sigma = \sqrt{np} = \sqrt{\text{counts}}$. For a large number of counts, the Poisson tends to a Gaussian (or normal) distribution [4]. The estimate of σ using square root statistics will therefore have properties of the normal distribution, i.e., approximately 68 % of observations are expected to fall within $\bar{x} \pm \sigma$, 95 % within $\bar{x} \pm 2\sigma$ and 99.7 % within $\bar{x} \pm 3\sigma$. This fact was used in the simulation of Chapter 3.

The notation used to express the binomial and Poisson distributions in Appendix A is similar to that generally found in books on Statistics. Somewhat different notations

$$b(x,n,p) = \frac{n!}{x!(n-x)!} p^x (1-p)^{n-x}, \; x = 0,1,2,\ldots n \tag{A.6}$$

and

$$P(x,np) = \frac{(np)^x \exp(-np)}{x!}, \; x = 0,1,2,\ldots n \tag{A.7}$$

were used in the main text, for added clarity and for agreement with one of the references [6].

References

[1] J. Foster, K. Kouris, I.P. Matthews, N.M. Spyrou, Binomial vs Poisson statistics in radiation studies, Nucl. Instr. and Meth. 212 (1983) 301.

[2] I. Salma, É. Zemplén-Papp, Experimental investigation of statistical models describing distribution of counts, Nucl. Instr. and Meth. A 312 (1992) 591.

[3] H.J. Larson, Introduction to probability theory and statistical inference, John Wiley & Sons, Inc., New York, 1969, pp. 106 – 129.

[4] G.F. Knoll, Radiation detection and measurement, third ed., John Wiley & Sons, Inc., New York, 2000, pp. 70 – 79.

[5] G.F. Knoll, Radiation detection and measurement, third ed., John Wiley & Sons, Inc., New York, 2000, pp. 2 – 3.

[6] R. Broda, K. Pochwalski, T. Radoszewski, Calculation of liquid-scintillation detector efficiency, Appl. Radiat. Isot. 39 (1988) 159.

APPENDIX B The figure-of-merit *P* (and *M*) for one-, two- and three-phototube detectors

It is shown in Section 2.3 how the liquid scintillation counting detection efficiency can be expressed in terms of a single floating parameter named the figure-of-merit. In this thesis the figure-of-merit mostly used is *P*, which was defined by Gibson [1] as the number of photoelectrons at the first dynode of a single phototube per keV deposited in the liquid scintillator. Thus,

$$P = \varepsilon_0 L/hv \tag{B.1}$$

if a single-phototube system is viewed, with ε_0 the optical efficiency of the complete scintillator/phototube system, L the factor for conversion of electron energy to light energy and hv the average energy of the emitted photons. Alternatively, some of the references (e.g. [2,3]) define the figure-of-merit M as the ratio of the energy deposited in the liquid scintillator and the average number of photoelectrons emitted by all photocathodes in the system. Thus, for a detection system with any number of phototubes,

$$M = hv/\varepsilon_0 L\,. \tag{B.2}$$

M is in effect the inverse of P but considers the whole detection system rather than a single phototube.

Fig. B.1 shows the interaction of an electron with a liquid scintillator and the different stages of detection by a three-phototube detection system. The optical efficiency of the complete scintillator/phototube system, ε_0, is given by the sum of the optical efficiencies of each operational phototube. Thus,

$$\varepsilon_0 = \xi_1 \varepsilon_{p1} \tag{B.3}$$

when only phototube 1 is operational. When phototubes 1 and 2 are operational,

$$\varepsilon_0 = \xi_1 \varepsilon_{p1} + \xi_2 \varepsilon_{p2}\,. \tag{B.4}$$

For all three phototubes,

$$\varepsilon_0 = \xi_1 \varepsilon_{p1} + \xi_2 \varepsilon_{p2} + \xi_3 \varepsilon_{p3}\,. \tag{B.5}$$

The total number of photoelectrons expected at the first dynode of all the phototubes is $\varepsilon_0 N$.

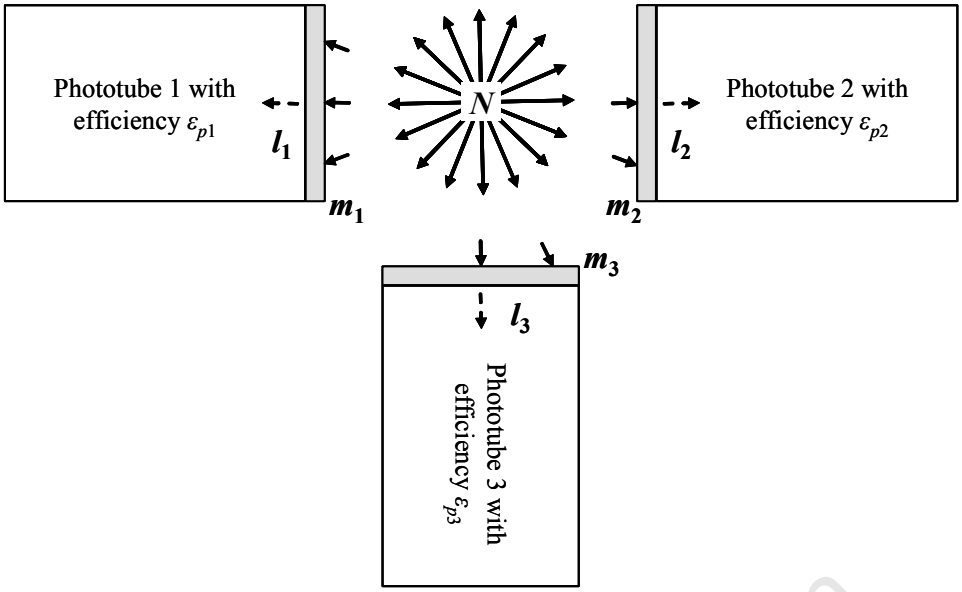

Fig. B.1 Schematic diagram of the detection of an electron by a three-phototube liquid scintillation detection system. This is an extension of Fig. 2.3. The interaction of an electron with a liquid scintillation source will result in the formation of N primary photons. For each of the i = 1 to 3 phototubes, m_i of the N photons will interact with the respective photocathode. The light collection efficiency of the scintillator as viewed by each individual phototube is given by ξ_i. For each phototube the overall photoelectric efficiency, ε_{pi}, describes the probability of formation and detection of photoelectrons so that l_i photoelectrons will be formed in response to the interaction of m_i photons.

Under conditions whereby an equal number of photons are incident on each phototube, i.e. $\xi_1 = \xi_2 = \xi_3 \equiv \xi$, and the photoelectric efficiency of each phototube is the same, i.e. $\varepsilon_{p1} = \varepsilon_{p2} = \varepsilon_{p3} \equiv \varepsilon_p$, then for one phototube

$$\varepsilon_0 = \xi\varepsilon_p \tag{B.6}$$

as in Section 2.3.1. For two phototubes

$$\varepsilon_0 = 2\xi\varepsilon_p \tag{B.7}$$

and for three phototubes

$$\varepsilon_0 = 3\xi\varepsilon_p . \tag{B.8}$$

Under the above assumptions, it follows from the definition of the figure-of-merit P given in Eq. (B.1) that, for one phototube,

$$P = \varepsilon_0 L/h\nu = \xi\varepsilon_p L/h\nu . \tag{B.9}$$

Since the figure-of-merit P is for a single phototube, extending the definition of P to a two-phototube detection system gives

$$P = \xi\varepsilon_p L/h\nu = \varepsilon_0 L/2h\nu \tag{B.10}$$

for each phototube. Similarly, for a three-phototube detection system

$$P = \xi\varepsilon_p L/h\nu = \varepsilon_0 L/3h\nu\,. \tag{B.11}$$

For a single-phototube detector the relationship between the figures-of-merit P and M is given by direct substitution of Eq. (B.2) into Eq. (B.9):

$$P = 1/M\,. \tag{B.12}$$

Substitution of Eq. (B.2) into Eq. (B.10) gives

$$P = 1/2M \tag{B.13}$$

for a matched two-phototube detection system and similarly, substitution of Eq. (B.2) into Eq. (B.11) gives

$$P = 1/3M \tag{B.14}$$

for a matched three-phototube detection system. These relationships were used for the adaptation of the CIEMAT program EFFY 2 [4], which calculates double-coincidence detection efficiencies in terms of M, to aid the calculation of double- and triple-coincidence detection efficiencies in terms of P for use with the TDCR method.

References

[1] J.A.B. Gibson, H.J. Gale, Absolute standardization with liquid scintillation counters, J. Phys. E. 1, ser. 2 (1968) 99.

[2] A. Grau Malonda, E. Garcia-Toraño, Evaluation of counting efficiency in liquid scintillation counting by pure β-ray emitters, Int. J. Appl. Radiat. Isot. 33 (1982) 249.

[3] A. Grau Malonda, B.M. Coursey, Calculation of beta-particle counting efficiency for liquid-scintillation systems with three phototubes, Appl. Radiat. Isot. 39 (1988) 1191.

[4] E. García-Toraño, A. Grau Malonda, EFFY, a new program to compute the counting efficiency of beta particles in liquid scintillators, Comp. Phys. Commun. 36 (1985) 307.

APPENDIX C Measurement of correction factors

Appendix C.1 Deadtime (τ_D)

A counting system consisting of a detector and its associated electronic equipment cannot process incoming signal pulses while it is still engaged in processing an earlier signal. Events arriving during this so-called deadtime are lost and the fraction of events lost increases with increasing counting rate. For any counting system, there is thus a minimum time interval, τ_D, by which two consecutive events must be separated for both to be recorded.

The equipment used in the NMISA laboratory makes use of a non-extending deadtime. This means that the deadtime is not extended by events arriving while the system is dead. Thus, if the system gives an average output count rate, n, the system will be dead for a fraction $n\tau_D$ and live for a fraction $(1 - n\tau_D)$ of the counting interval, t. If the input events arrive randomly at an average rate N that does not vary significantly during t, the measured count rate is $n = N(1 - n\tau_D)$, or rearranging, the deadtime corrected count rate, N, is given by [1]

$$N = n/(1 - n\tau_D). \tag{C.1}$$

The two-detector paired-source method [2] was applied to determine the intrinsic deadtime of equipment used in these experiments. Two similar NaI(Tl) detector/preamplifier systems were terminated into a 50Ω power divider at the input of an amplifier. It was assumed that the detectors are fast and do not contribute significantly to the deadtime. The shapes of the β spectra obtained in counting were simulated as well as possible with γ sources and the attenuation effect of the power divider compensated for by increasing the signal amplification. Each detector viewed a similar source, source 1 being counted by detector 1 and source 2 by detector 2. The high-voltage supply to each detector was alternatively switched on and off in the order 1, 1 + 2, 2, with the sources remaining advantageously fixed in position.

Briefly, let S_1, S_2 and S_{12} be the actual source count rates corrected for deadtime and N_1, N_2 and N_{12} be the observed count rates, including background, again corrected for deadtime. All these rates are thus "true" rates. Conservation of the source activities gives:

$$S_1 + S_2 = S_{12}, \tag{C.2}$$

and so

$$(S_1 + B_1) + (S_2 + B_2) = S_{12} + B_1 + B_2, \tag{C.3}$$

where B_1 and B_2 are the corrected background rates recorded by each detector. Hence

$$N_1 + N_2 = N_{12} \tag{C.4}$$

since $B_1 + B_2$ is the corrected background rate when both detectors are on. Thus if n_1, n_2 and n_{12} are the measured rates, including background, uncorrected for deadtime, the equality becomes

$$\frac{n_1}{1 - n_1\tau_D} + \frac{n_2}{1 - n_2\tau_D} = \frac{n_{12}}{1 - n_{12}\tau_D}, \tag{C.5}$$

where Eq. (C.1) was used to express the deadtime corrected count rates. Eq. (C.5) can be solved for τ_D:

$$\tau_D = \frac{1}{n_{12}}\left(1 - \sqrt{1 - \frac{n_{12}(n_1 + n_2 - n_{12})}{n_1 n_2}}\right). \tag{C.6}$$

$\tau_D = \frac{1}{n_{12}}\left(1 + \sqrt{1 - \frac{n_{12}(n_1 + n_2 - n_{12})}{n_1 n_2}}\right)$ is also an analytical solution to Eq. (C.5), but it gives non-physical deadtime corrected count rates since the condition, $\tau_D < 1/n_{12}$, [3] is not satisfied.

To derive an expression for the uncertainty of the deadtime, Eq. (C.6) is written in terms of counts, m_1, m_2, m_{12}, recorded in a common time interval t

$$\tau_D = \frac{t}{m_{12}}\left(1 - \sqrt{1 - \frac{m_{12}(m_1 + m_2 - m_{12})}{m_1 m_2}}\right). \tag{C.7}$$

The paired sources are usually set up to provide similar counting rates to within about 15% or so. Under conditions that $m_1 \approx m_2 \approx m_{av}$, where $m_{av} = (m_1 + m_2)/2$, τ_D can be approximated by

$$\tau_D \approx \frac{2t}{m_{12}} - \frac{t}{m_{av}}. \tag{C.8}$$

Since the observables m_1, m_2 and m_{12} are independent measurements, the uncertainty in the deadtime can be found by applying the uncertainty propagation formula to Eq. (C.8). Thus

$$\sigma(\tau_D) = \sqrt{\left(\frac{\partial \tau_D}{\partial m_{12}}\right)^2 \sigma^2(m_{12}) + \left(\frac{\partial \tau_D}{\partial m_{av}}\right)^2 \sigma^2(m_{av})} \tag{C.9}$$

so that

$$\sigma(\tau_D) = t\sqrt{\frac{4}{(m_{12})^3} + \frac{1}{2(m_{av})^3}}, \tag{C.10}$$

where $\sigma(m_{12}) = \sqrt{m_{12}}$, $\sigma(m_{av}) = \sqrt{m_{av}/2}$ and the counting period t is the same for each of the three required measurements. It was shown [2] that Eq. (C.10) gives a good estimate of the uncertainty for deadtimes of the order of 1 μs. For larger deadtimes, the radioactive events do not follow a Poisson distribution and $\sigma m = (1 - n\tau_D)\sqrt{m}$ [1], where n is the count rate and $m = nt$ is the total counts in the time interval t.

Appendix C.2 Afterpulse correction (θ)

Afterpulses are satellite pulses that will sometimes follow a true signal pulse after a short delay period. They are formed [4] by the emission of light from the latter stages of the multiplier structure which finds its way back to the photocathode. Alternatively, an imperfect vacuum within the phototube allows traces of residual gas to be ionised by the passage of electrons through the multiplier structure. Positive ions that are formed will drift in the reverse direction and some may find a path back to the photocathode.

Afterpulsing was measured simultaneously with counting for each of the three double-coincidence channels in turn. Afterpulsing for the triple-coincidences was found to be negligible. A gating technique [5] was used which compares the count rates corresponding to the intrinsic deadtime, τ_D, and a considerably longer non-extending deadtime, τ, that is introduced electronically with the start of a genuine pulse. The signal width chosen corresponds to $\tau \approx 94$ μs [6], during which time most of the afterpulsing will have occurred. The probability, θ, for the production of one of more spurious pulses per genuine pulse is given by

$$\theta = \frac{q - n_0}{n_0} - (\tau - \tau_D)\frac{q}{t}, \tag{C.11}$$

where t is the counting period, q is the total number of counts corresponding to τ_D and n_0 the number of counts associated with the longer deadtime. To achieve accurate measurements of

θ it is important to determine ($\tau - \tau_D$) as accurately as possible and to keep the count rate of sources low (generally < 2 000 s^{-1}), since any uncertainty in ($\tau - \tau_D$) is multiplied by the count rate q/t.

The uncertainty in the afterpulse correction, $\sigma\theta$, is obtained [5] by rewriting Eq. (C.11) in terms of the independent variables n_0, the number of gated counts, $n_g = q - n_0$, and ($\tau - \tau_D$), and applying the uncertainty propagation formula to give

$$\sigma\theta = \sqrt{\frac{(q-n_0)q}{(n_0)^3} + q\frac{(\tau-\tau_D)^2}{t^2} + \frac{q^2}{t^2}\sigma^2(\tau-\tau_D)} \qquad \text{(C.12)}$$

after re-substitution of q.

Appendix C.3 ($\tau - \tau_D$)

($\tau - \tau_D$), the difference between the lengthened deadtime and the inherent deadtime, can be found from Eq. (C.11) if θ is set to zero [5]. This is possible if experimental conditions are such that the detection of spurious pulses is highly unlikely. This is the case when relatively high-energy gamma radiation is observed by means of a NaI detector. Then

$$(\tau-\tau_D) = \frac{(q-n_0)}{n_0}\frac{t}{q}. \qquad \text{(C.13)}$$

An equation for the uncertainty of ($\tau - \tau_D$) was derived by re-writing Eq. (C.13) in terms of the independent variables n_0 and n_g and applying the uncertainty propagation formula. This gives

$$\sigma(\tau-\tau_D) = t\sqrt{\frac{(q-n_0)(q^2+qn_0-n_0^2)}{q^3n_0^3}} \qquad \text{(C.14)}$$

after re-substitution of q.

To measure ($\tau - \tau_D$), the same electronic set-up as that for the measurement for satellite pulses was used, with the exception that a ^{137}Cs point source and a NaI(Tl) detector were used. The electronic settings were adjusted so that the pulse distribution resembled that obtained with the pure β-emitters.

Appendix C.4 Coincidence resolving time (τ_R)

The coincidence resolving time, τ_R, gives the maximum time interval by which two consecutive events can be separated for a coincidence to be recorded by the coincidence unit. τ_R was measured for the NMISA TDCR coincidence unit by providing two uncorrelated inputs from ^{137}Cs sources viewed by two NaI(Tl) detectors and measuring both the singles rates, m_1 and m_2, and the resulting chance coincidence rate, c, in a measurement time t. The resolving time was calculated from [7]

$$\tau_R = \frac{ct}{2m_1m_2}. \tag{C.15}$$

References

[1] NCRP Report No. 58, A handbook of radioactivity measurements procedures, second ed., National Council on Radiation Protection and Measurements, Bethesda, 1985, pp. 60-73.

[2] B.R.S. Simpson, Deadtime measurement and associated statistical uncertainty by means of a two-detector paired-source method, Appl. Radiat. Isot. 42 (1991) 811.

[3] W.S. Diethorn, Counter deadtime: a question of poor textbook advice, Int. J. Appl. Radiat. Isot. 25 (1974) 55.

[4] G.F. Knoll, Radiation detection and measurement, third ed., John Wiley & Sons, Inc., New York, 2000, pp. 281 – 282.

[5] J. Steyn, S.M. Botha, International comparison of the radioactivity of a ^{139}Ce solution (March 1976): The effect of spurious pulses on the accuracy of the final result, NPRL research report FIS 102 (1976).

[6] B.R.S. Simpson, Radioactivity standardization in South Africa, Appl. Radiat. Isot. 56 (2002) 301.

[7] G.F. Knoll, Radiation detection and measurement, third ed., John Wiley & Sons, Inc., New York, 2000, pp.668 – 673.

APPENDIX D The statistical uncertainty in N_t/N_d

The TDCR value, N_t/N_d, is given by the triple-coincidence count, T, divided by the average of three double-coincidence counts, D_1, D_2 and D_3, all collected simultaneously in a time interval t. Each double count is made up of the triple count and a portion exclusive to the double count, X_1, X_2 and X_3, so that

$$D_i = X_i + T\,,\ i = 1 \text{ to } 3. \tag{D.1}$$

To derive a formula to estimate the statistical uncertainty in the measured TDCR value, $\sigma(N_t/N_d)$, N_t/N_d is written in terms of the independent variables T, X_1, X_2 and X_3:

$$\frac{N_t}{N_d} = \frac{3T}{3T + X_1 + X_2 + X_3}\,. \tag{D.2}$$

Applying the uncertainty propagation formula [1]

$$\sigma(N_t/N_d) = \sqrt{\left(\frac{\partial(N_t/N_d)}{\partial T}\right)^2 \sigma_T^2 + \sum_{i=1}^{3}\left[\left(\frac{\partial(N_t/N_d)}{\partial X_i}\right)^2 \sigma_{X_i}^2\right]} \tag{D.3}$$

to Eq. (D.2) gives the predicted uncertainty as

$$\sigma(N_t/N_d) = \frac{3\sqrt{(X_1 + X_2 + X_3)^2 T + (X_1 + X_2 + X_3)T^2}}{(3T + X_1 + X_2 + X_3)^2}\,. \tag{D.4}$$

Square root statistics were used to estimate the standard deviations of the numbers of counts, i.e. $\sigma_T = \sqrt{T}$ and $\sigma_{X_i} = \sqrt{X_i}$, with

$$\frac{\partial(N_t/N_d)}{\partial T} = \frac{3(X_1 + X_2 + X_3)}{(3T + X_1 + X_2 + X_3)^2} \tag{D.5}$$

and

$$\frac{\partial(N_t/N_d)}{\partial X_i} = \frac{-3T}{(3T + X_1 + X_2 + X_3)^2}\,, \text{ for } i = 1, 2 \text{ or } 3. \tag{D.6}$$

Eq. (D.4) is an extension of the formula derived for a three-detector system where two double-coincidence counts and one triple-coincidence count are collected [2,3]. Because this is the uncertainty of a ratio, $\sigma(N_t/N_d)$ is usually relatively small and N_t/N_d can be measured to a high precision even for relatively low count rates and short counting intervals [3].

References

[1] Guide to the expression of uncertainty in measurement, first ed., first printing, International Organization for Standardization, Geneva, 1993, pp. 19 – 20.

[2] B.R.S. Simpson, B.R. Meyer, Direct determination of the activity of non-gamma-emitting radionuclides by the TDCR efficiency calculation technique: a review of the present status, NAC Report NAC/92-02 (1992).

[3] B.R.S. Simpson, B.R. Meyer, Direct activity measurement of pure beta-emitting radionuclides by the TDCR efficiency calculation technique, Nucl. Instr. and Meth. A 339 (1994) 14.